STRENGTHENING OF REINFORCED CONCRETE BEAMS USING EXTERNALLY BONDED FRP PLATES

by

Savaş Atmaca

B.S. in C.E., Dokuz Eylül University, 1997

Submitted to the Institute for Graduate Studies in
Science and Engineering in partial fulfillment of
the requirements for the degree of
Master of Science
in
Civil Engineering

Boğaziçi University

2001

Dedicated to my mother,

my sister,

my father

and

my older brother, Halim Alanyalı.

ACKNOWLEDGEMENTS

I would like to express my sincere gratitude to my thesis supervisor, Prof. Cengiz KARAKOÇ, for his valuable guidance and encouragement throughout this thesis.

I owe special thanks to the members of thesis jury, Prof. Turan ÖZTURAN and Assistant Prof. Şevket ÖZDEN, for their useful suggestions and comments.

I would like to express my deepest gratitude to Halim ALANYALI for his continuous support, guidance and encouragement.

The supply of materials from SIKA and Nuh ready mixed concrete is also acknowledged.

I am also grateful to research assistant Onur ERTAŞ for his continuous support that he provided throughout the preparation of the thesis.

I would like to thank to Idil YURDAKUL for her assistance and valuable suggestions.

I would like to express my appreciation to research assistants Osman KAYA and Haydar ARSLAN for their assistance throughout this thesis.

I am also grateful to Güray Özgün for his assistance during application of FRP materials.

I would like to thank to technicians, H. Şenel, H. Ayar, I. Gültekin, for their assistance during the tests of the beams.

Finally, I would like to express my sincere gratitude to my dear family for their continuous support and endless encouragement.

ABSTRACT

STRENGTHENING OF REINFORCED CONCRETE BEAMS USING EXTERNALLY BONDED FRP PLATES

In recent years, occurrence of great earthquakes in Turkey has resulted in important damages in structures. Due to this phenomenon, repair and/or retrofit of the existing structures have become an important issue. In addition, increasing of serviceability loads, upgrading of provisions or deterioration of the structures due to corrosion or other types of degradation have caused emerging the necessity of repair and/or strengthening. Although a variety of strengthening techniques are available such as jacketing or strengthening with externally bonded steel plates, it is getting popular to use FRP material due to their excellent properties.

An experimental and analytical study on the behaviour of FRP-strengthened beams has been performed. All beams have the same material properties and dimensions. The effect of FRP ratio and reinforcement ratio on the behaviour of test specimens has been investigated.

ÖZET

BETONARME KiRiŞLERiN FRP ŞERiTLERLE GÜÇLENDiRiLMESi

Son yıllarda Türkiye'de meydana gelen büyük depremler yapılarda önemli hasarlara neden olmuştur. Bu nedenle mevcut yapıların onarım ve güçlendirilmesi önemli bir konu olmuştur. Ayrıca kullanım yüklerinin artması, yönetmeliklerin yenilenmesi yada yapıların korozyon gibi çeşitli nedenlerle kötüleşmesi onarım ve/veya güçlendirme gerekliliğinin ortaya çıkmasına neden olmuştur. Mantolama yada Çelik plakaların kirişlerin çekme bölgesine yapıştırılmasıyla elde edilen çeşitli güçlendirme tekniklerinin olmasına rağmen FRP malzemelerin çeşitli özelliklerinden dolayı güçlendirme malzemesi olarak kullanılmaları gittikçe yaygınlaşmaktadır

Bu tez çalışmasında FRP ile güçlendirilmiş kirişlerin davranışları deneysel ve analitik olarak incelenmiştir. Bütün test kirişleri aynı malzeme özelliklerine ve aynı boyutlara sahiptir. FRP ve donatı oranlarının kirişlerin davranşları üzerindeki etkileri incelenmiştir.

TABLE OF CONTENT

LIST OF FIGURES

LIST OF TABLES

LIST OF SYMBOLS/ABBREVIATIONS

a	Crack spacing
$A_{f\,min}$	Minimum FRP area for the cross section
A_{frp}	FRP cross-sectional area
A_s	Area of tension steel re-bars
A_s'	Area of compression steel reinforcement
b	Width of the cross section
c	Neutral axis depth
d	Effective depth
d'	Depth to the centroid of the compression steel
d_p	Depth to the centroid of the FRP plate
E_c	Young's modulus of concrete
E_s	Young's modulus of tension steel
E_s'	Young's modulus of compression steel
F_c	Concrete compression force
F_p	FRP plate force
F_s	Tension steel force
F_s'	Compression steel force
f_c'	Concrete compressive strength
f_c''	Maximum stress in concrete
f_{cv}	Stress in concrete
f_r	Ultimate strength in steel
f_s	Stress in tension steel
f_s'	Stress in compression steel
f_y	Yield strength of tension steel
f_y'	Yield strength of compression steel
h	Height of cross section
k	Coefficient needed to evaluate shear capacity of FRP-plated beams
L_{max}	Maximum load corresponding to max moment
M	Bending moment

M_{max}	Maximum moment in the cross section
R_E	Enhancement ratio
s	Stirrup spacing
t_p	Thickness of FRP plate
V_{up}	Shear capacity of plated beams
y'	Depth of centroid of the concrete stress block
α	Mean stress factor
Δ	Deflection
$\ddot{\varepsilon}_c$	Strain at centroid of area under concrete stress-strain diagram
ε_{oo}	Initial strain at the extreme tensile fiber of concrete
ε_0	Strain in concrete at maximum stress
ε_p	Strain in FRP plate
$\varepsilon_{p\ ult}$	Ultimate strain for the FRP plate
ε_{cu}	Ultimate concrete compressive strain
ε_s	Strain in tension steel
ε_r	Ultimate strain in steel
ε_s'	Strain in compression steel
ε_y	Yield strain in tension steel
ε_y'	Yield strain in compression steel
ϕ	Curvature
γ	Centroid factor
μ_D	Deflection ductility
μ_ϕ	Curvature ductility
λ	Constant
ρ	Percentage of tension steel
σ	Normal stresses at the cut-off point
σ_y	Yield stress of tension steel
σ_y'	Yield stress of compression steel
$\sigma_{p\ ult}$	Ultimate stress for the FRP plate

$\Sigma(GA)$	Shear stiffness
τ	Shear stresses at the plate curtailment

1. INTRODUCTION

In recent years, repair and retrofit of existing structures have been among the most important challenges in civil engineering. The primary reasons for strengthening of structures can be summarized as follows:

- Upgrading of resistance to withstand underestimated loads,
- Increasing the load-carrying capacity for higher load permits,
- Eliminating premature failure due to inadequate detailing,
- Restoring lost load carrying capacity due to corrosion,
- Other types of degredation caused by aging, etc.[1].

Repairment might be necessary either as a result of lack of durability or after a disaster such as fire or earthquake. One of the methods to repair the damaged structures is filling the cracks with a polymeric resin, such as epoxy. Externally bonded steel plates have been used for both repair and strengthening purposes [2].

Strengthening of concrete members has been usually accomplished by construction of external reinforced concrete or shotcrete jackets, by epoxy bonding of steel plates to the tension faces of the members or by external post-tensioning. A relatively new technique involves the replacement of steel plates by fiber reinforced polymers (FRP), or simply composites, in the form of thin laminates or fabrics [3].

Fiber reinforced plastic (FRP) plates or fabrics are becoming increasingly popular materials for strengthening of reinforced concrete (RC) beams and girders. This strengthening technique has involved epoxy bonding FRP plates or fabrics to the tension face of the beam, increasing both the strength and stiffness of the beam [4].

These fiber reinforced plastic materials has provided the engineer an opportunity for an outstanding combination of properties, such as low weight (making them much easier to handle on site), immunity to corrosion, excellent mechanical strength and stiffness, and the ability of formation in very long lengths, thus eliminating the need for lapping at joints [3].

The main disadvantages in using these materials are high material cost and brittle failure modes. Carbon fibre reinforced polymer (CFRP) materials have been around ten times more expensive than mild steel but material cost has usually constituted around 20 per cent of the total cost of a strengthening project, the remaining 80 per cent being labour cost. The easy handling of FRP plates has reduced labour costs considerably. The problem of having to join limited lengths of steel plate has been overcome by the fact that FRP plates may be delivered to site in rolls of 300 m or more [5].

2. LITERATURE REVIEW

2.1. Introduction

Concrete structures deteriorate due to reasons including internal reinforcement corrosion, freeze-thaw action, excessive loading and poor initial design. Many bridges and other structures have been no longer considered satisfactory in terms of load carrying capacity for these reasons or changes in the loading specifications of design codes. In order to maintain efficient highway networks and to keep buildings operational, older structures must be upgraded so that they meet the same requirements demanded of structures built today and in the future. To upgrade structures rather than to rebuild them, particularly if rapid, effective and simple strengthening methods both environmentally and economically preferable have been available. The choice between upgrading and rebuilding has been based on factors specific to each individual case, but several issues should be considered in every case. These have been the length of time during which the structure would be out of service or providing a reduced service, relative costs upgrading and rebuilding in terms of labour, materials and plant, and disruption of other facilities. For example the need to upgrade bridges has been a worldwide one which has placed considerable importance on strengthening techniques [5].

The strengthening of reinforced concrete members by externally bonded steel plates has become very popular throughout the beginning of 1970s to the beginning of 1990s Irvin 1975, Solomon *et al.* 1976, MacDonald 1978, Jones *et al.*, 1982, Rybicki *et al.* 1987 have been some of the researchers studying on this field [6].

The first recorded strengthening case was in Durban, South Africa, in 1964, where epoxy-bonded steel plates were used to strengthen concrete beams in an apartment complex, where part of the reinforcing steel in the building had been accidentally omitted during construction. Four bridges at Swanley, Kent, in England, was strengthened by using steel plates in 1975 and 1977, respectively [7].

The disadvantages of steel plates can be summarised as follows:

- Transporting, handling and installing heavy plates have been difficult,
- Corrosion of plates has resulted in deterioration of the bond at concrete-steel interface,
- The steel plates have had limited delivery lengths which have necessitated the work and difficulty of forming joints,
- The need for massive and expensive falsework in order to hold plates in position during adhesive cure,
- The need to prepare the steel surface for bonding (this being labour intensive and time consuming) [8].

Since the use of steel plates has had several severe disadvantages, researchers have tried to find an alternative material. Fibre reinforced plastic materials have emerged at that time. FRP materials have had mechanical and physical properties superior to those of steel, particularly with respect to tensile and fatigue strengths, and these qualities have been maintained under a wide range of temperatures [8].

The FRP laminates have been typically made of continuous fibers, glass, aramid and carbon, bonded with a polymeric matrix such as epoxy. Regarding the FRP material selection, it has been believed that, given its superior properties over other composites, carbon fiber reinforced plastics (CFRP) has offered the highest potential for retrofitting concrete structures [9].

Table 2.1 has shown which fiber is most suitable for such strengthening applications [10]. It can be easily seen from Table 2.1 that carbon has been ranked as the first with total points of 55. Aramid has been placed in the second place with the total points of 41 and glass has had the third place with total points of 32.

Using fiber reinforced plastic materials (FRP), many bridges and buildings have been strengthened. For example, Kattenbusch bridge in Germany has been strengthened by using glass fiber reinforced plastic (GFRP) plates. Ibach bridge in Switzerland using

carbon fiber reinforced plastic (CFRP) sheets, tall chimneys in Japan using CFRP tapes and winding strands [9].

Table 2.1. Rating of the fiber types [10]

Criterion	Weighting factor (1-3)	Weighted rating[a] for laminates with fibers of		
		Carbon	Aramid	E-glass
Tensile strength	3	9	9	9
Compressive strength	2	6	0	4
Young's modulus	3	9	6	3
Long term behaviour	3	9	6	3
Fatigue behaviour	2	6	4	2
Bulk density	2	4	6	2
Alkaline resistance	2	6	4	0
Price	3	6	6	9
Total points		55	41	32
Ranking		1	2	3
[a] rating: very good=3, good=2, adequate=1, inadequate=0 points				

2.2. Carbon Fiber Materials for Strengthening

2.2.1. Carbon Fiber Filament

Carbon fiber filaments have been manufactured by chemical transaction using a Rayon belonging in a highly continued organic molecular compound and an organic Mesophase-Pitch belonging in a petroleum or a liquefied coke pitch. The stretched and stabilized Rayon has been carbonized by the heat of 2500~3000 ^{0}C and the Rayon has been changed into the high performance carbon fiber filament. Those filaments have had approximately the diameter of 7~10 μm included uni-directionally aligned molecular fibers. Mesophase-Pitch originally having a uni-directional molecular fiber alignment has

been changed easily into the high performance carbon fiber filament by the carbonization under the heat of 2500~3000 ^{0}C [11].

The carbon fiber filament has had an excellent high tensile strength reaching about 5000 MPa but its load carrying capacity at tension has not been so great as 0.2 N per each filament because of a very small sectional area of 7~10 μm diameter. Figure 2.1 has shown the relationship between tensile strength and strain of the high performance carbon fiber in comparison with the other materials [11]. It can be noted that the modulus of elasticity of the carbon fiber filament has been greater than aramid fiber and glass fiber. Besides, there has been a little difference between young's modulus of the high performance carbon fiber filament and young's modulus of steel. Nevertheless, it should be noted that many kind of carbon fiber have been available. That's why, young's modulus of carbon fiber can change widely.

Moreover, according to the angle of applied load with respect to the fibers the behaviour of fibers has been linear elastic for 0^0 or 90^0 or non-linear as shown in Figure 2.2 [12]. It has shown that longitudinal fibers have possessed greater load-carrying capacity than angled fibers and transverse fibers.

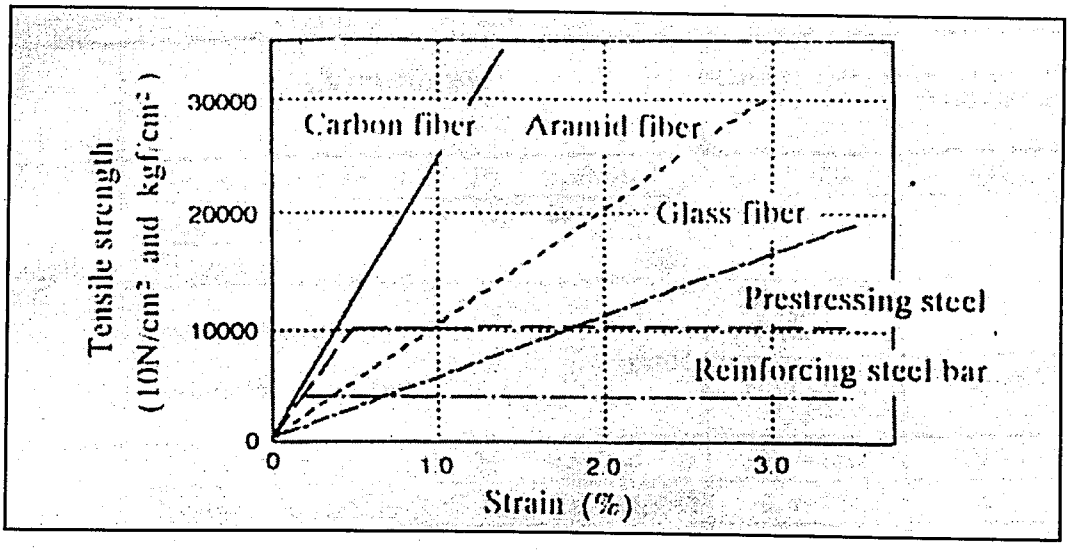

Figure 2.1. Stress-strain diagrams of different materials [11]

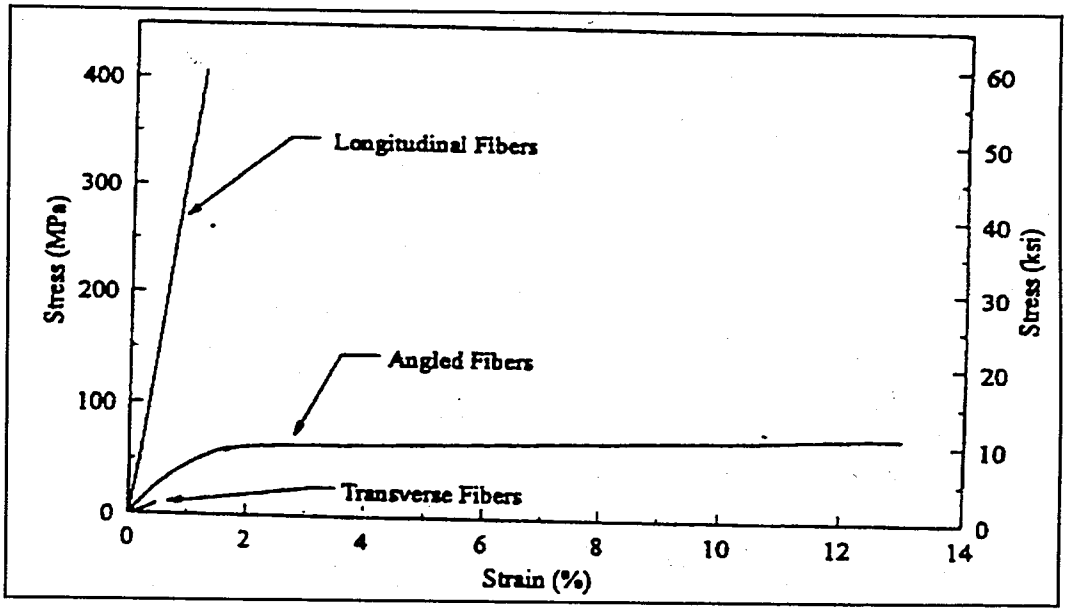

Figure 2.2. Stress-strain diagrams of different fiber orientations [12]

2.2.2. Carbon Fiber Strand

Carbon fiber strand has been composed of 12000 high performance carbon fiber filaments. They have had the superior mechanical and chemical characteristic and flexibility. Carbon fiber strand has been used to retrofit columns and beams by a winding around them. Figure 2.3 has depicted a view of carbon fiber strand and Figure 2.4 has shown how to be applied carbon fiber strand [11].

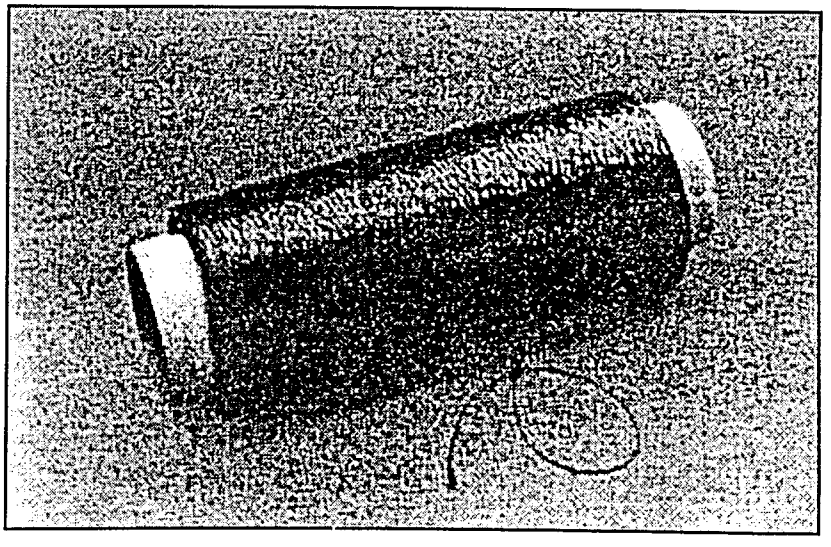

Figure 2.3. Carbon fiber strand [11]

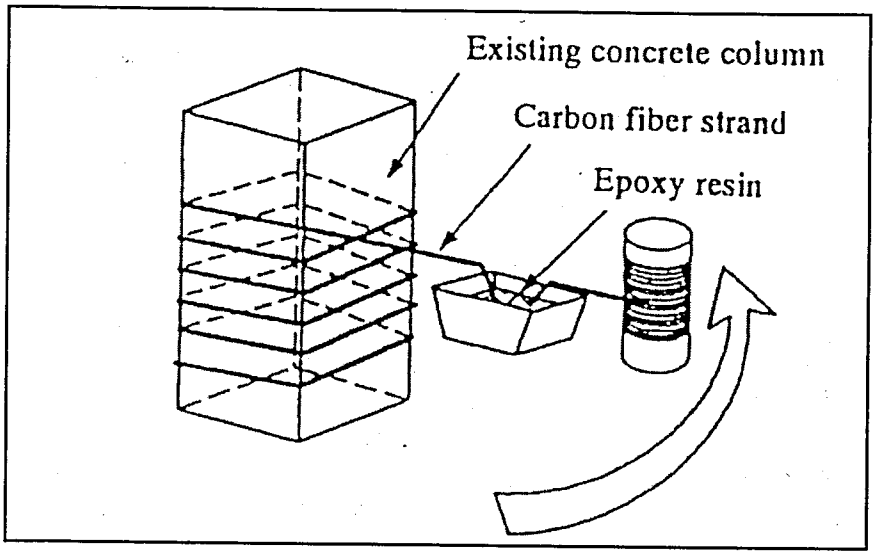

Figure 2.4. Winding of column with carbon fiber strand [11]

2.2.3. Carbon Fiber Plastic Sheets and Plates

Fiber composites have been made of thin fibers bonded together with a resin matrix. Fibers can be oriented in any direction to enhance the strength and stiffness of the composite in the desired direction. The structural qualities of the product have depended primarily on the type and amount of fibers used in the direction of measurement [13].

Continuous fiber sheets (CFRP sheets) have been made of parallel filaments attached to a flexible backing tape for handling. Fabrics have been made of filaments stitched into a geometric form. The filaments can run uni-directionally like the continuous fiber sheets, or can be woven at different angles into a fabric. Because there has not been any adhesion between individual fibers, a polymer or resin matrix has been utilized to transmit forces between fibers [12].

2.3. Adhesives

Recently, there has been a rapid development of adhesive bonding to be parallel the development of science and technology as an economical and effective method for the fabrication of various components and assemblies. According to 1980 Book of Standards, an adhesive is a substance capable of holding materials together by surface attachment.

Kinloch defines the adhesive as a material which when applied to substrate surfaces can join them together and resist separation [14].

The use of adhesives may offer various advantages in comparison with conventional techniques such as welding, riveting etc.

Some of the advantages can be summarized as follows:

- It has the ability to join efficiently thin sheets or different materials,
- It makes an increase in design flexibility,
- It supplies an improved stress distribution in the joint which leads to an increase in fatigue resistance of the bonded components,
- It is a convenient and cost effective technique [14].

There have been many kind of adhesives such as PVA, PVC, polyamides, amino-plastics, epoxies etc. These varieties have supplied us to select the material which has more proper properties. Epoxy adhesives have had two components namely basic resin or just resin and hardener or accelerator. These materials have been mixed in a definite range of temperatures and different volume or weight so as to produce epoxy adhesives.

Epoxy resins have been from thermosetting resins [15]. The physical properties of a cured epoxy resin have depended upon many factors such as type and amount of curing agent, cure history, type of filler, type of reinforcement etc [14].

The basic characteristics of epoxy resins can be listed in the following:

- Outstanding adhesive qualities to such materials as concrete and steel,
- Resistance to a wide range of chemicals,
- Rather vulnerable to organic solvents,
- Low shrinkage when the compound has cured and changed form the liquid to the solid state,
- High coefficient of thermal movement compared with concrete,

- High compressive, tensile and flexural strength,
- Appreciable loss of strength at temperatures over about 80 ^{0}C,
- High rate of gain of strength,
- Rather poor resistance to fire compared with concrete and clay bricks [16].

Since there exists many advantages, the use of epoxy adhesives have been increasing widely in construction such as externally bonding CFRP plates and sheets to a concrete surface. Strength increase of epoxy adhesives used can be clearly seen in the following Figures 2.5, 2.6 and 2.7, obtained from SIKA, with respect to time.

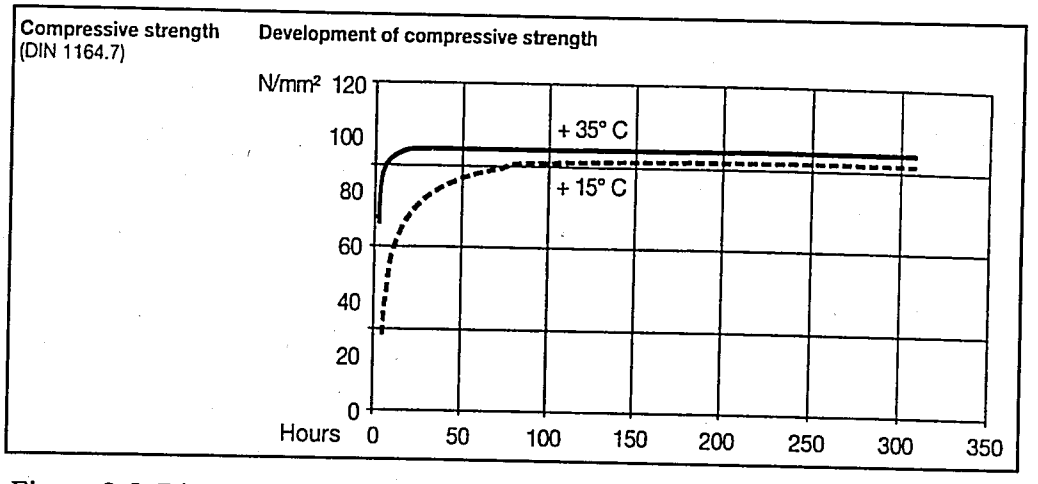

Figure 2.5. Diagrams of compressive strength versus time of the adhesive used

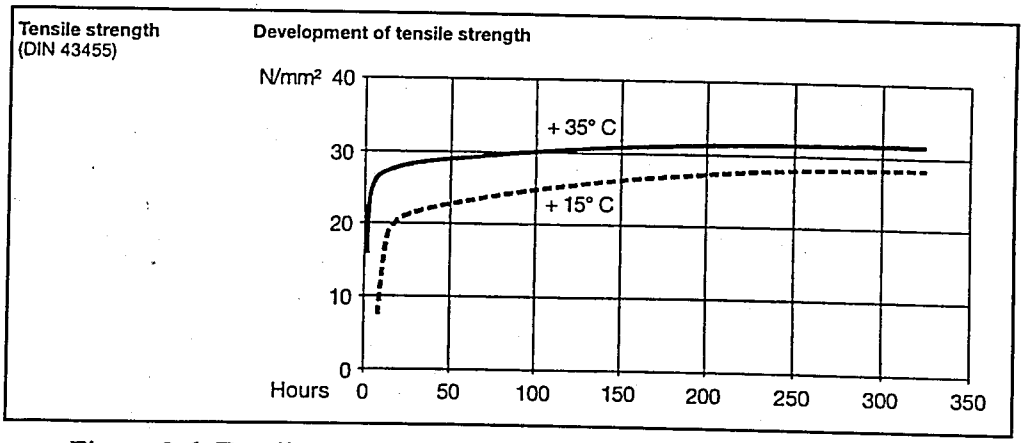

Figure 2.6. Tensile strength with respect to time of the adhesive used

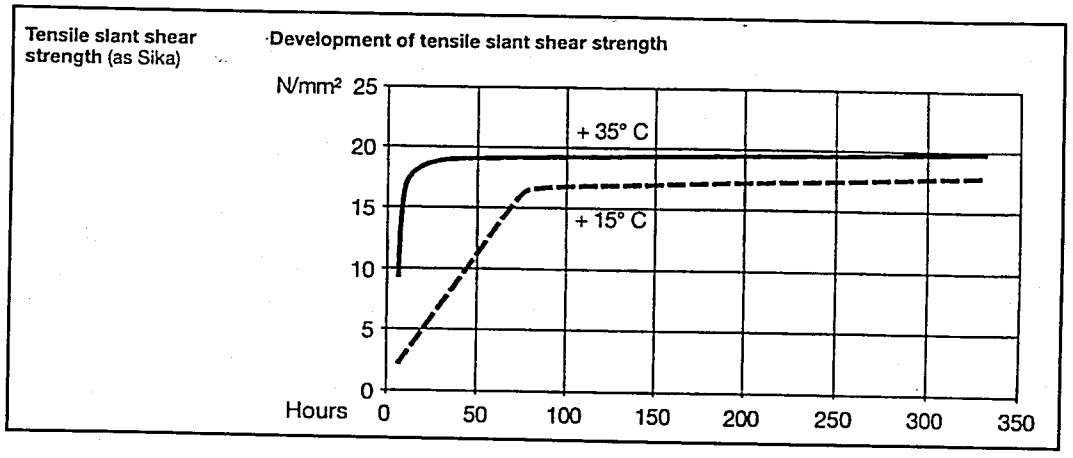

Figure 2.7. Tensile slant shear strength with respect to time of the adhesive used

2.4. Factors Affecting Durability of Strengthening System

Durability of the retrofitting system can be affected by many parameters some of which have been presented as follows.

2.4.1. Temperature

During an application of CFRP sheets and plates, temperatures should satisfy some requirements. Otherwise, the application couldn't be started. In order to start strengthening work dew point should be lower than the substrate temperature. Dewpoint obtained from dewpoint table is a function of ambient temperature of the air and relative air humidity. If temperature requirements are not satisfied, temperature of the air can be increased by heating or the relative air humidity can be decreased by using fans. Besides, minimum ambient temperature of the air and substrate temperature should satisfy some conditions. For example, according to SIKA for Sikadur-330 application temperature should be in the range of +15 ^{0}C to +35 ^{0}C (for substrate and ambient temperature).

Almost all materials can have loss of strength while temperature increases under service loads. That's why, strengthening of the system with CFRP plates or sheets also should be protect against sudden loss of strength such as resulting from fire. According to the study of Koga and Ohtsu [11], carbon fiber has had a high resistant ability against the high temperature but epoxy resin has not resisted against high temperature.

2.4.2. Surface Preparation

Surface preparation is very important. The surface of concrete should be roughened by using different techniques such as grinding using grinding wheel, sandblasting etc. All loose particles and other laitance can be removed with a vacuum cleaner. If CFRP sheets will be used, the sharp corner should be rounded prior to application. In addition, the concrete surface should be dry and age should be minimum at the age of 3~6 weeks. The CFRP plates should be cleaned with a solvent such as colma cleaner produced by SIKA.

2.5. Factors Affecting The Load-Carrying Capacity

2.5.1. Adhesive Type

Adhesives have different mechanical and physical properties. Thus, they should be selected in accordance with the work done. They have transferred forces from beam to the CFRP materials. Therefore, they have played an important role over failure mode and load-carrying capacity.

In the study of Hamoush and Ahmad [6], has been shown that an increase of adhesive thickness has resulted in a decrease in the strain energy release rate. Thus, it should be taken into account that adhesive thickness should be homogenous and not be greater than approximately 2~3 mm. Many researchers [2,17] have fixed adhesive thickness in order to prevent adverse effect of adhesive thickness on test results within this range.

2.5.2. Effect of Anchorage

In the application, different types of anchorage can be met. L shaped carbodur laminates, CFRP sheets or fabrics, steel bolts and steel U-strips have been some of the anchorage types seen in practice. The most important issue is to determine anchorage type and to design them carefully. Many researchers have investigated the effectiveness of the anchorage.

The behaviour of composite RC beams with externally bonded CFRP with external anchorages has been investigated by Spadea *et al.*, [17]. In this study externally bonded steel anchorages were used. Additional anchorages along the span have reduced the slip between the plate and concrete face of the beam. This control of slip has led to an extension of composite action up to as near failure as possible. The beams (A3.2, A3.3) with anchorage used in that study have carried about 70 per cent additional loads compared to the virgin specimen (A3). Due to these anchorages, it has been shown that concrete compressive strains and CFRP plate strains have increased with respect to the beam of A3.1 which has been without anchorage. The study has also shown that it is possible to increase structural ductility of the composite beams with adequate anchorages [17].

In the study of Sharif *et al.*, [7], strengthening of initially loaded RC beams using FRP plates has been investigated and different anchorage types have been used in the study. It has been reported that steel anchorage bolts have eliminated plate separation at the curtailment zone but the failure has become due to the formation of diagonal tension cracks shown in Figure 2.8. I-jacket GFRP plates have provided the best anchorage system in the study so as to eliminate plate separation and diagonal tension failure and to develop flexural strength of the repaired beams depicted in Figures 2.9 and 2.10 [7].

Mechanical behaviour of RC beams strengthened or repaired by CFRP sheets bonding has been examined by David [18].

The techniques shown in Figure 2.11 has been used and explained as follows:

- Using of steel bolts at the ends of the CFRP sheets,
- Bonding of lateral vertical or inclined sheets,
- Wrapping of shear spans.

It has been reported that the second and the third applications have had very good results in comparison with the first one in order to enhance the load-carrying capacity. As seen from Figure 2.12 and Figure 2.13 ultimate load for beam 10 has reached 168 kN for beam 11 has reached 176 kN and for beam 12 has become 183 kN [18].

In the study of Spadea *et al.*, [19], external anchorages have been examined as one of the variables. It has been also reported that the strengthened beams with the various external anchorage systems have carried higher loads than those of beams without external anchorages and their failure modes have been characterized by greater ductility, slow de-bonding and slippage of the CFRP plates [19]. Location of anchorages used in the study for A3 series have been shown in Figure 2.14.

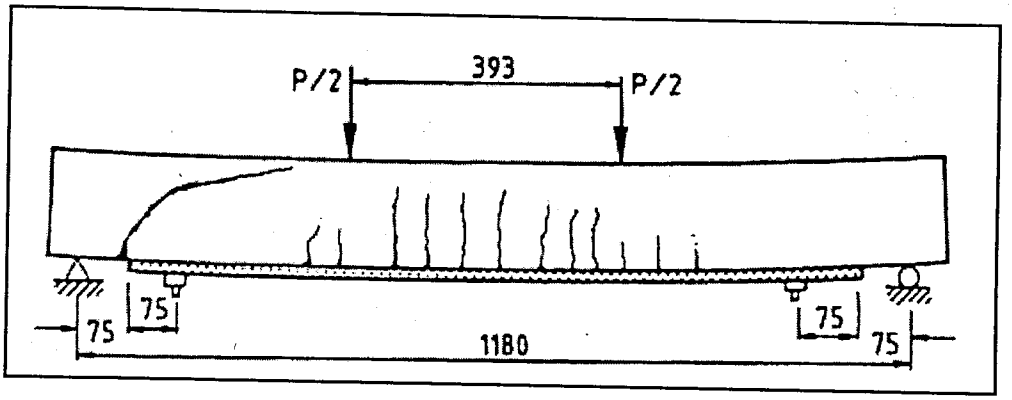

Figure 2.8. Formation of diagonal tension cracks with steel anchorage bolts [7]

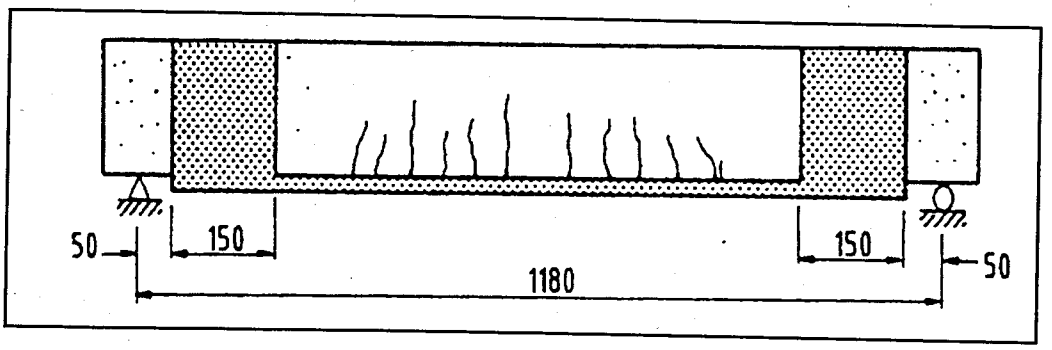

Figure 2.9. I-jacket GFRP plates side view [7]

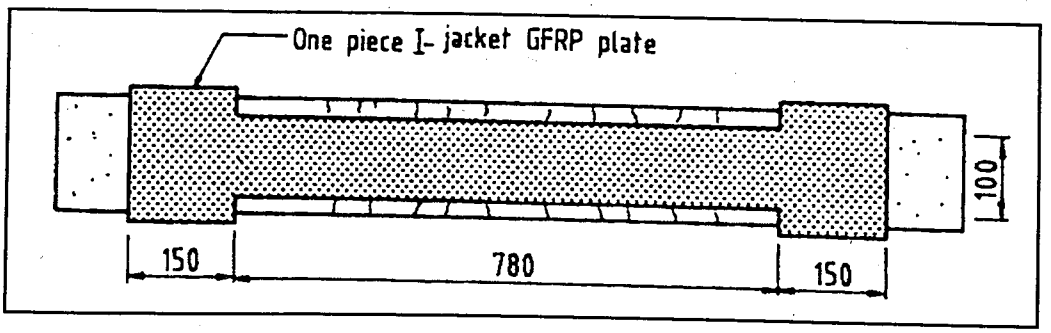

Figure 2.10. I-jacket GFRP plates bottom view [7]

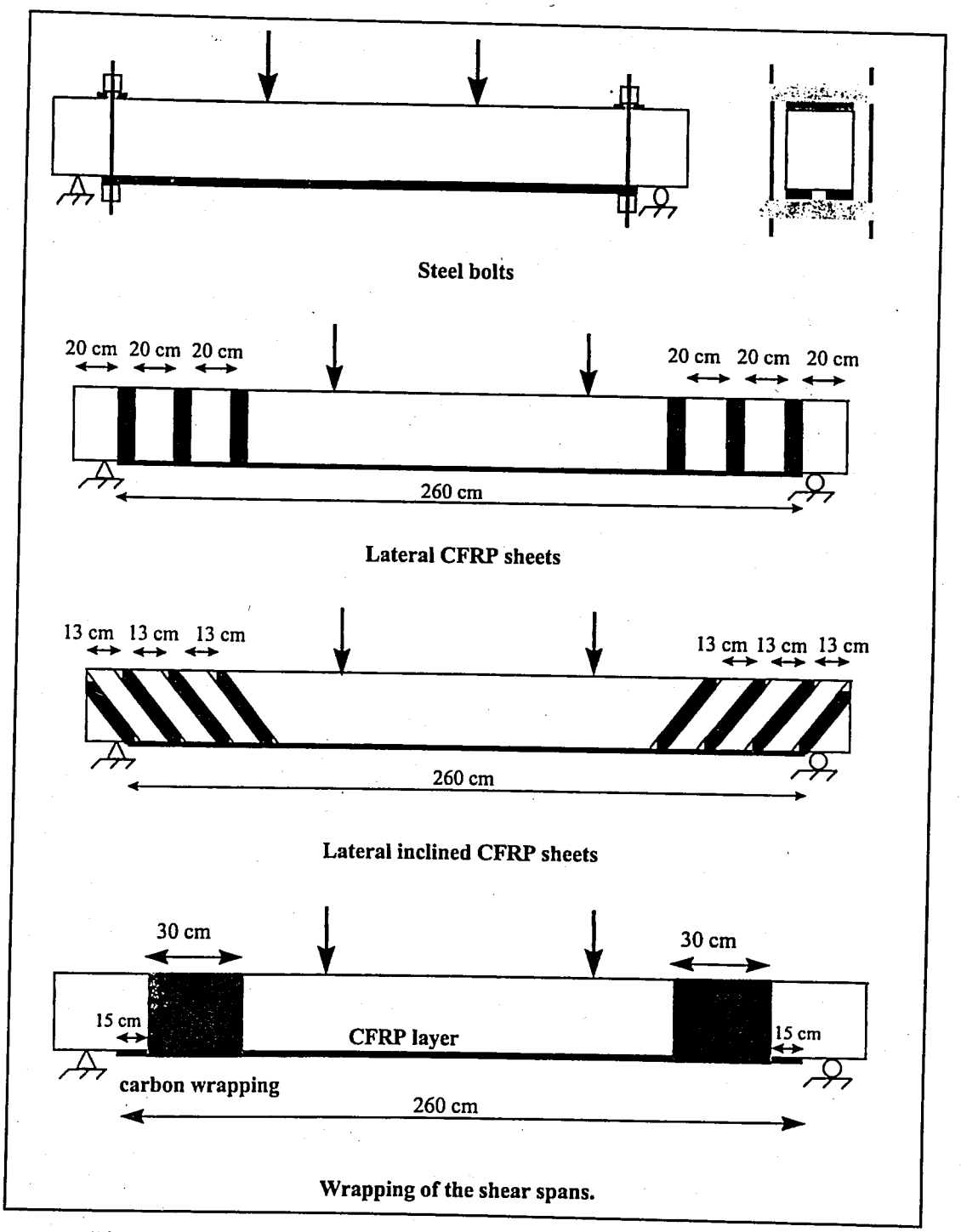

Figure 2.11. Strengthening of beams by using different methods [18]

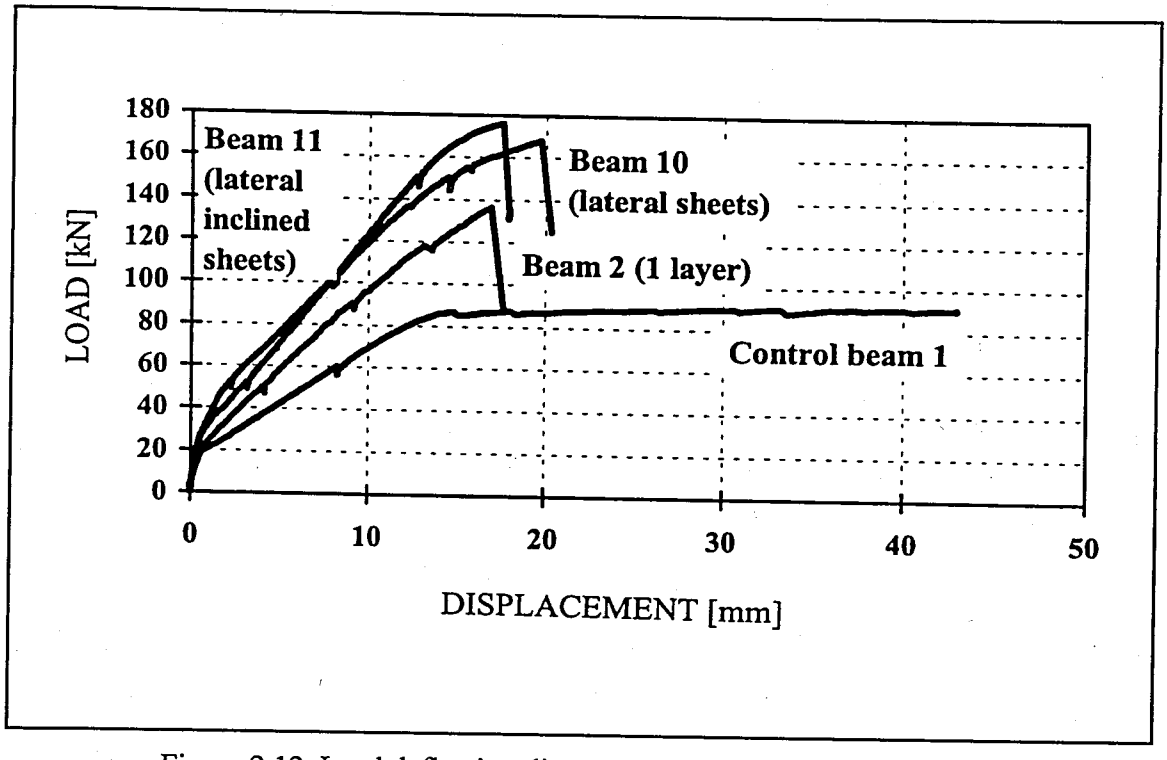

Figure 2.12. Load deflection diagram of the beams 10 and 11 [18]

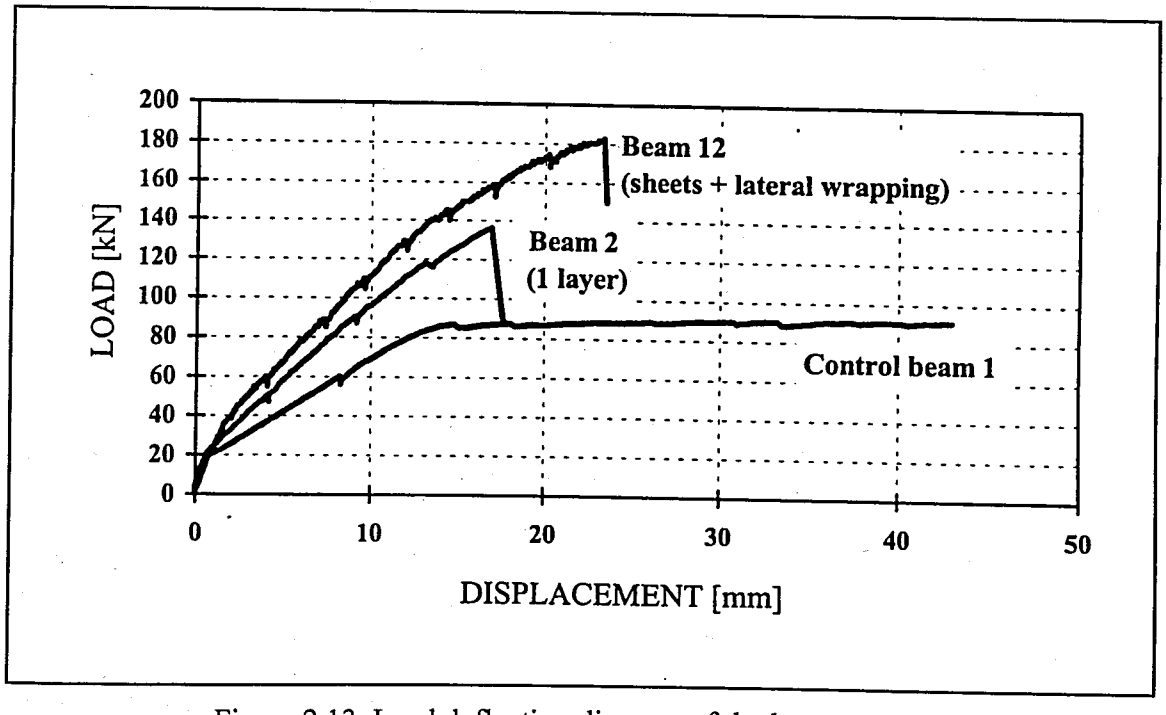

Figure 2.13. Load deflection diagram of the beam 12 [18]

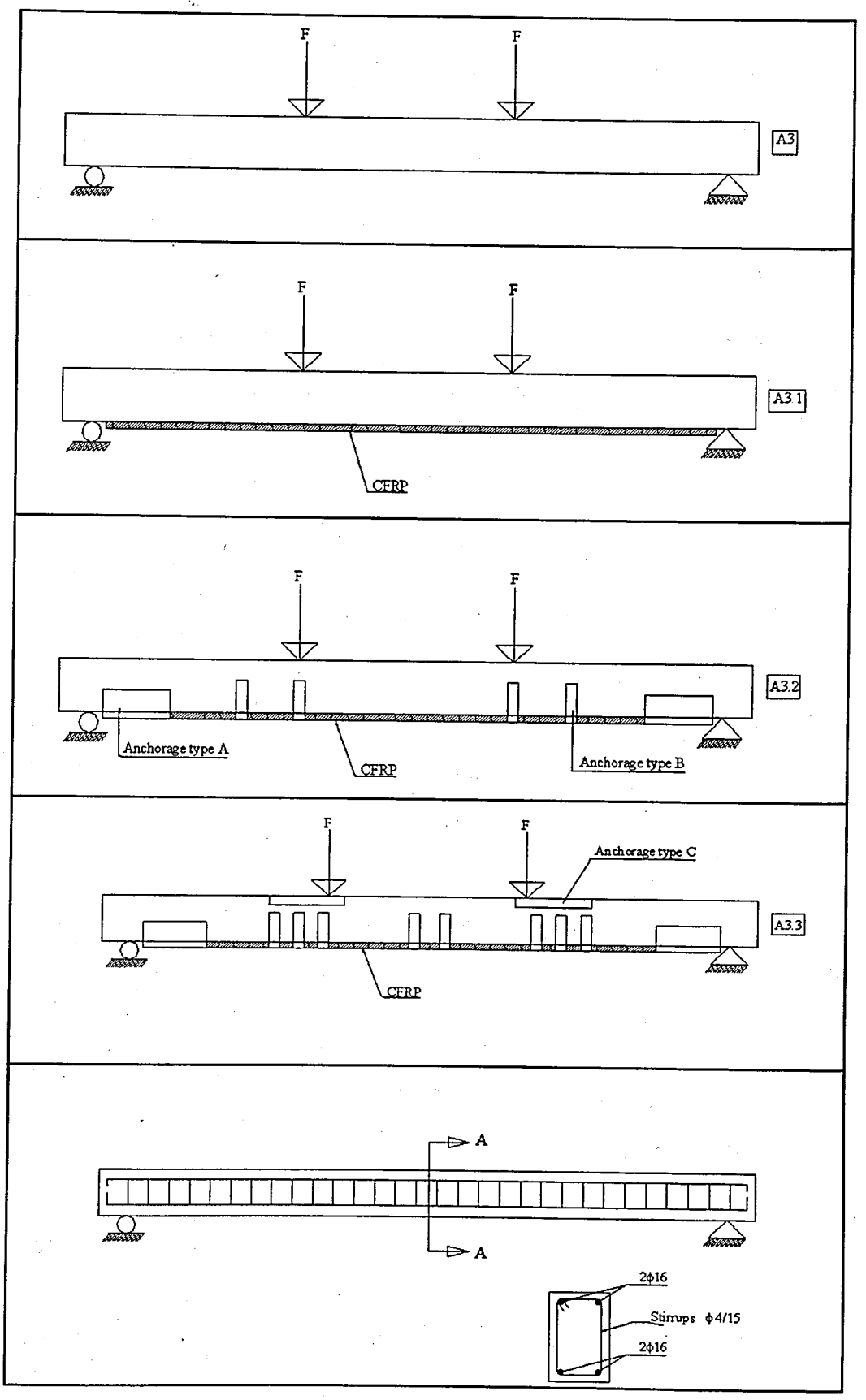

Figure 2.14. Illustrating of different anchorage types [19]

2.5.3. Effect of Fiber Orientation

Fiber orientation of CFRP sheets has resulted in changing of load-carrying capacity of the beams and changing of failure modes. That's why, fiber orientation should be determined in order to increase the effect of FRP in the desired direction.

In the research of Norris *et al.*, [12], the effect of fiber orientation on the behaviour of composite beams has been examined. For this purpose, three types of fiber orientation have been employed namely, 0^0 90^0 and $\pm 45^0$ with respect to the beam axis. Beam 1A has had the fibers oriented longitudinally on both the tension flange and web. Ultimate strength of this beam has been about 138 kN and failure type has been due to peeling of the CFRP laminate from the concrete. Beam 1B has been bonded as [0^0/ 90^0] cross ply layup. Ultimate strength of this beam has been less than that of beam 1A but the failure has been less explosively than beam 1A. Beam 1C has had the fibers applied $\pm 45^0$ to the axis of the beam. Ultimate strength of this beam has been less than that of beam1B but the overall behaviour of this beam was more ductile than the first two beams [12].

Thus, this study has shown that when the CFRP fibers have been placed perpendicular to the cracks in the beam, a great increase in stiffness and strength and a brittle failure have been noticed. When CFRP fibers have been placed obliquely to the cracks in the beam, a smaller increase in stiffness and strength have been noticed but the mode of failure has been more ductile due to the off-axis application of CFRP [12].

2.5.4. Effect of Plate Thickness and FRP Ratio

Increase of plate thickness and FRP ratio has probably led to an increase of load-carrying capacity but it has changed failure mechanisms. Many researchers have investigated the effect of these parameters. The findings have supported the increase of load-carrying capacity.

A series of tests on mechanical behaviour of RC beams strengthened with CFRP sheets has been fulfilled by David [18]. Different parameters, which of them have been plate thickness and plate ratio has been investigated. Four beams has been tested so as to

find the effect of these parameters on the behaviour namely, P2, P3, P4 and P5. P2 and P3 have had a single layer of two sikadur plates and the others named as P4 and P5 have had two layers of two sikadur plates. It has been reported that increase of thickness has resulted in enhancement of the ultimate loads and stiffness of the beams. Likewise, increase of plate ratio has led to an increase in ultimate load and stiffness. Increases in ultimate loads have been 51 per cent and 58 per cent for P2 and P3 with respect to P1. Increases in ultimate loads have been 73 per cent and 77 per cent for P4 and P5 over P1 respectively [18].

A research over initially loaded RC beams using FRP plates has been performed by Sharif *et al.*, [7]. Three different plate thickness that have been 1 mm for P1, 2 mm for P2 and 3 mm for P3 have been used. While plate thickness has increased, loads at yield have also increased but ductility index has decreased. Besides, failure mechanisms have changed. While the failure mode has been due rupture of plate for P1 beam, the other beams have failed by virtue of plate separation accompanied by local shear failure in the concrete along the longitudinal tension steel re-bars [7].

The effect of FRP ratio has been also investigated by Triantafillou and Plevris, [20]. Load-deflection curves obtained from the experiments have been shown in Figure 2.15 [20]. Test specimens used in this study has been a clear span of 1220 mm with equal point loads which have been applied symmetrically at a distance of 305 mm on either side of the midspan [20]. It can be easily seen that increase in FRP ratio has enhanced the ultimate load capacity and the stiffness. However, while FRP ratio increases, failure mechanism has converted form FRP rupture to de-bonding.

2.5.5. Reinforcement Ratio

Strengthening of RC beams with FRP plates has been more effective for low reinforcement ratios.

The effect of reinforcement ratio has been studied by Ross *et al.*, [21]. Six different reinforcement ratios have been used namely, 1-6. It has been shown that while reinforcement ratio has increased, ultimate loads of beams have increased but contribution

of FRP has decreased. Figure 2.16 and Figure 2.17 have shown load-displacement curves of lightly reinforced beams and heavily reinforced beams [21].

These figures have depicted that the increase rate in ultimate loads for low reinforcement ratio have been greater than that of high reinforcement ratio. Because the ratio of A_s /A_{frp} has been higher for the lightly reinforced beams. Moreover, displacements of beams which have had low reinforcement ratio have been greater.

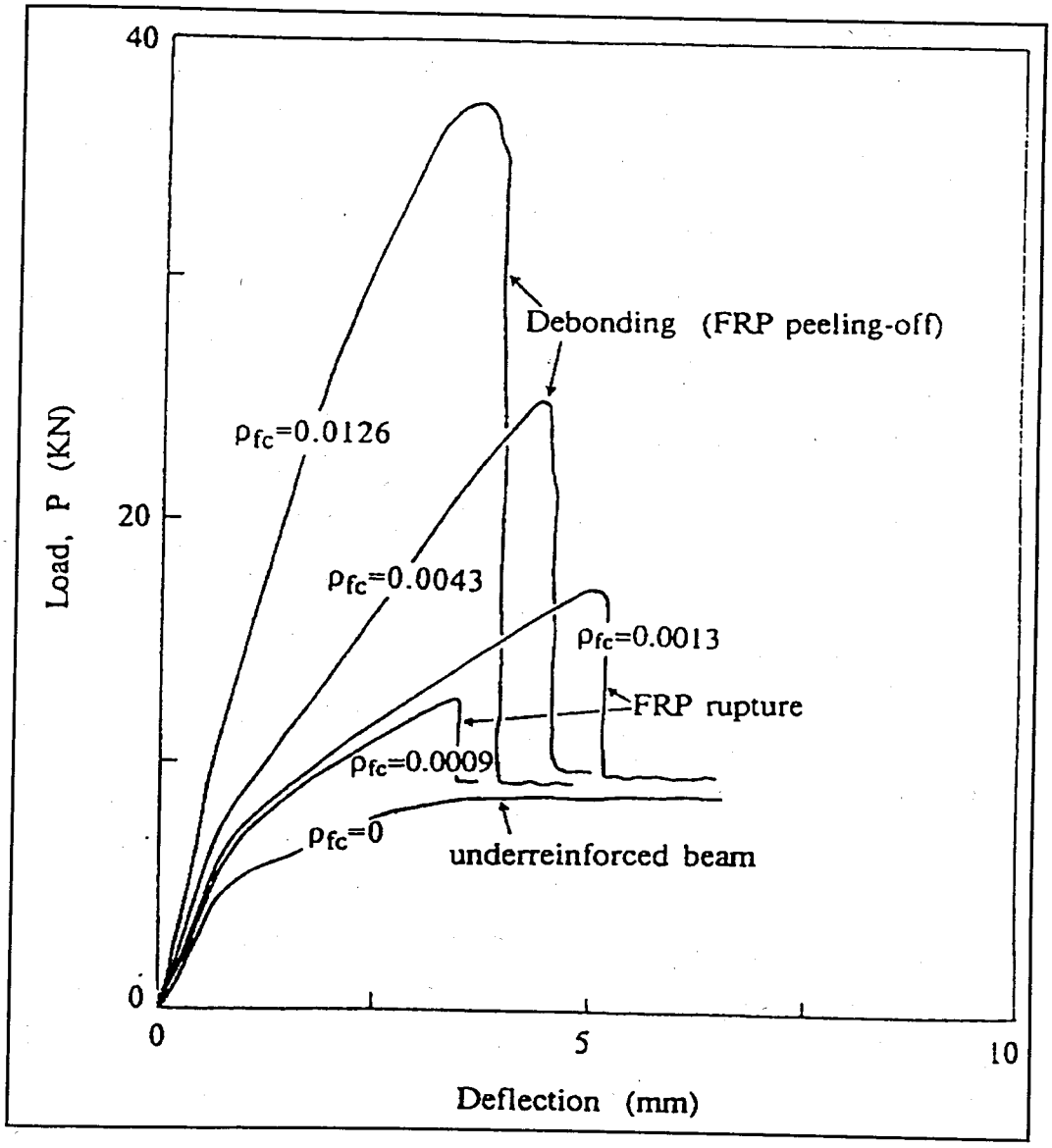

Figure 2.15. The effect of FRP ratio over load-carrying capacity [20]

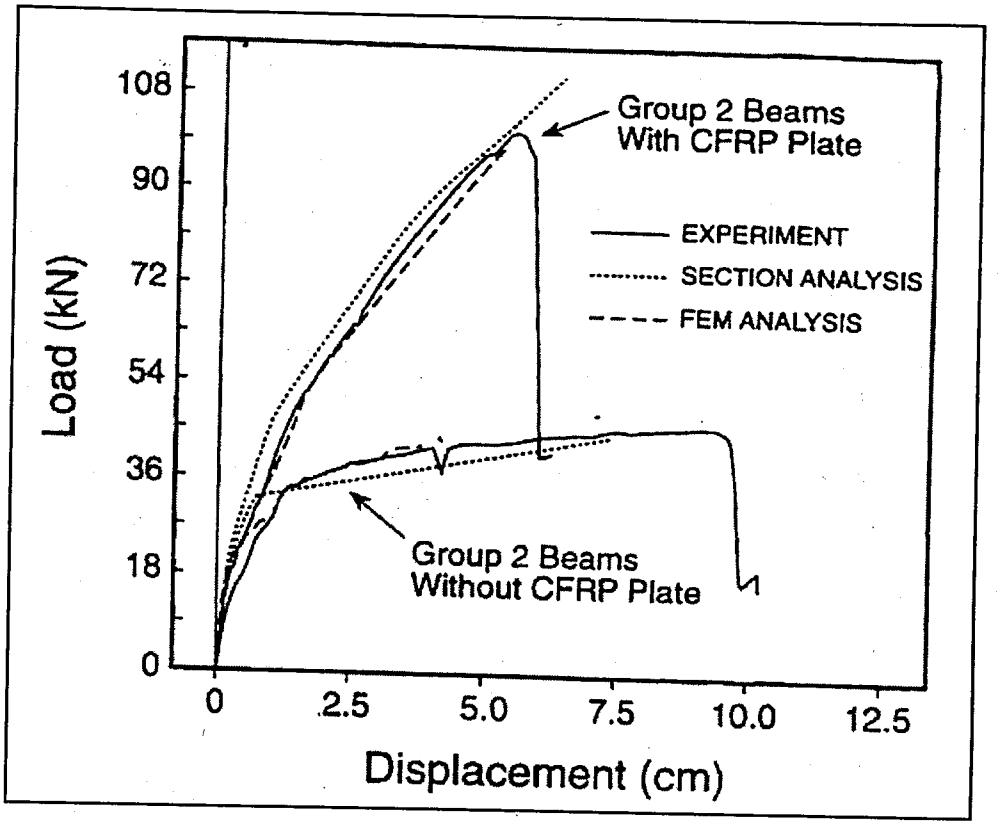

Figure 2.16. Load-deflection curves of lightly reinforced beams [21]

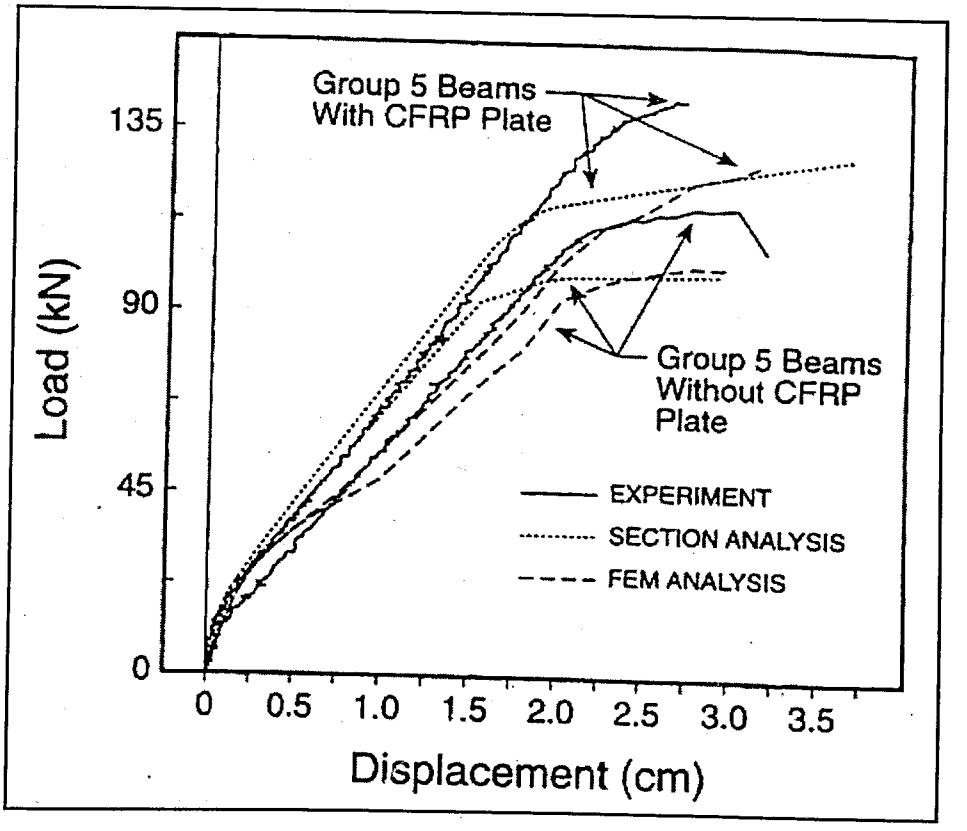

Figure 2.17. Load-deflection curves of heavily reinforced beams [21]

2.5.6. Concrete Compressive Strength

Increase in concrete compressive strength has resulted in an increase at capacity because section has had an addition moment couple. This phenomenon can be seen more clearly by added plate.

A parametric study has been carried out by An *et al.*, [22] so as to investigate the effects of design variables on the mechanical behaviour of beams which of them has been concrete compressive strength. Two types of concrete compressive strength 20.6 MPa and 41.4 MPa have been used. It has been seen that increasing of the compressive strength with the addition of the composite plate has raised the ultimate moment and ultimate load [22].

2.6. Design Assumptions

While the necessary formulations have been maintained, some simplifications done would be necessary so as to facilitate the calculations.

Assumptions done have been as follows:

- Plane sections before bending have remained plane after bending,
- Tensile resistance of the adhesive and concrete have been neglected,
- Perfect bond between FRP plates and concrete has been assumed,
- Linear strain distribution in the cross section until failure has been assumed.

2.7. Types of Failure Modes

Investigations of failure modes and failure mechanisms have been taken into account by many researchers. Grace *et al.*, [23], Triantafillou and Plevris [20], Buyukozturk and Hearing [24], have been some of them. Actually, in order to be strengthened of concrete structures effectively, to understand the behaviour of concrete structures retrofitted and to determine what kind of strengthening is better, failure modes and failure mechanisms has needed investigations in advance.

Different failure modes have been presented on RC beams strengthened with FRP materials. These failure modes can be divided into two main categories namely, flexural failure and local failure. Local failure can be also separated into two parts which are shear failure and de-bonding.

Flexural failure has been defined as concrete crushing in compression or plate rupturing in tension. However, local failure has been described as the peeling of the FRP plate at the location of high interfacial stresses and shear failure of the concrete layer between the plate and the longitudinal reinforcement [1].

Flexural failure can be separated into three components [25]:

- Steel yields and FRP ruptures (FRP rupture),
- Yielding of the reinforcing steel in tension followed by concrete crushing (Tension failure),
- Crushing of concrete in compression zone before reinforcing steel yields in tension or FRP ruptures (Compression failure),

Shear failure of local failure can be analyzed as follows [25,20]:

- Diagonal tension failure resulting from shear in the section (Shear failure)[25,20],

The last failure mode namely, de-bonding, can be divided into two parts [25,20]:

- Shear/Tension failure of the concrete substrate, in other words, shear failure of the concrete layer between the FRP plate and longitudinal reinforcing steel re-bars (Anchorage failure),
- FRP peeling-off or de-bonding of adhesive bond line due to vertical section translation resulting from cracking (De-bonding failure) [25,20].

2.7.1. Tension Failure

According to this mode, which has been the most desirable, failure of the critical cross section has occurred by yielding of tensile steel re-bars followed by crushing of concrete, while FRP has been intact [26]. The tension failure mechanism have been more preferable, because it has had a ductile manner, the FRP rupture mode can have dominated if FRP cross sectional area has been less than the minimum FRP area, $A_{f\,min}$, for the cross section seen in Figure 2.18 [25].

When the FRP plate has been thick enough and the tension steel area fraction of the section has been small, this failure mechanism has occurred [20].

The following formulations have been valid for tension failure mechanism. The variables used have been shown in Figure 2.19.

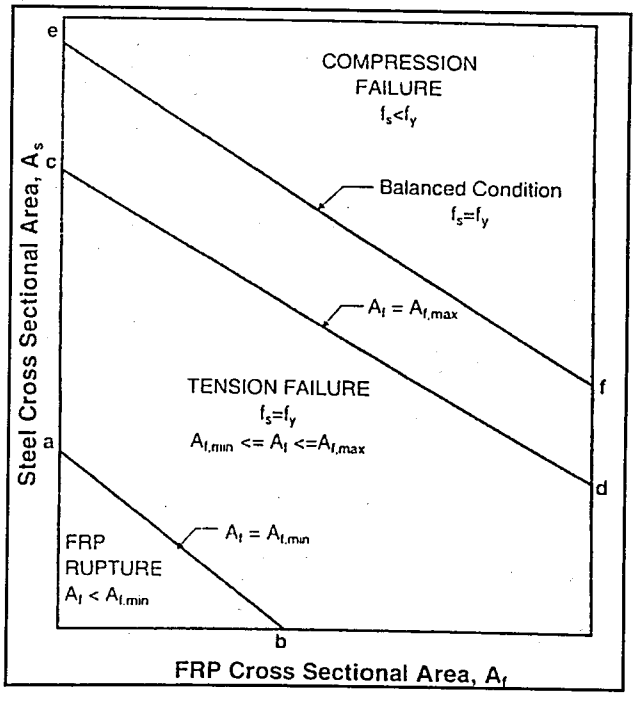

Figure 2.18. Classification of failure modes with respect to A_s and A_f [25]

$$\varepsilon_s' = \varepsilon_{cu} * \frac{(c-d')}{c} \tag{2.1}$$

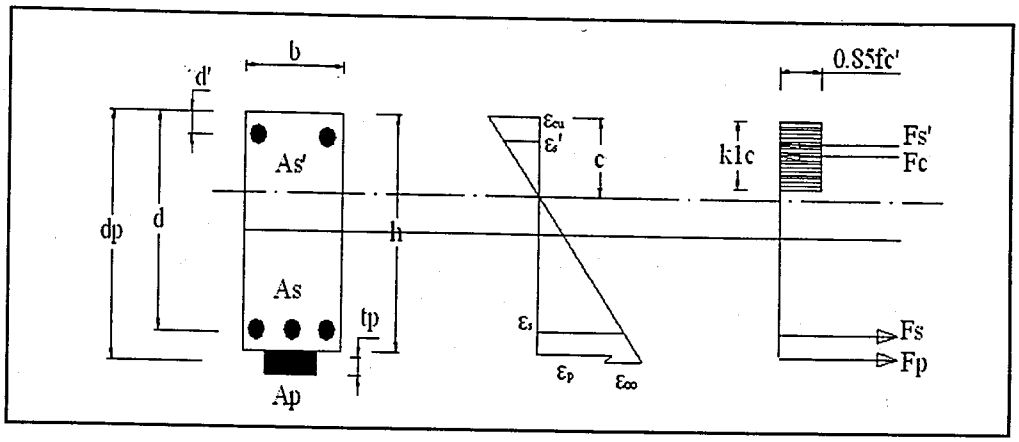

Figure 2.19. Variables of the section

$$\varepsilon_p = \varepsilon_{cu} * \frac{(d_p - c)}{c} - \varepsilon_{oo} \tag{2.2}$$

$$M_U = A_s * f_y * (d - \frac{k_1 * c}{2}) + A_p * E_p * \varepsilon_p * (d_p - \frac{k_1 * c}{2}) + A_s' * E_s * \varepsilon_s' * (\frac{k_1 * c}{2} - d') \tag{2.3}$$

In order to satisfy the above equations to be valid, the following assumptions should be checked [26]:

- Tensile steel has yielded.

$$\varepsilon_s \geq \frac{f_y}{E_s} \tag{2.4}$$

- Strain of FRP plate has been less than ultimate strain of the FRP plate.

$$\varepsilon_p \leq \varepsilon_{p,ult} \tag{2.5}$$

- For the above equations the assumption that compression steel reinforcement has not yielded has been accepted [26].

$$\varepsilon_s' \leq \frac{f_y}{E_s} = \varepsilon_y \tag{2.6}$$

2.7.2. FRP Rupture

When the flexural strength has been reached because of yielding of the tension steel reinforcement followed by rupture of the FRP laminate, FRP rupture failure mechanism has appeared. For this failure mode, tension steel and FRP area fractions have been quite small [20]. FRP rupture failure mechanism has been depicted in Figure 2.21 [24]. The forces have been shown in Figure 2.20.

For FRP rupture mode, strains and ultimate moment capacity have been summarized as the following. Ultimate moment has been obtained by summing the moments of all internal forces about the axis of the concrete compression force.

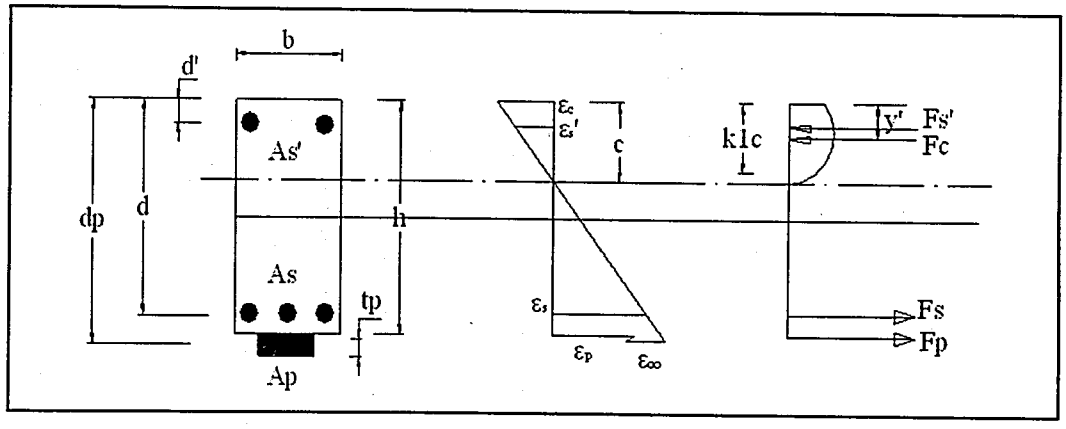

Figure 2.20. Variables and forces affecting the section

$$\varepsilon_s^{'} = \varepsilon_c * \frac{(c-d')}{c} \tag{2.7}$$

$$M_U = A_s * f_y * (d-y^{'}) + A_p * E_p * \varepsilon_{p,ult} * (d_p - y^{'}) + A_s^{'} * E_s * \varepsilon_s^{'} * (y^{'} - d^{'}) \tag{2.8}$$

Note that the above moment calculation has been valid for the assumption which the compression steel has not yielded. If compression steel has yielded, yield strength of the compression steel re-bars, (f_y), should be used in the moment formulation instead of (E_s*ε_s').

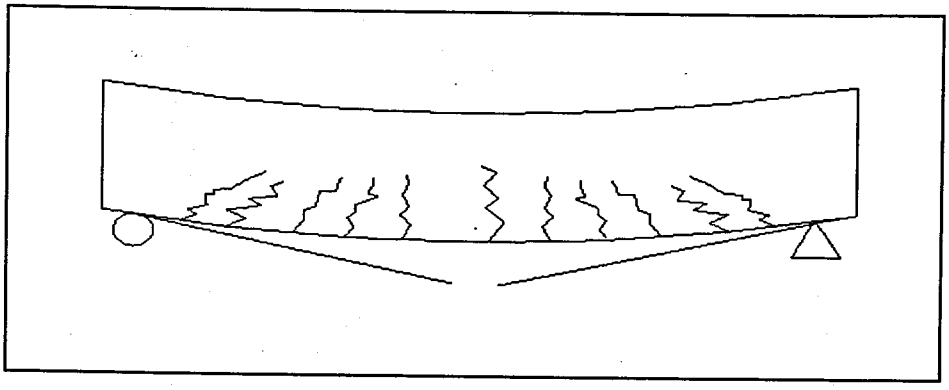

Figure 2.21. Failure mechanism of FRP rupture [24]

2.7.3. Compression Failure

In case of the tension steel area fraction and/or the FRP area fraction of the section have been quite high, the concrete would reach its maximum capacity before the tension steel has yielded and before the composite laminates have ruptured. For this type of failure the strain at the extreme compression fiber of the concrete has been 0.003 [20]. In order to avoid the compression failure mechanism, the cross sectional area of the FRP laminate should not exceed the maximum FRP cross sectional area, $A_{f\,max}$, for the section as shown in Figure 2.18 [25].

The schematic diagram of the compression failure mechanism has been shown in Figure 2.22 [24].

$$\varepsilon_s' = \varepsilon_{cu} * \frac{(c - d')}{c} \tag{2.9}$$

$$\varepsilon_s = \varepsilon_{cu} * \frac{(d - c)}{c} \leq \varepsilon_y = \frac{f_y}{E_s} \tag{2.10}$$

$$\varepsilon_p = \varepsilon_{cu} * \frac{(d_p - c)}{c} - \varepsilon_o \leq \varepsilon_{p,ult} \tag{2.11}$$

$$M_U = A_s * E_s * \varepsilon_s * (d - \frac{k_1 * c}{2}) + A_p * E_p * \varepsilon_p * (d_p - \frac{k_1 * c}{2}) + A_s' * E_s * \varepsilon_s' * (\frac{k_1 * c}{2} - d') \quad (2.12)$$

The above equation has been valid if compression steel has not yielded. Otherwise, yield strength of the compression steel re-bars, (f_y), should be used in the moment formulation instead of (E_s*ε_s').

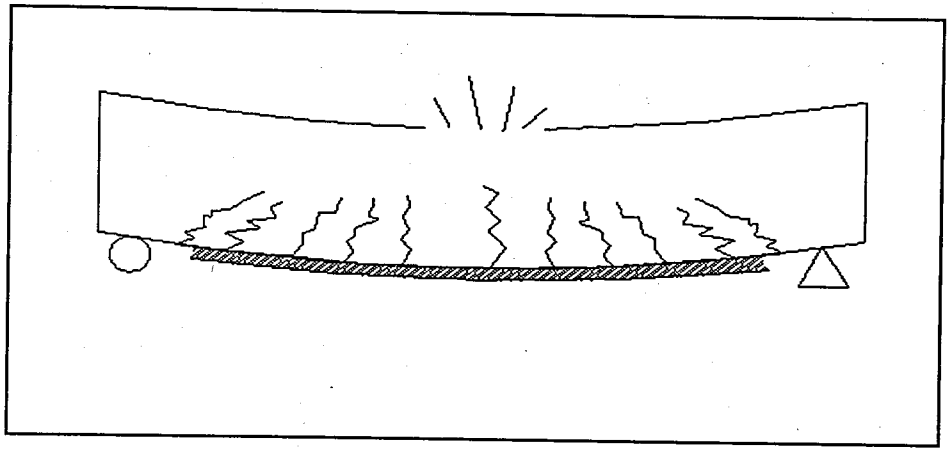

Figure 2.22. Compression failure mechanism [24]

2.7.4. Local Failures

The bond between the composite laminate and concrete surface may fail in a sudden manner as a result of the catastrophic propagation of a crack along the FRP-concrete interface [20].

Some possible reasons for the occurrence of such a crack have been reported as follows [20]:

- Imperfections in the spreading of the adhesive,
- Flexural cracking in the concrete leading to horizontal interface cracks developed from the bottom tip of the flexural cracks,
- Peeling-off of the composite laminate when the concrete tensile face has not been perfectly flat,

- Fatigue loads.

The interfacial shear and normal (peeling) stresses in the concrete beam at the cut-off point may result in premature local failure in the concrete and separation of the plate. In other words, shear and normal stress concentrations at the cut-off point or around flexural cracks have been the main reason for local failures [4].

2.7.4.1. Shear Failures. Shear failures of strengthening sections have occurred when the shear capacity of the section have been exceeded prior to the load level reaching the flexural strength [24].

The main characteristic of this failure mode has been cracking through the concrete layer just below the longitudinal reinforcement but in the rather remote case of RC structures without stirrups, such cracking can propagate in a diagonal form. A schematic diagram of shear failure has been shown in Figure 2.23 [26].

Shear capacity of FRP-strengthened beams, V_{up}, based on conventional reinforced concrete shear theory has been presented as follows in the research of Ziraba *et al.*, [27], in accordance with ACI 318-95 [28]. This method has not considered new shear-reinforcement retrofit techniques such as wrapping of FRP fabric or strip [24].

$$V_{up} = (V_c + k * V_s) \tag{2.13}$$

$$V_c = \frac{1}{6} * \left[\sqrt{f_c'} + 100 * \rho_s\right] * b * d \tag{2.14}$$

$$V_s = \frac{A_w * f_{wy} * d}{s} \tag{2.15}$$

$$k = 2.4 * e^{(-0.08 * C_{R1} * C_{R2} * 10^6)} \tag{2.16}$$

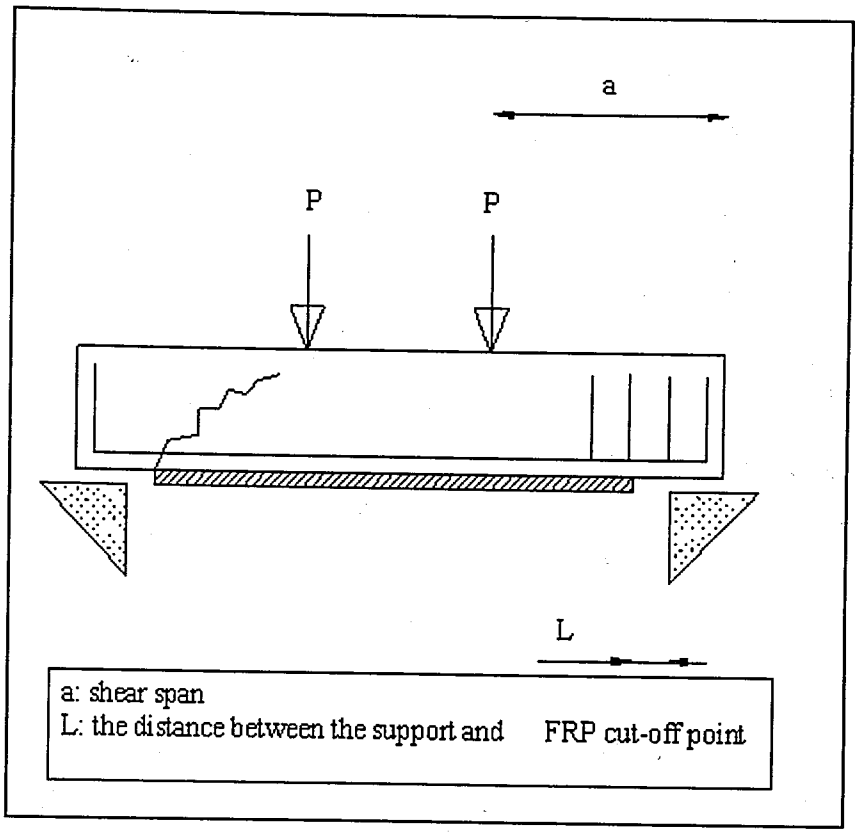

Figure 2.23. Shear failure mechanism [26]

2.7.4.2. Anchorage Failures. Shear-tension failure in the concrete initiating at the FRP plate end may have resulted in the beam shear failure or de-bonding of a concrete layer at the flexural reinforcement. These complex failure mechanisms have been investigated by many researchers such as Kaiser and Arduini *et al.*, [24].

Anchorage failure mechanism has been quite common, and has been occurred due to excessive shear stresses at the concrete-FRP interface near the ends. Anchoring the FRP ends by wrapping with sheets or strips onto the concrete may prevent this type of failure [26]. Schematic diagram of the anchorage failure has been illustrated in Figure 2.24 [24].

The shear and normal stresses at the plate curtailment zone have been obtained as follows [7, 27]:

$$\tau = \left\{ V + \left[\frac{k_s}{E_p * b_p * t_p} \right]^{\frac{1}{2}} * M \right\} * \frac{b_p * t_p}{I * b_p} * (d_p - c) = V * C_{R1} \qquad (2.17)$$

$$\sigma = \tau * t_p * \left[\frac{k_n}{4 * E_p * I_p} \right]^{\frac{1}{4}} = \tau * C_{R2} \qquad (2.18)$$

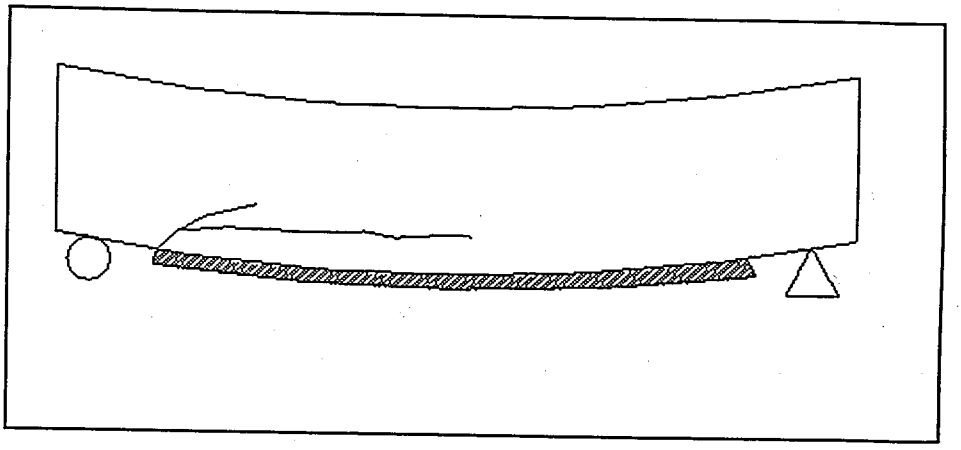

Figure 2.24. Anchorage failure mechanism [24]

2.7.4.3. FRP Peeling-off Failures. Peeling of the FRP from the concrete may have initiated from the ends of the plate or from existing cracks in the concrete [24]. Besides, roughness of the concrete surface may have led to localized de-bonding which may have caused the peeling-off. Figure 2.25, Figure 2.26, and Figure 2.27 have shown schematic diagrams of this failure mode [26].

Shear cracks in concrete beams have been associated with both horizontal and vertical openings, mainly because of the dowel action and aggregate interlock mechanisms as depicted in Figure 2.28. According to the assumption that the dowel deformations in the tension steel and the FRP at the crack location have been mainly due to shear, peeling-off of the FRP would occur when the ratio (v/w) has reached $(v/w)_{cr}$. What's more, the shear force has been proportional to the external load, P. Thus, the de-bonding load has been found as a linear function of the total shear stiffness, (Σ GA) [20].

$$P = \lambda * \sum (G * A) \qquad (2.19)$$

In order to eliminate local failures, some cautions can be taken some of which are that:

- Special mechanical anchoring devices can be utilized,
- The voids on the concrete substrate can be filled up properly with special mortars [26].

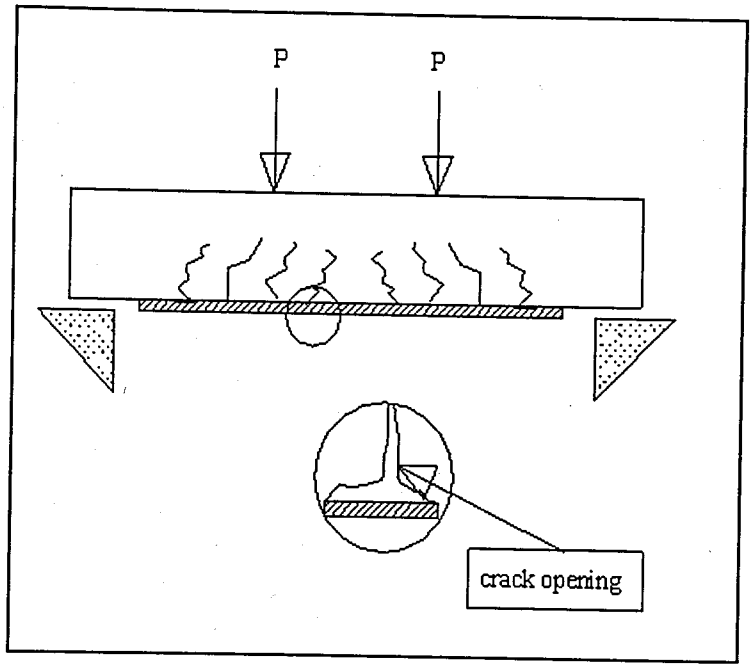

Figure 2.25. FRP peeling-off at flexural cracks [26]

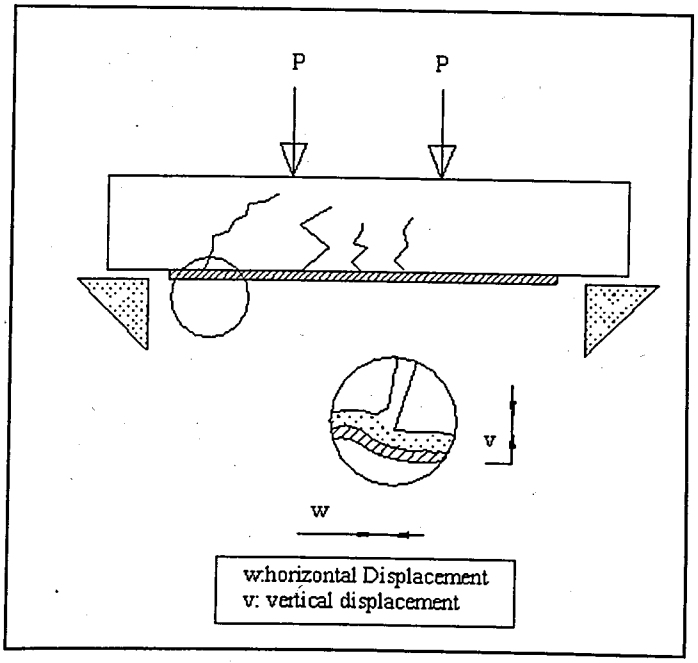

Figure 2.26. FRP peeling-off at diagonal cracks [26]

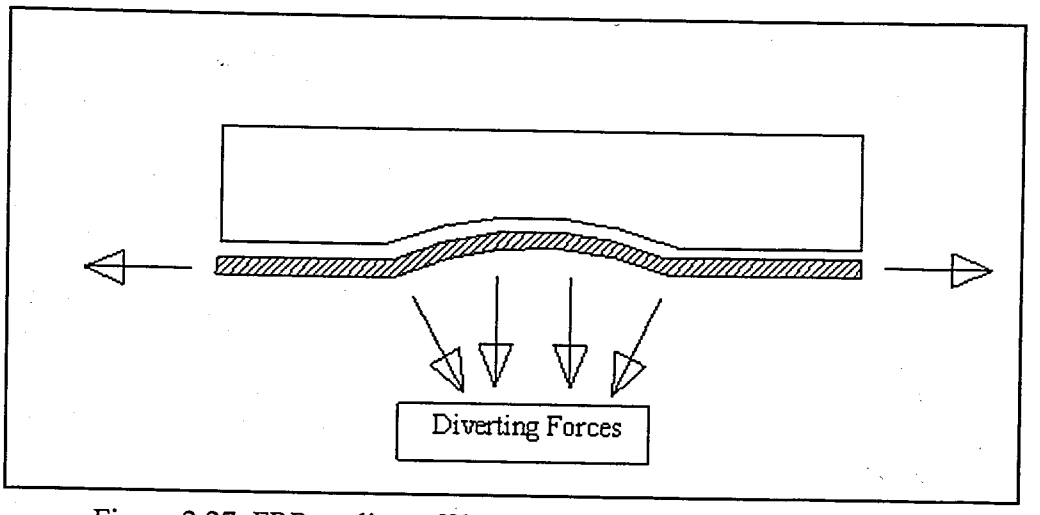

Figure 2.27. FRP peeling-off because of roughness of surface [26]

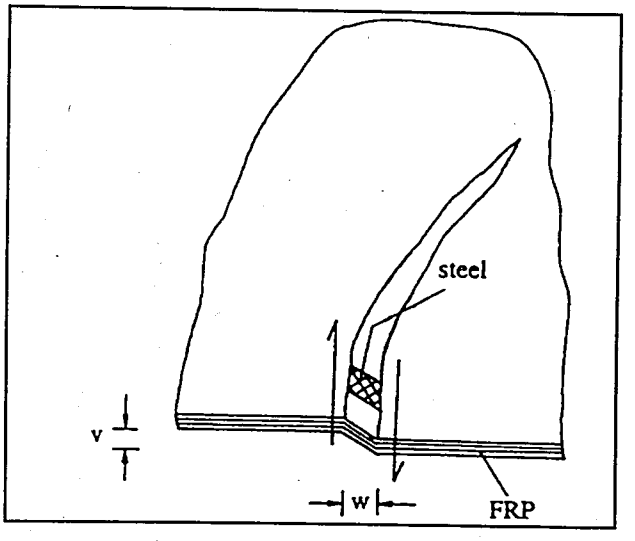

Figure 2.28. FRP peeling-off mechanism [20]

3. EXPERIMENTAL STUDY

3.1. Objectives and Scope

This study includes a variety of R.C. beams strengthened with externally bonded FRP Plates and their control beams. There are totally 11 beams eight of which are strengthened with FRP plates and the others are virgin specimens tested under four point loading up to failure. In order to eliminate the size effect on the behaviour of test beams, all beams have been chosen in the same size. Two main variables have been investigated. Those are the effect of reinforcement ratio on the behaviour of the beams and the effect of the CFRP ratio on the behaviour of the test specimens. What is more, it has been investigated the effect of plate end anchorage at both sides of the beams on the behaviour of R.C. beams. In order to investigate how those variables influence the behaviour of the beams, two types of FRP ratio and three types of Reinforcement Ratio have been employed. The effect of the variables on the behaviour has been examined by comparing different curves. Moreover, experimental moment-curvature diagrams have been compared with analytical moment-curvature diagrams by using proposed formulation by An *et al.*, [22].

3.2. Material Properties

3.2.1. Concrete

Concrete used in this study has been obtained from Nuh ready-mixed concrete. During the production of test specimens the nominal 150x300 mm test cylinders have been moulded. The mean compressive strength (f_c') of test specimens at 28-day was approximately 30 MPa. To determine compressive strength of concrete 20 cylinder samples were moulded by the size of 150x300 mm. Since it was ready-mixed, mixture proportions have been supplied from the manufacturer.

The special concrete mix had a maximum particle size of 10 mm. While the maximum particle size was chosen, it has been noticed that ready-mixed concrete must have passed the clear distance between the tension bars.

Concrete mix design values have been listed in Table 3.1.

3.2.2. Steel Re-bars

Two types of reinforcing steel bars have been used in the test specimens. Tension tests were carried out on a set of six deformed steel bar specimens so as to specify mechanical properties of the steel bars (Table 3.2). Three specimens were diameter of 8 mm and the others were diameter of 12 mm. In order to determine elongation at yield and elongation at rupture extensometer was used. Test set-up is shown in Figure A.1 and Figure A.2.

Table 3.1. Concrete mixture proportions

Aggregate (#10)	901 kg/m³
Sand (P)	535 kg/m³
Sand (S)	536 kg/m³
Cement (PC-42.5)	254 kg/m³
Water	105 kg/m³
Superplasticizer	3.80 kg/m³
W/C Ratio	0.42

Table 3.2. Mechanical properties of deformed steel bars

Type	ϕ12	ϕ8
Area	113.1 mm²	50.3 mm²
f_y	341.89 Mpa	530.52 MPa
f_r	489.25 MPa	782.51 MPa
ε_y	0.00155	0.00218
ε_r	0.29167	0.21417
E_s	220127 MPa	240110 MPa

3.2.3. Carbon Fiber Reinforced Plastic (CFRP) Plates

In all experiments, types of S512 laminates have been utilized, which of them have been obtained from SIKA. Besides, CFRP materials have been applied to all test specimens by an expert from SIKA.

A single layer of one CFRP laminate for four test beams and a single layer of two CFRP laminates the other four specimens have been bonded by epoxy adhesives two of which (R1P1W and R1P2W) have been wrapped with carbon fiber fabrics (SikaWrap 230C) at a distance of 100 mm to the cut off points of the laminates throughout 300 mm at the supports.

Material properties of S512 laminate and SikaWrap 230C obtained from SIKA have been listed in Table 3.3 and Table 3.4.

3.2.4. Epoxy Adhesives

Two types of adhesives, which were Sikadur 30 and Sikadur 330, have been employed throughout the applications. Both adhesives had two components.

Sikadur 30 has consisted of white resin and black hardener. When resin and hardener have been mixed, emerging light grey colour has indicated adequate mixing of them. Even though material properties of Sikadur 30 has been provided by SIKA, flexural tests on a set of three epoxy specimens have been carried out at Bogazici University Material Laboratory using "Ele Autotest 2000" flexural test machine (Figure A.3). Those specimens had the size of 40x40x160 mm. Average of the results of the flexural tests have been presented in Table 3.5.

Table 3.3. Material properties of CFRP laminates

Type	S512
Dimensions (w x t)	50x1.2 mm
Density	1.5 g/cm^3
Modulus of Elasticity	165000 MPa
Tensile Strength	2800 MPa
Shelf Life	Unlimited

Sikadur 330 has also been composed of two components which were white resin and grey hardener. Mixture has had light colour.

Both Sikadur 30 and Sikadur 330 adhesives have been prepared carefully. Material properties of the epoxy adhesives have been listed in Table 3.5 and Table 3.6 respectively.

3.3. Test Specimens

Twelve rectangular underreinforced beams have been tested one of which was a pilot beam in order to determine the deficiencies of test set-up and test procedure. All beams were 200x205 mm in cross section and 2840 mm long. The effective depth of the beams was 181 mm. Each beam was a clear span of 2600 mm.

The beams were divided into three different groups as compared to reinforcement ratios and CFRP ratios. Three different deformed steel bar ratios and two different CFRP

Table 3.4. Matarial properties of carbon fiber fabrics

Type	SikaWrap 230C
Areal Weight	225 g/m²
Design Thickness	0.13 mm
Tensile Strength of Fibers	3500 MPa
Modulus of Elasticity	230000 MPa
Fabric Witdh	610 mm
Shelf Life	Unlimited

Table 3.5. Material properties of Sikadur 30

Mix Ratio (by weight and volume)	A:B = 3:1
Density	1.77 kg/l (A+B)
Static Young Modulus	12800 MPa
Pot life	40 minutes (at 35 °C)
Flexural Strength	53.87 MPa

Table 3.6. Material properties of Sikadur 330

Mix Ratio (by weight)	A:B = 4:1
Density	1.31 kg/l (A+B)
Flexural Young Modulus	3800 MPa (at 7 days, 23 °C)
Pot life	90 minutes (at 15 °C)

ratios have been employed. As each beam has been designated, variables to be used can be summarized in the following. R1, R2, R3 have represented reinforcement ratios of ρ_1=0.0094, ρ_2=0.0125, ρ_3=0.0156 respectively. P1 and P2 have stood for CFRP ratios of ρ_{P1}=0.0017, ρ_{P2}=0.0033 respectively. Finally W has stood for whether the beam had carbon fiber fabric at the end of the CFRP at a distance of 100 mm to the cut-off point of the plate on both supports. These variables have been indicated in Figure 3.1. Name and description of each beam has been summarized in Table 3.7.

The beams which were in three batch were reinforced with 3ϕ12, 4ϕ12, 5ϕ12, tension steel re-bars respectively each one of which was also reinforced with 2ϕ8 compression steel re-bars. All longitudinal reinforcing bars have been made with 90° end hooks in accordance with TS-500 [29]. The stirrups have been made with 135° end hooks. Since there was no shear the zone between the applied loads, no stirrups have been used at the zone between loads. The zone outside of the applied loads has been reinforced with vertical stirrups of 8 mm diameter at a spacing 90 mm center to center (Figure A.4).

At all beams a/d ratio was the same and chosen approximately 4.81, which was in the range of 3 ~ 7. Details of the reinforcements of the test beams have been depicted in Figure 3.2.

CFRP plates, which were used to improve the structural behaviour of the beams, have been 1.2x50 mm in cross section and 2500 mm long. CFRP strips were applied

support to support so as to neglect undesirable failure mode due to distance effect between supports and CFRP cut-off points.

CFRP strips have been bonded to the tension face of the beams by using epoxy adhesives provided by SIKA, Sikadur 30 and Sikadur 330 namely. Both materials have had two components; component A (resin) and component B (hardener). For both materials these components contained of different contents.

Sikadur 30 has been used to bond CFRP to the concrete surface and Sikadur 330 has been used to wrap carbon fiber fabric to the concrete substrate.

3.4. Test Set-up and Procedures

The first step of the study was to specify necessary values for deformed steel re-bars such as yield stress, modulus of elasticity, yield strain and elongation at rupture. After determining of necessary values for reinforcing steel bars design of the beams have been done.

3.4.1. Casting and Curing of Test Specimens

Since ready-mixed concrete was used, the concrete have ordered after timber and steel moulds have prepared (Figure A.5). Both test beams and 150x300 mm test cylinders have been cast at the same day. An internal vibrator has been used so as to get an optimum compaction. All moulds have been oiled in order to ease the stripping process. All specimens were cured for three days with wet sacks. Then, they were left air-cured at the laboratory. Test specimens and cylinder samples have been demoulded seven days later after casting of them. 150x300 mm three cylinder samples have been tested so as to specify 150x300 mm cylinder compressive strength of concrete specimens gained at seven days.

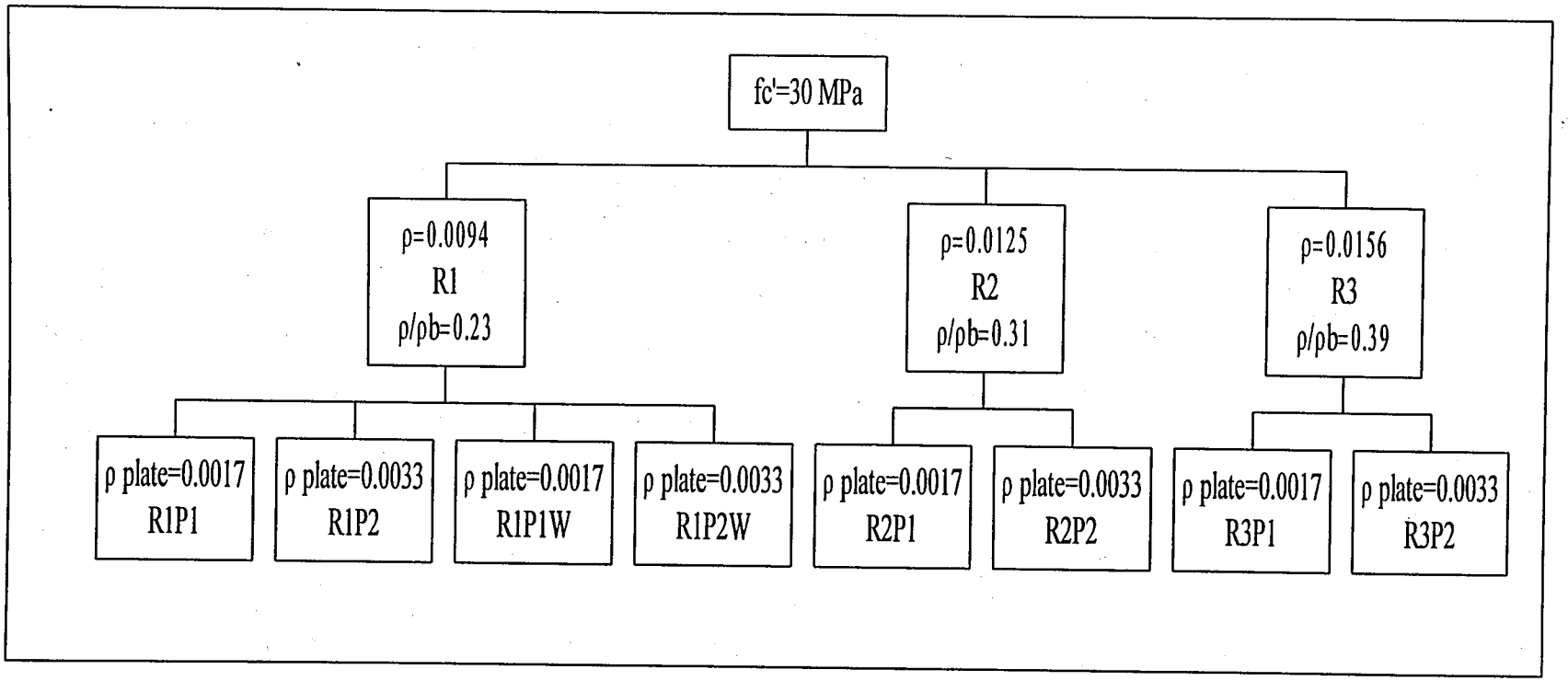

Figure 3.1. Chart of variables

At the same day, each test beam have been reversed in order to dry the surface which CFRP would be applied using a "CESAN" brand crane of 10 ton capacity (Figure A.6).

3.4.2. Application of CFRP Strips and Fabrics

Tension faces of the eight beams have been blasted down to aggregate by using mosaic hammer prior to application of strips. In addition, the zone which fabrics would have been applied have been prepared in the same way. All these work have lasted for three days. Blasted width for the beams which would have been bonded a single layer of one CFRP was 80 mm. Blasted width for the others was approximately 130 mm throughout the beams from support to support. Next, tension faces of the beams were cleaned up with a brush to remove great particles and cleaned with a vacuum cleaner to remove all leftover dust and loose particles from the concrete substrate. It was noted that concrete surface were free from oil and grease.

The second step was to wipe of CFRPs. Since CFRP plates were being cut at the factory, the procedure of cleaning up the strips was begun. CFRP plates being applied were wiped using a clean white cloth at the required direction with a solvent named as Colma Cleaner obtained from SIKA until all carbon dust was removed.

After wiping the surfaces of CFRP plates, epoxy adhesive named Sikadur 30 were started to prepare. Using an electric low speed hand mixer (400 mhp-600 mhp) resin (Component A) and hardener (Component B) have been stirred in their containers separately. Then, Component B were added to Component A with a proportion of 1:3 respectively. The mixture has been stirred approximately 3 minutes until coloured streaks disappeared (Figure A.7).

A fair amount of prepared epoxy were applied to the substrate using a spatula and then using a special instrument which contains of a roof-shaped spatula and a plywood set

Table 3.7. Descriptions of the eleven beams

R1	Rectangular beam whose reinforcement ratio was 0.0094 (control beam for group one)
R1P1	Rectangular beam which has a reinforcement ratio of 0.0094 and a single layer of one CFRP
R1P1W	Rectangular beam which has a reinforcement ratio of 0.0094, a single layer of one CFRP and wrapping
R1P2	Rectangular beam which has a reinforcement ratio of 0.0094 and a single layer of two CFRP
R1P2W	Rectangular beam which has a reinforcement ratio of 0.0094, a single layer of two CFRP and wrapping
R2	Rectangular beam whose reinforcement ratio was 0.0125 (control beam for group two)
R2P1	Rectangular beam which has a reinforcement ratio of 0.0125 and a single layer of one CFRP
R2P2	Rectangular beam which has a reinforcement ratio of 0.0125 and a single layer of two CFRP
R3	Rectangular beam whose reinforcement ratio was 0.0156 (control beam for group three)
R3P1	Rectangular beam which has a reinforcement ratio of 0.0156 and a single layer of one CFRP
R3P2	Rectangular beam which has a reinforcement ratio of 0.0156 and a single layer of two CFRP

epoxy was applied successfully to the CFRP strips. Dimensions of roof-shaped spatula is depicted Figure 3.3. Then, CFRP plates were placed on the concrete substrate. Both materials (strip and test beam) have had epoxy adhesives on their surfaces. A laminating roller was used to force out the adhesive on both side of the strip, to eliminate air voids in glue layer and to maintain a uniform thickness throughout the laminates. Surplus epoxy on

both side of the laminate was carefully removed. Adhesive thickness was about 3 mm. Four beams have had a single layer of two CFRP plates. The distance between those laminates was approximately 10 mm.

Since necessary conditions (dew point, relative humidity, temperature of substrate etc.) weren't satisfied by four beams, application of all CFRP plates and fabrics has not been done in the same day. The four beams named R1P1, R1P1W, R1P2W, R3P1, which have been satisfied necessary requirements due to being closer to the open fans at the structure laboratory, have been applied CFRP strips at the same time.

The other four beams which were R1P2, R2P1, R2P2, R3P2 namely were applied CFRP strips when the temperature requirements were satisfied. In order to provide vital conditions for application a nylon tent was constructed within a small fan for three days (Figure A.8). Application procedure of CFRPs was the same as previous four beams.

Sikadur 330 used to place the fabrics to the two beams have been prepared as the same as Sikadur 30. But the proportions of component A and component B were 4:1 by weight. Besides whole mixture was stirred 1 minute extra at a clean pail with an electric low speed hand mixer in order to keep air entrainment at a minimum. Then, the impregnating resin (Sikadur 330) was applied to the substrate by using a roller and the previously prepared fabric were mounted on to the adhesive in the required direction. The fabrics were cut with a scissor 300 mm long and they were overlapped 150 mm fiber direction prior to the application.

Since the surface of the fabrics would be sticky the day after the application day, their surface were wiped with a sponge saturated with water under the recommendations of manufacturer and impregnating resin hanging down from the surface was cut by a scissor.

3.4.3. Test Procedure

The beams were tested under four point bending up to failure. The test machine has been manually controlled hydraulic ram which had 20 ton capacity. A schematic drawing of test set-up is depicted in Figure 3.4. Tests of eleven beams have lasted for 4 days. Each day three 150x300 mm cylinders were tested under compression and it was seen that their strengths have been in the same range. Compressive strength of concrete was about 30 MPa. Compression tests were done at "Ele Autotest 2000" compression test machine seen in Figure A.9. Pace rate was chosen 3.5 kN/s.

The test specimens were instrumented by a various electronic sensors. They were six displacement-measuring devices named dial gage or LVDT, 50-ton load cell, analog to digital converter and computer program Data Collect v1.0. Before testing of specimens, all devices were calibrated. Moreover, all cables were kept in the same channel number on the converter throughout the tests.

During the tests, two dial gages (Linear Voltage Displacement Transducers) were placed at two supports so as to measure vertical settlements (Figure A.10). Two dial gages mounted at midspan 50 mm to the tension face at both sides of the beams were used to determine vertical deflection at midpoint. These two dial gages have been placed on two straight steel bars which were mounted in the holes drilled both sides of the beams. One of the other two dial gages was placed over the beam using clamps and the other one was located bottom of the beam. Both were at a distance of 100 mm to the midpoint at both sides. The former has been used to determine the shortening at the top fiber of midspan and the latter has been used to determine the elongation at the bottom fiber of midspan. Locations of LVDTs and details of the test beams were illustrated in Figure 3.5 and Figure 3.6 respectively. Average of these two-dial gage values were used in order to determine curvature at midspan. Besides, at every stage crack opening was measured by a pair of crack binoculars and noted.

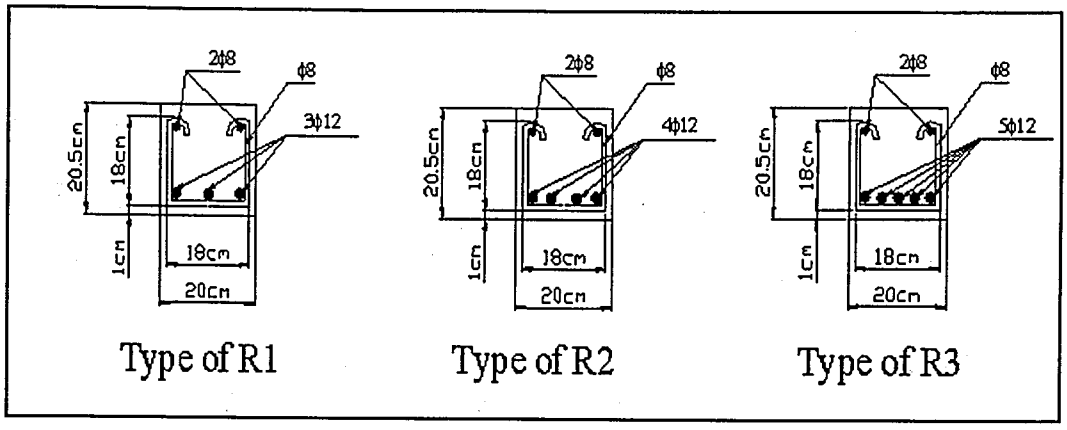

Figure 3.2. Details of reinforcement

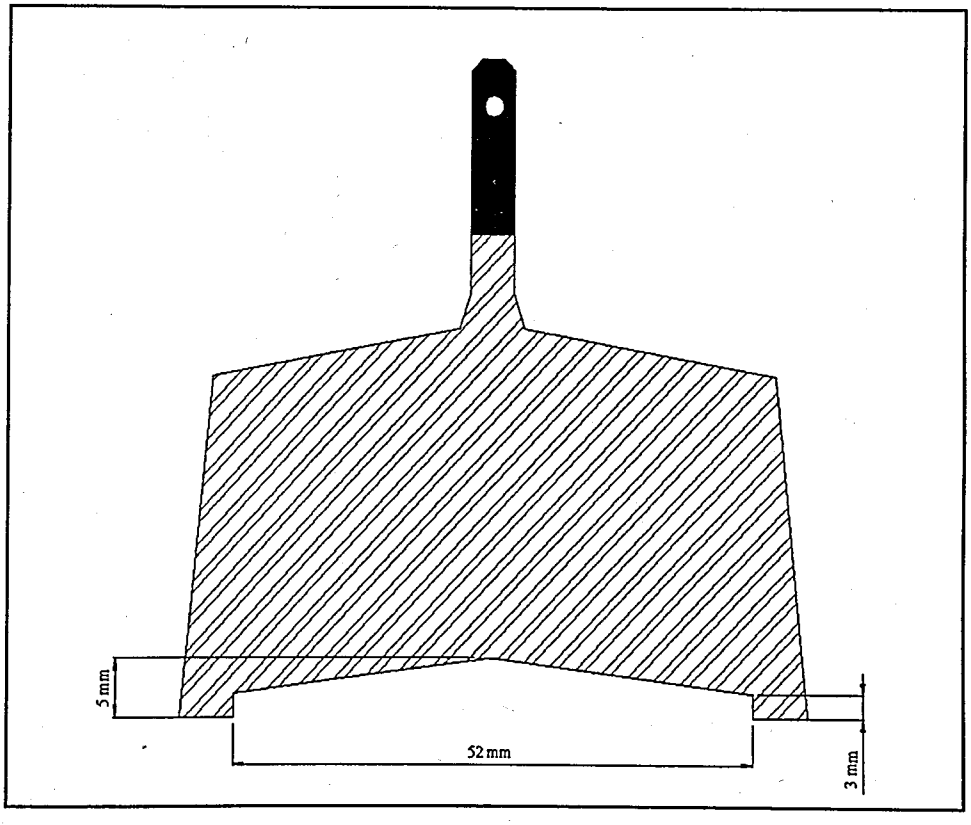

Figure 3.3. Dimensions of roof-shaped spatula

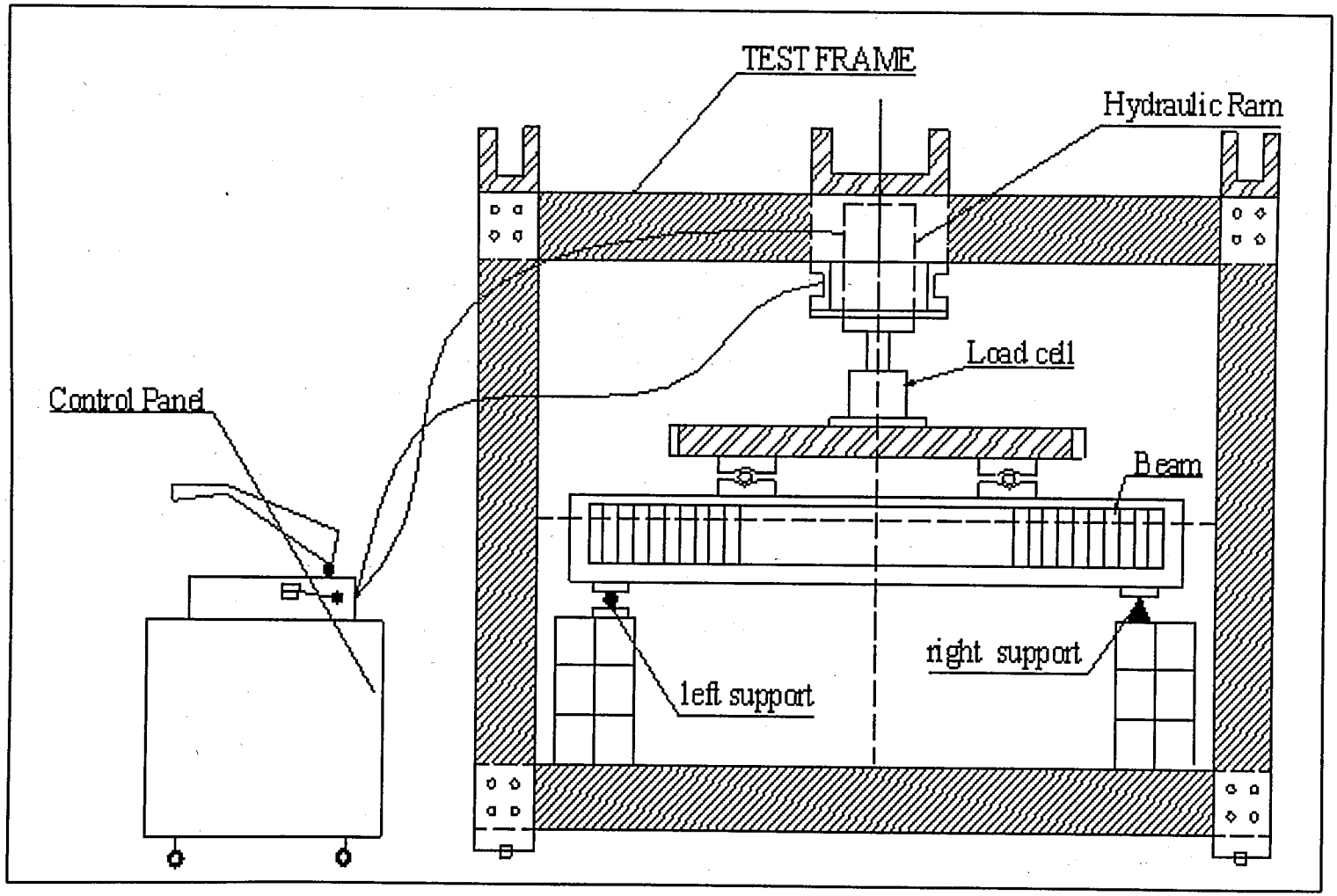

Figure 3.4. Test set-up

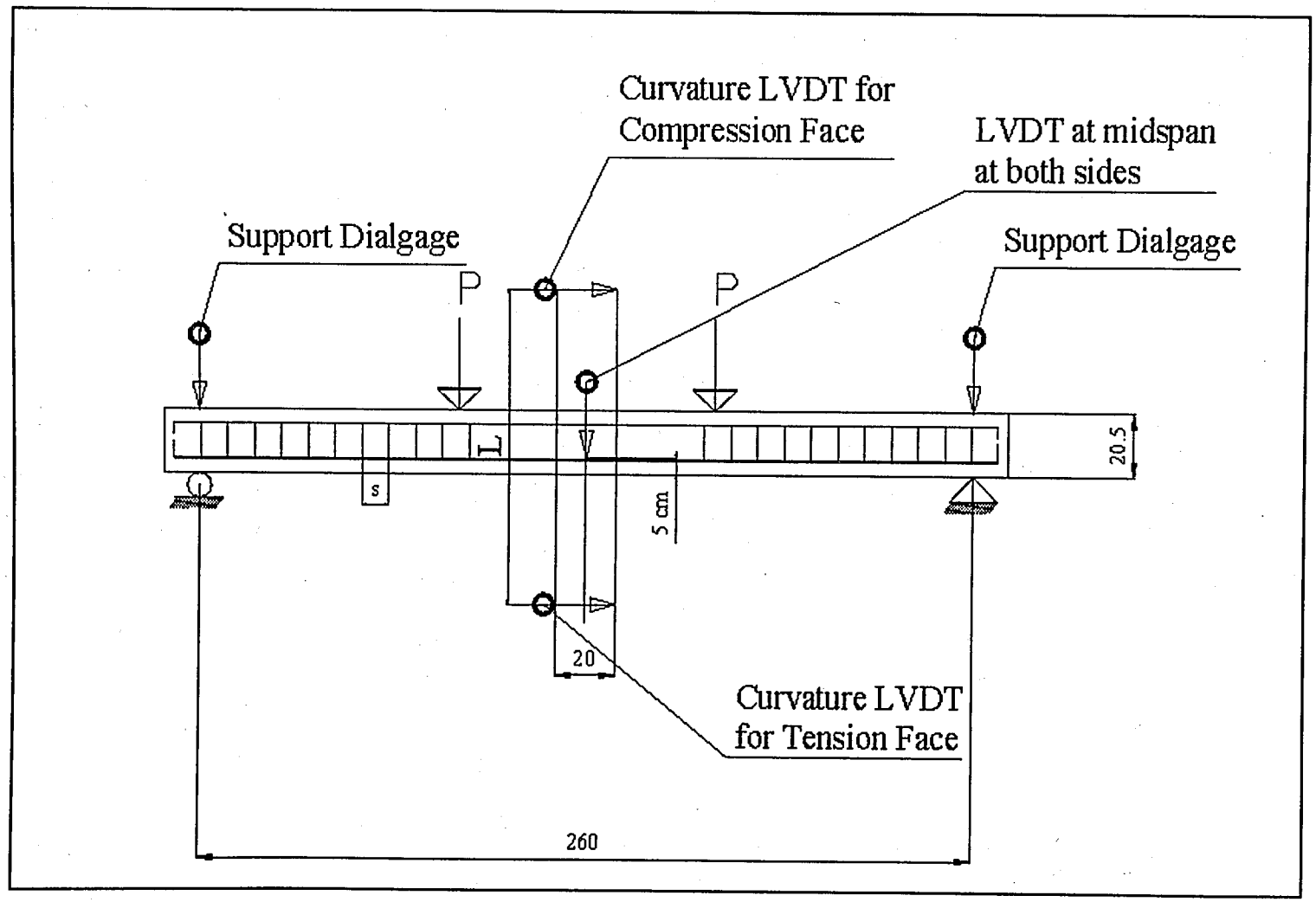

Figure 3.5. Locations of LVDTs

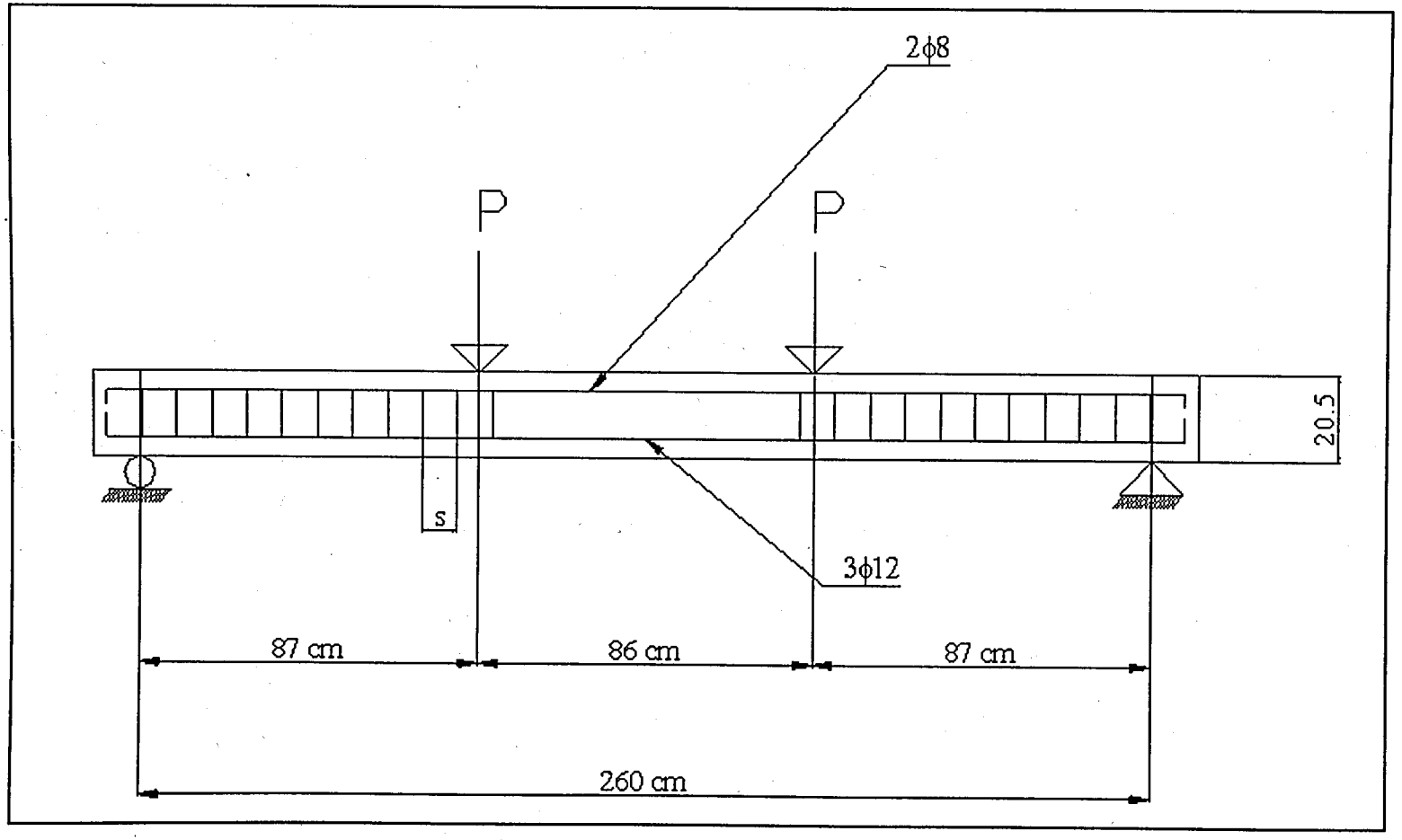

Figure 3.6. Details of the test beams

4. TEST RESULTS

4.1. General

Prior to the testing of the samples, in order to determine concrete compressive strength 150x300 mm cylinder samples have been tested in the structural laboratory. The loading speed was 3.5 kN/s for cylinder compression tests. Average value obtained from these tests has been 30 MPa. Moreover, three 4x4x16 cm epoxy adhesive samples have been moulded. When these samples were cured, they have been demoulded and tested under three-point loading so as to determine flexural strength of the epoxy adhesive. Pace has been selected as 0.5 kN/s. The average value of these tests has been recorded as 53.87 MPa.

4.2. Structural Tests

Thanks to six LVDTs, necessary deflection and load values have been transferred into computer through an analog to digital converter. Data has been recorded per second.

During the tests of the beams, the load which first crack has initiated has been recorded for every beam. Besides, max crack width values have been measured at different load levels up to failure. It has been seen that the first crack load has generally increased while FRP ratio and tension steel ratio have enhanced. Experimental results can be summarized as in Table 4.1. In this table the loads in which tension steel has yielded, max loads, the first cracking loads, residual loads and deflections corresponded to these loads can be seen, respectively.

While the test specimens have been tested, load-controlled type of loading has been employed up to failure. Behaviour of the samples under four point bending can be depicted in Figure 4.1 to 4.22.

Table 4.1. Summary of test results

LOADS AND DEFLECTIONS	BEAMS										
	R1	R1P1	R1P1W	R1P2	R1P2W	R2	R2P1	R2P2	R3	R3P1	R3P2
$P_{max\ load}$ (kN)	50.40	79.06	91.57	99.81	109.03	62.92	91.57	116.94	77.08	105.41	124.84
$P_{steel\ yields}$ (kN)	40.85	62.92	56.66	78.07	75.10	60.28	72.80	64.56	47.10	68.19	92.56
$P_{first\ crack}$ (kN)	29.00	35.00	48.40	56.00	63.00	37.00	36.00	46.00	26.00	44.00	75.00
$P_{residual}$ (kN)	****	44.14	45.79	33.93	35.91	****	56.66	52.38	****	69.17	67.53
$\delta_{steel\ yields}$ (mm)	7.6	11.4	9.3	14.5	11.7	10.9	11.2	8.1	6.2	9.2	11.6
$\delta_{for\ max\ load}$ (mm)	39.1	26.8	44.1	26.7	35.4	35.0	31.0	30.1	36.1	32.9	29.9
$\delta_{first\ crack}$ (mm)	4.5	4.7	7.5	8.1	9.2	5.9	4.4	5.4	2.7	5.3	9.0
δ_{max} (mm)	39.4	44.5	44.9	40.9	46.1	39.5	38.9	40.5	39.1	41.2	40.1

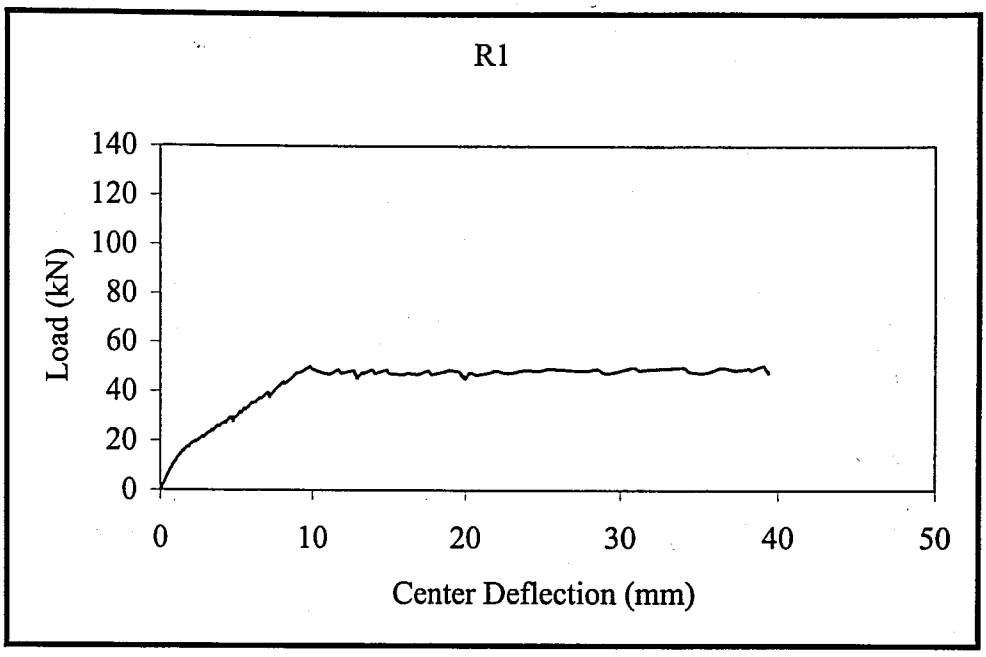

Figure 4.1. Load deflection curve of the beam of R1

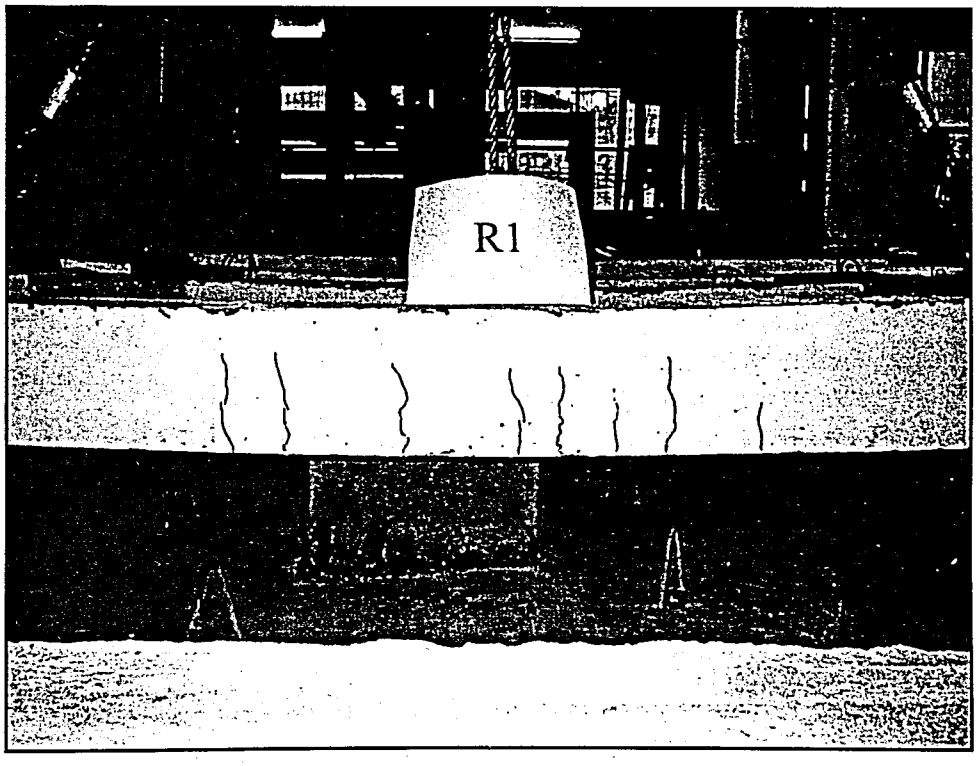

Figure 4.2. Crack propagation of the beam of R1 after testing

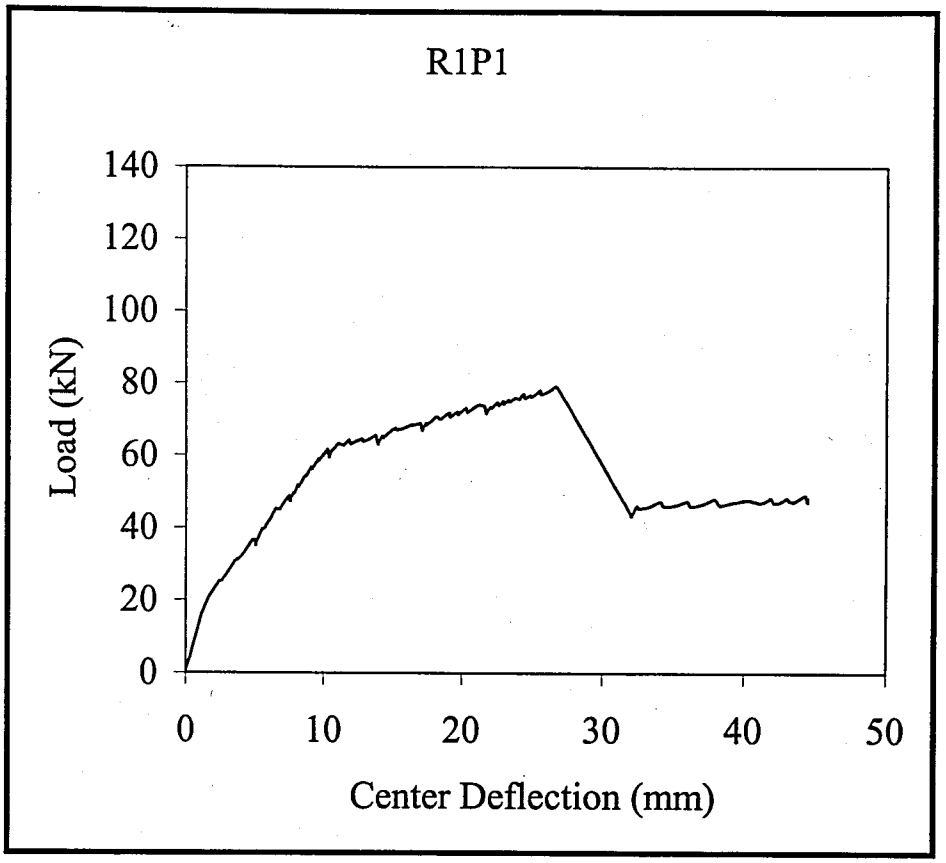

Figure 4.3. Load deflection curve of the beam of R1P1

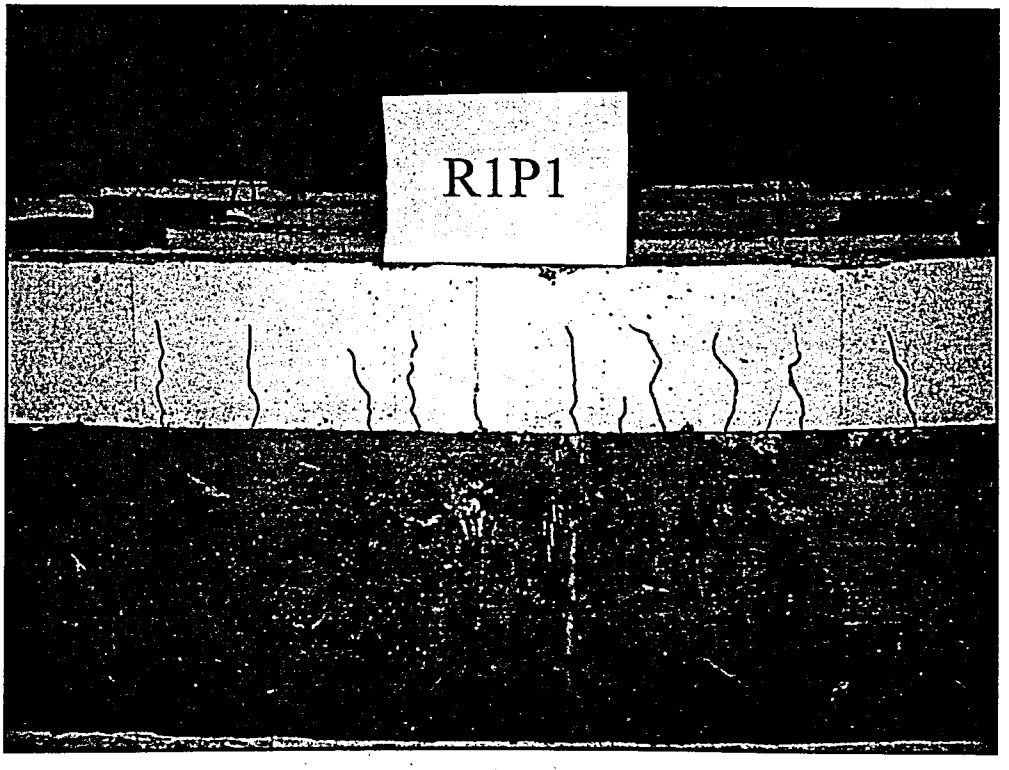

Figure 4.4. Crack propagation of the beam of R1P1 after testing

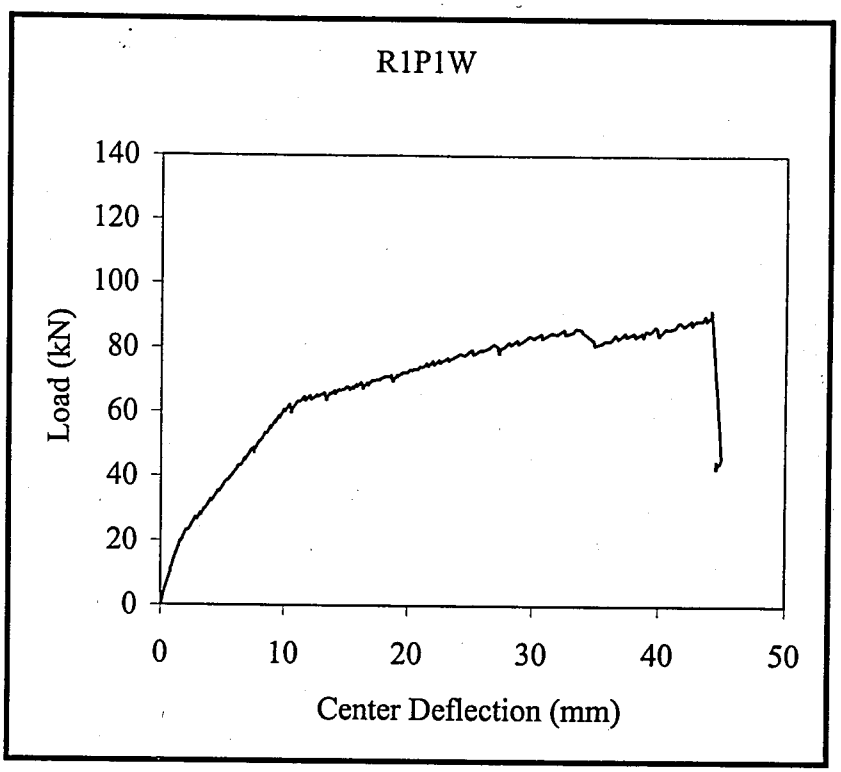

Figure 4.5. Load deflection curve of the beam of R1P1W

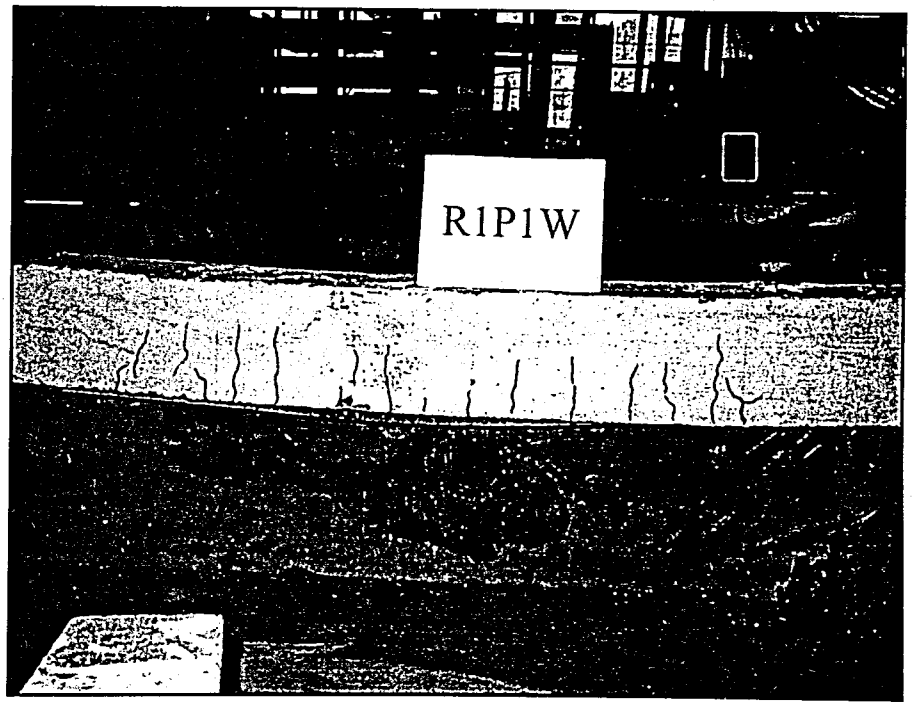

Figure 4.6. Crack propagation of the beam of R1P1W after testing

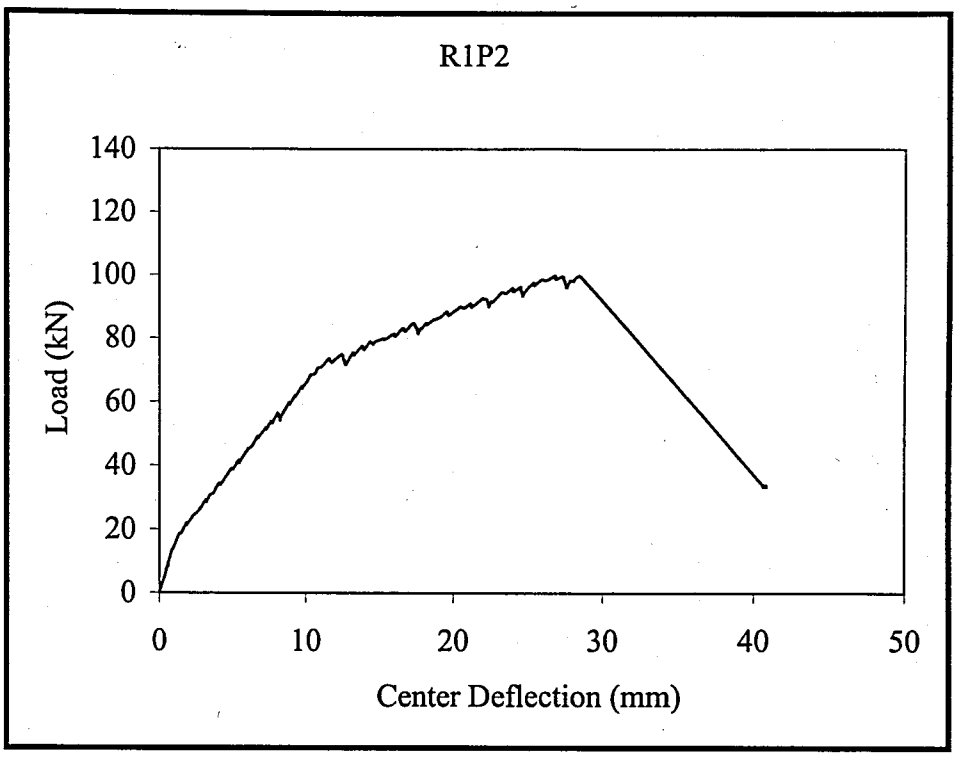

Figure 4.7. Load deflection curve of the beam of R1P2

Figure 4.8. Crack propagation of the beam of R1P2 after testing

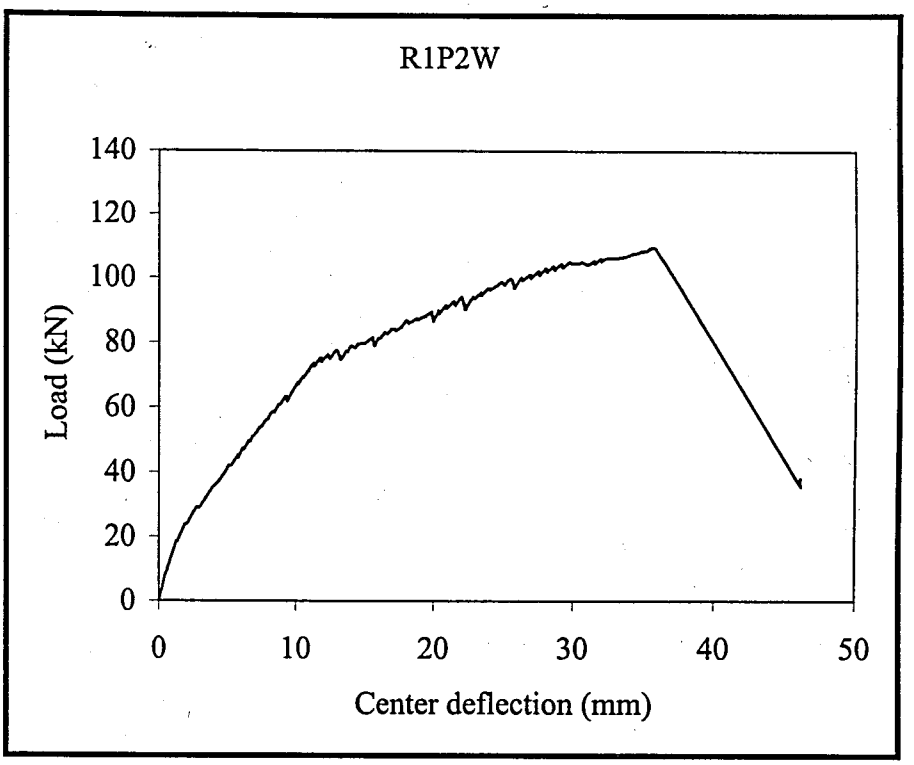

Figure 4.9. Load deflection curve of the beam of R1P2W

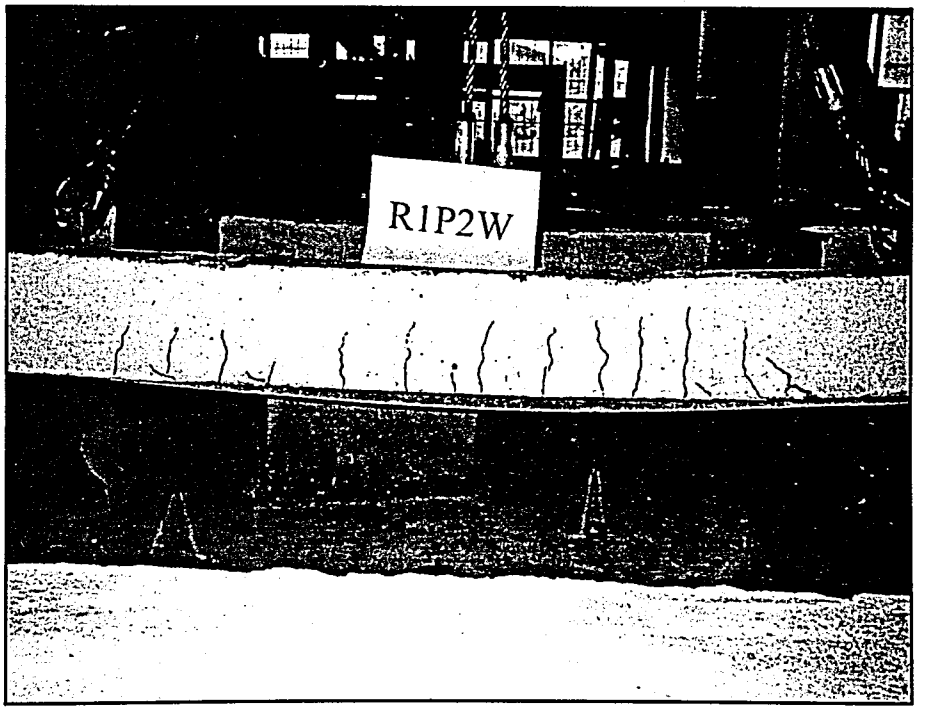

Figure 4.10. Crack propagation of the beam of R1P2W after testing

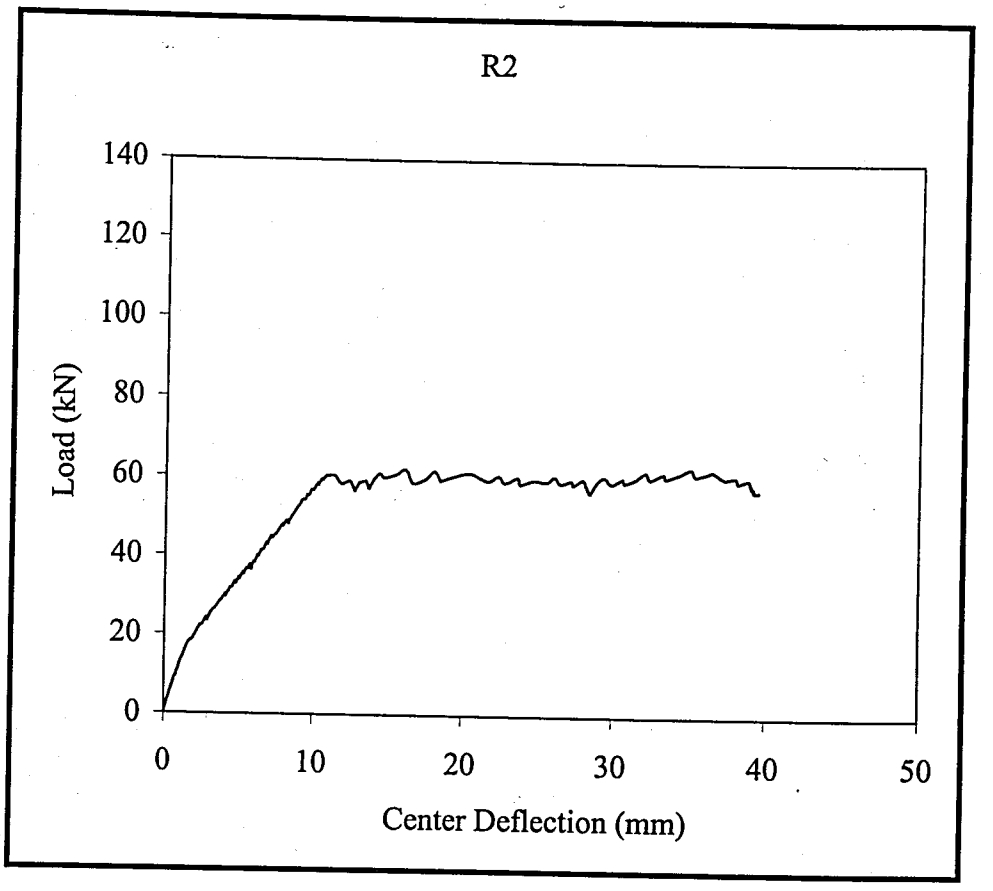

Figure 4.11. Load deflection curve of the beam of R2

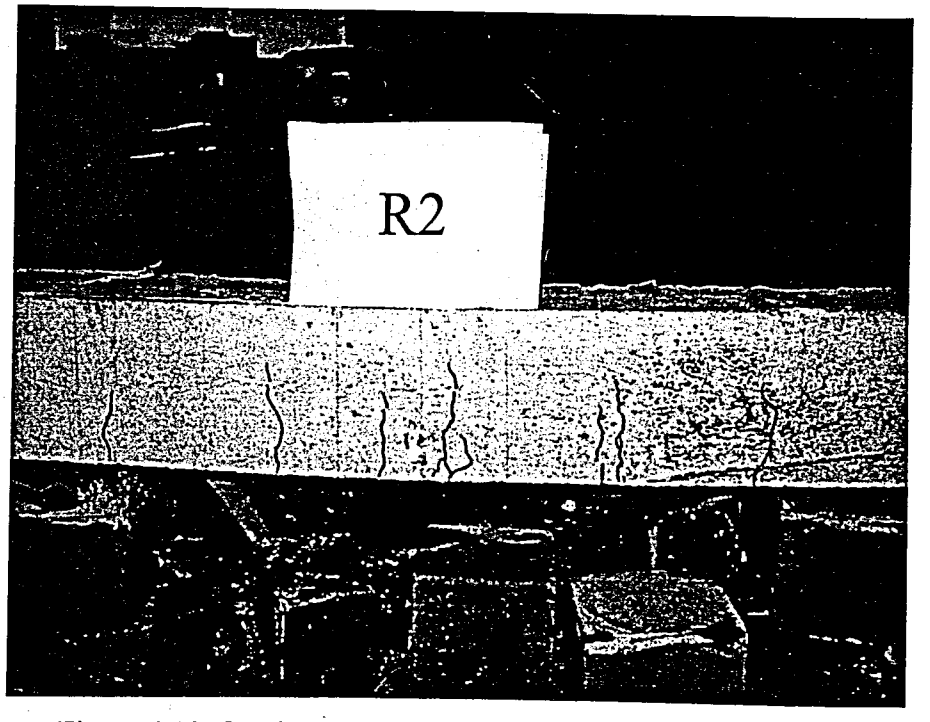

Figure 4.12. Crack propagation of the beam of R2 after testing

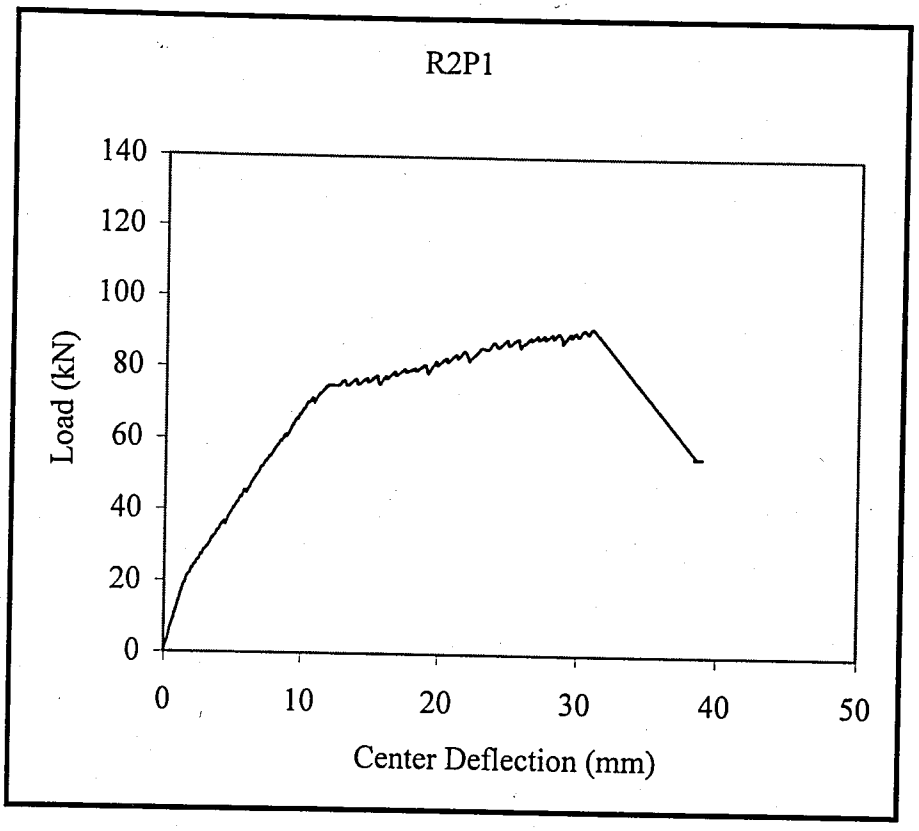

Figure 4.13. Load deflection curve of the beam of R2P1

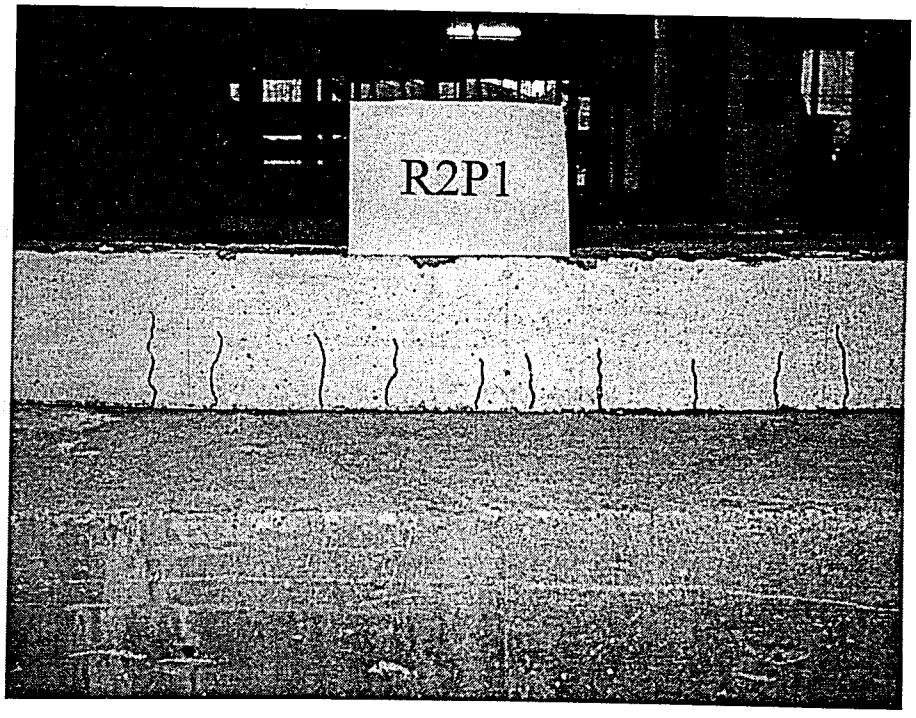

Figure 4.14. Crack propagation of the beam of R2P1 after testing

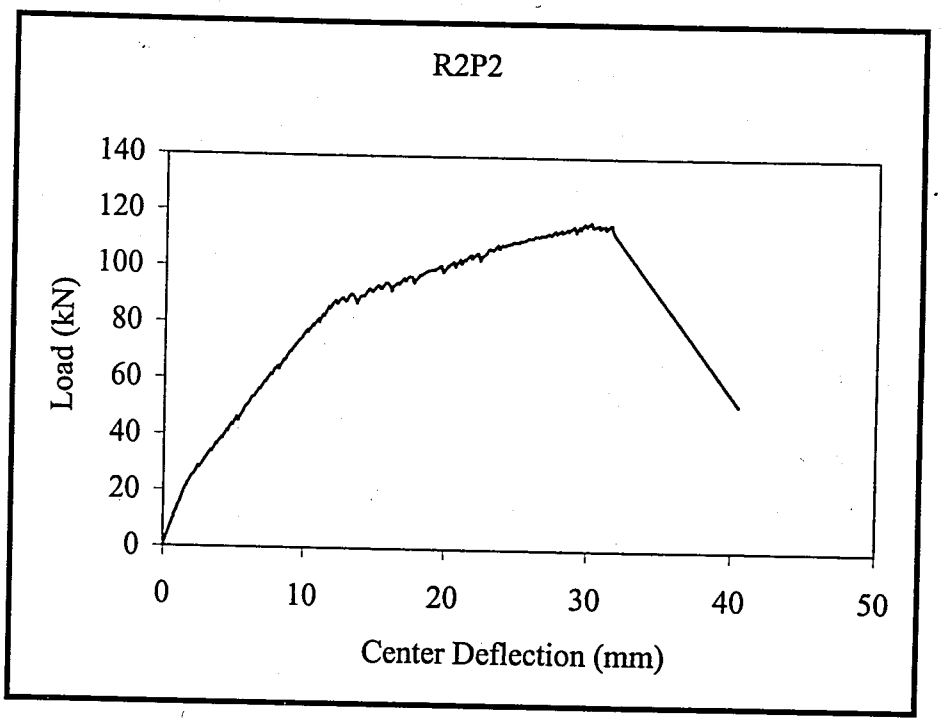

Figure 4.15. Load deflection curve of the beam of R2P2

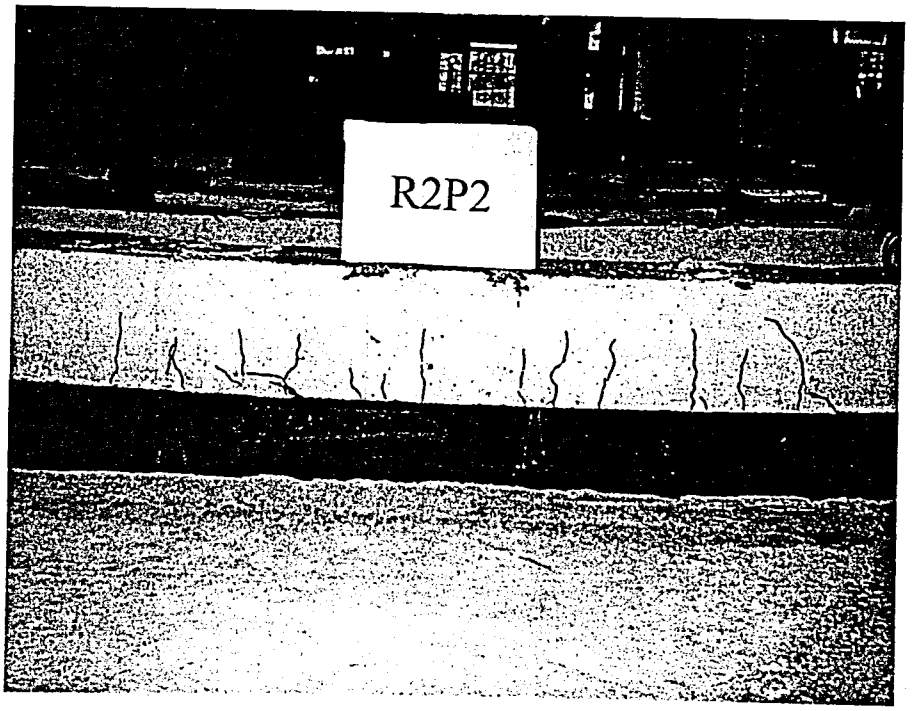

Figure 4.16. Crack propagation of the beam of R2P2 after testing

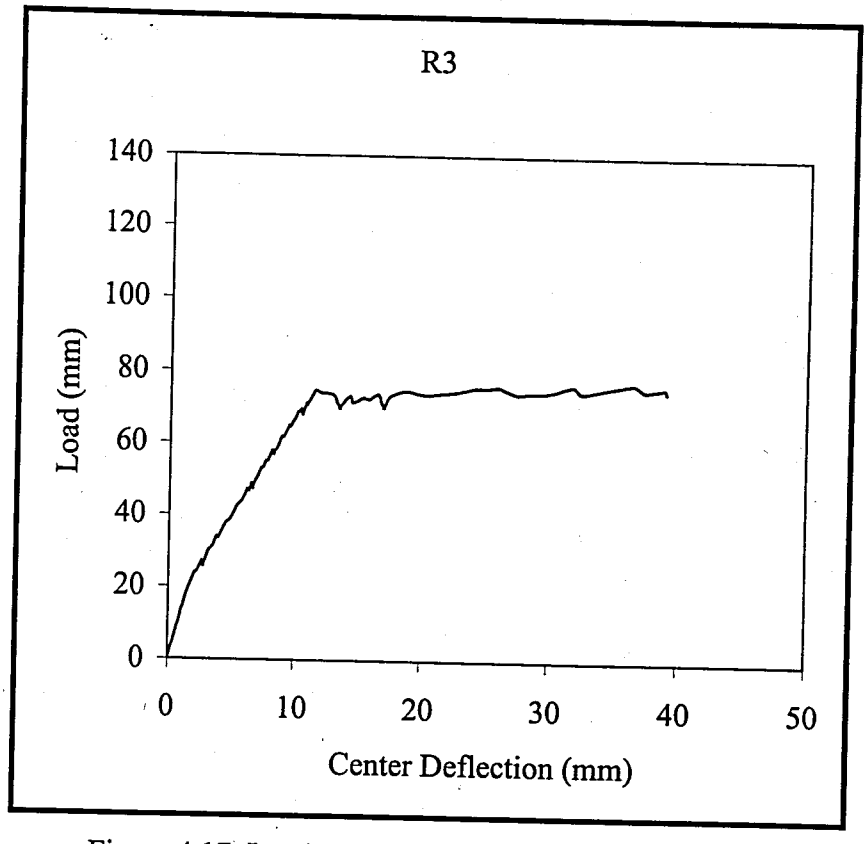

Figure 4.17. Load deflection curve of the beam of R3

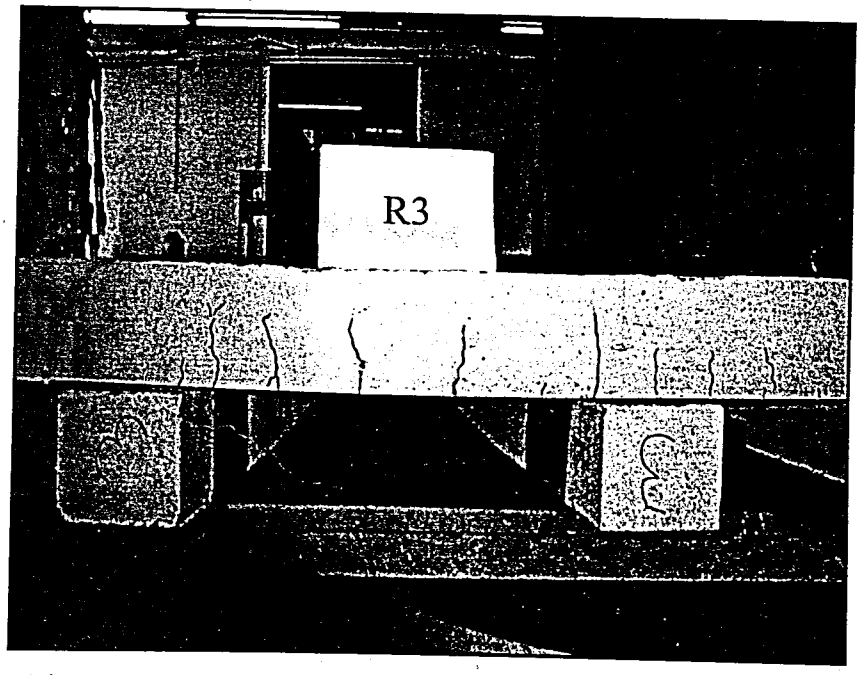

Figure 4.18. Crack propagation of the beam of R3 after testing

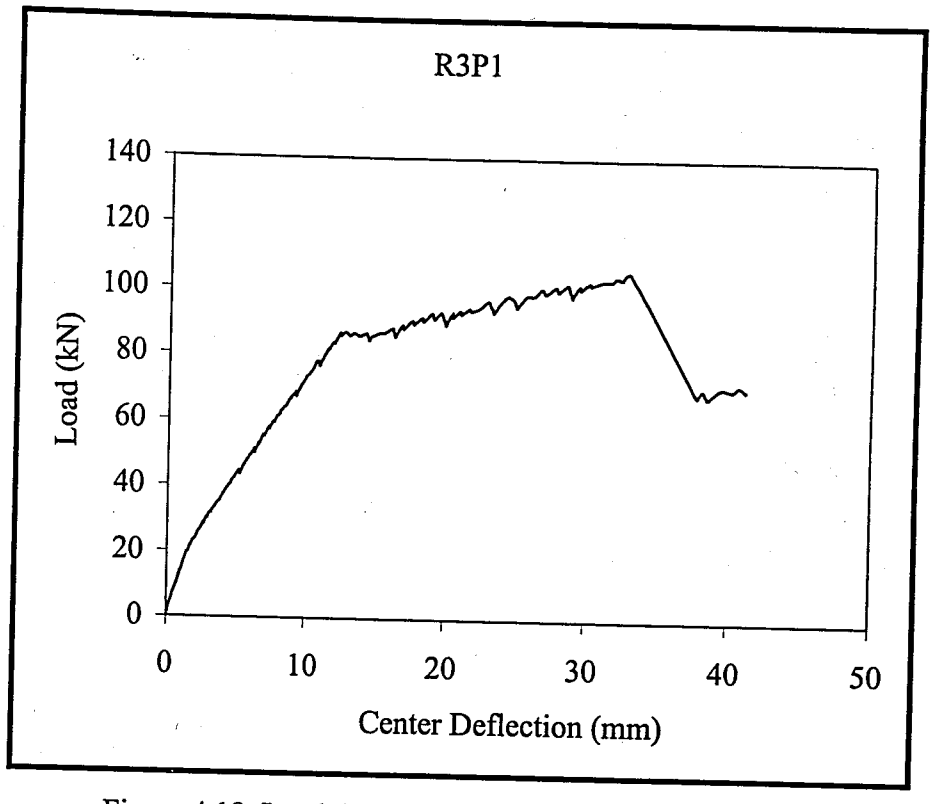

Figure 4.19. Load deflection curve of the beam of R3P1

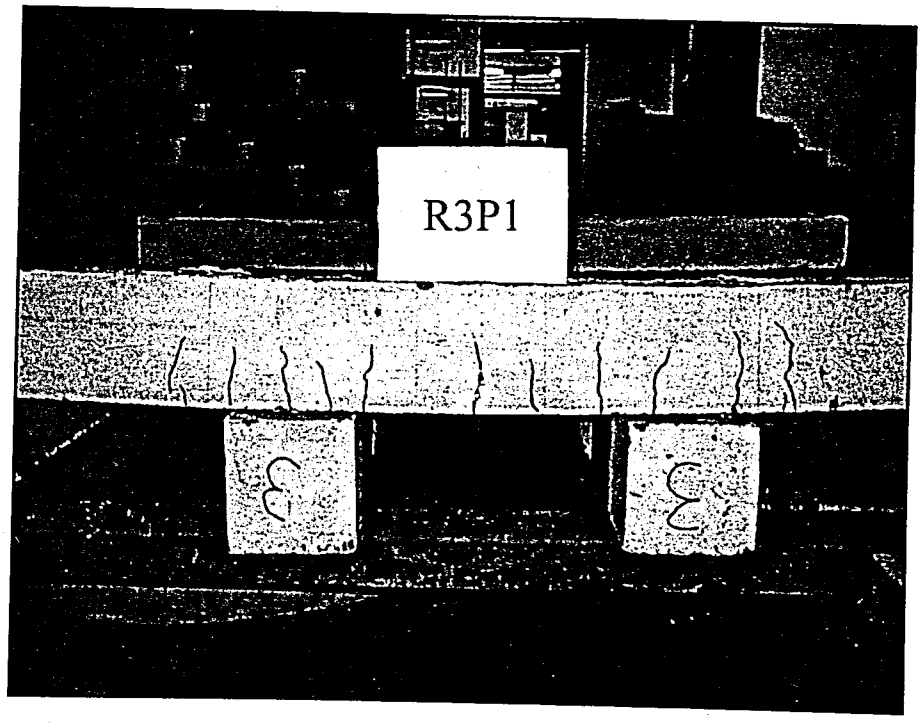

Figure 4.20. Crack propagation of the beam of R3P1 after testing

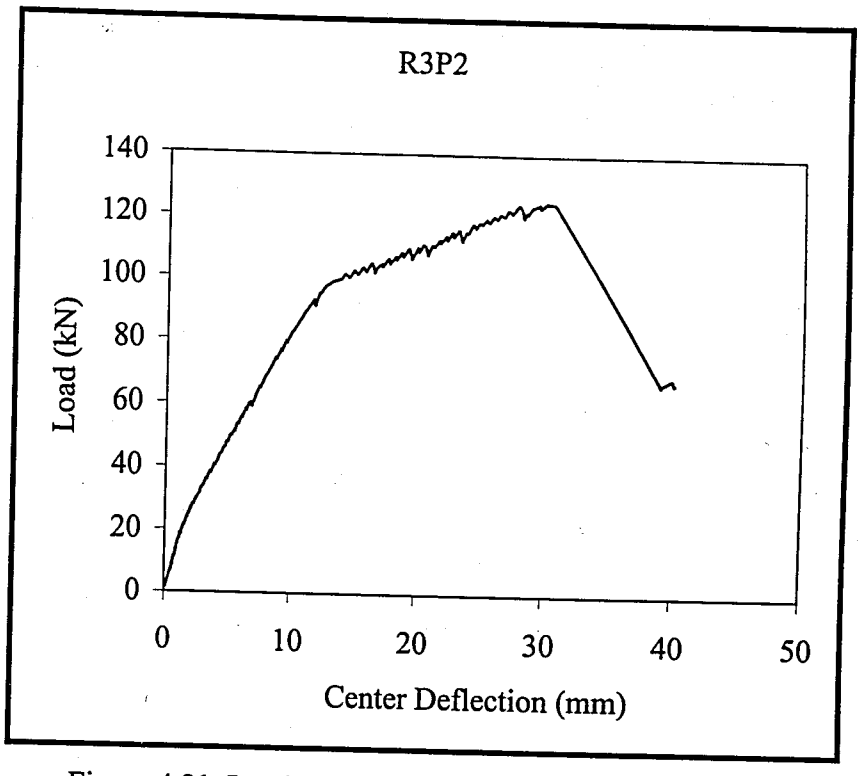

Figure 4.21. Load deflection curve of the beam of R3P2

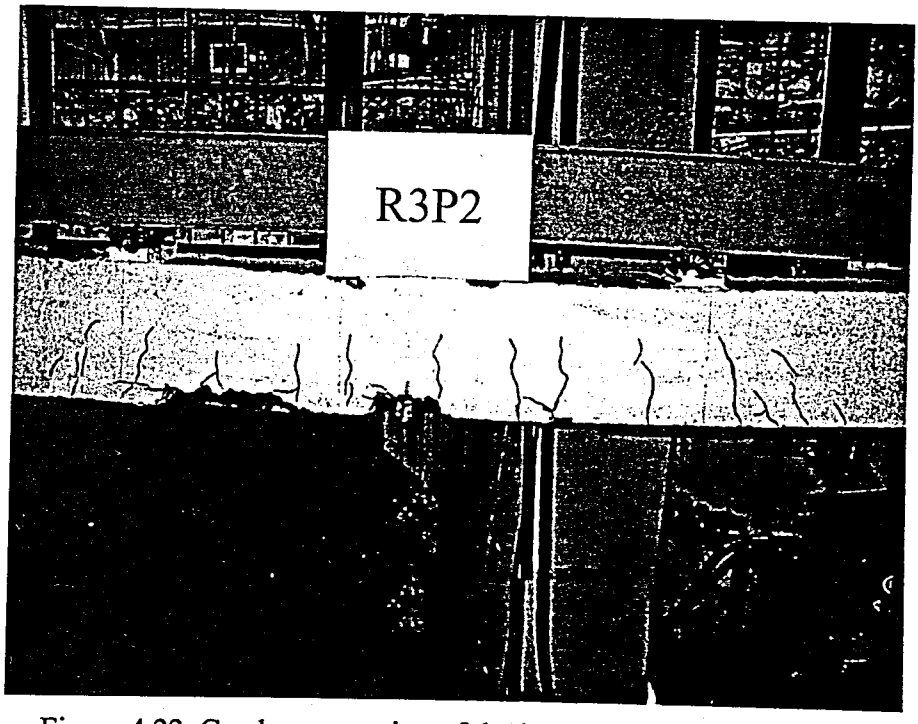

Figure 4.22. Crack propagation of the beam of R3P2 after testing

5. EVALUATION OF TEST RESULTS

5.1. Factors Affecting Specimen Behaviour

In the scope of this study, they have been mainly investigated the effect of reinforcement ratio and CFRP ratio on the behaviour of the specimens. In addition to that, it has been tried to be examined the effect of wrapping shear span but for this research only the series of R1 beams have been used. The effects of these parameters are presented in the following.

5.1.1. Effect of Reinforcement Ratio

The Results have been discussed for virgin specimens, a single layer of one FRP plated beams and a single layer of two FRP plated beams. It can be seen that an increase in reinforcement ratio has resulted in a decrease of crack width gradually. Moment versus crack width diagrams for virgin specimens and CFRP-plated specimens are depicted in Figure 5.1 to 5.3. From these figures it can be easily seen that while reinforcement ratio increases, crack width decreases for the same moment after approximately 0.11 mm crack width for virgin specimens and nearly 0.19 mm crack width for a single layer of one CFRP-plated beams.

Crack width values around 0.4 mm which is a limit case for interior beams in TS 500 [29] have been calculated using recorded data. It has been noticed that reinforcement ratio has increased the loads corresponded to the 0.4 mm-crack width for the test specimens. For virgin specimens the increase was about 18 per cent for R2 beam and 44 per cent for R3 beam with respect to R1 beam. For a single layer of one FRP plated beams those values were about 20 per cent for R2P1 and 30 per cent for R3P1 beam with respect to R1P1 beam. For a single layer of two FRP-plated beams, the ratios which were similar to the previous one were 20 per cent for R2P2 and 31 per cent for R3P2 beam. Table 5.1 and Figure 5.4 can explain the trend for loads corresponded to the max crack width precisely.

Reinforcement ratio is one of the major factors which influences flexural capacity or load-carrying capacity. Table 5.2 is the summary of loads and deformations for each beam. Different researches have been done so as to investigate the effect of reinforcement ratio on the behaviour of the beams. Ross *et al.*, [21], Spadea *et al.*, [19] have been some of them. It is found that an increase in reinforcement ratio has resulted in an enhancement in the ultimate load capacity or the ultimate moment capacity. Enhancement ratios which are defined as the ratio of the peak load of the strengthened beam to the ultimate load of the virgin specimen in each group [21] are listed in Table 5.3. It has shown that while tension steel ratio increases enhancement ratio decreases for both virgin specimens and CFRP-plated specimens. In other words, for lightly reinforced beams, enhancement ratio is greater than those of the heavily reinforced beams. According to the Table 5.3 while R1P1 beam sustains 57 per cent much more than R1 beam, R3P1 which is heavily reinforced beam can sustain only 37 per cent much more than R3 beam. Figure 5.5 shows the relationship between enhancement ratio and composite ratio (A_{frp}/A_s=x). Enhancement ratio versus composite ratio trend-line which was drawn by Ross *et al.*, [21] is also shown in Figure 5.5. It can be concluded that reinforcement ratio has an explicit effect to be increased load-carrying capacity or ultimate moment capacity. Load-center deflection curves obtained are depicted in Figure 5.6 to 5.8. Load-deflection curves are associated with moment-curvature diagrams. Figure 5.9 to 5.11 depict moment-curvature diagrams obtained from test data for different reinforcement ratios. From those figures, an increase in stiffness and strength with increasing reinforcement ratio for plated beams can be seen more explicitly for the series of P1 beams. Besides, these moment-curvature diagrams show that an increase in the reinforcement ratio generally results in strength enhancement of the beams.

In addition to load-deflection curves, moment versus strain relationships have been also examined. For various reinforcement ratios, moment-strain curves are shown from Figure 5.12 to Figure 5.25. These strains are calculated using compatibility equations at different levels.

An increase in the reinforcement ratio generally results in a decrease in the strain of top fiber of the concrete for the same load level. This is better visualized in the figures drawn for a single layer of one CFRP-plated beams and virgin specimens. Moreover, for

different load levels moment and corresponding strain values at the top fiber of the concrete section are given in Table 5.4. At failure, ultimate strains at the top fiber of the concrete section, which are seen in Table 5.4 are usually increased with increasing reinforcement ratio.

The strains in the level of tension steel and the level of bottom fiber of the concrete are similar to each other. For the same moment, an increase in reinforcement ratio decreases strain values for those levels generally. However, ultimate strain values usually increase with increasing reinforcement ratio for strengthened beams. Moment-strain at tension steel level and moment versus strain at bottom fiber level of the concrete section are illustrated in Figure 5.18 to 5.23. Besides, strain values at ultimate moment and at the moment which steel yields are summarized in Table 5.5 and Table 5.6.

For CFRP-plated beams, using compatibility equations, strains at the level of FRP were calculated. With an increase in reinforcement ratio ultimate strains are generally inclined to increase. It means that the stress values of FRP level come close to tensile strength of FRP. This can be seen clearly in Figure 5.24 and Figure 5.25. However, for a single layer of two FRP-strengthened beams strain values at ultimate moments appear smaller than that of one plated beams generally. Therefore, it can be concluded that tensile capacity of FRP could not be used effectively for these beams. Strain values in max moments, the strains which top fiber of the concrete reaches 0.003 strain in compression zone and the strains which tension steel yields are shown in Table 5.7.

In the results of the tests, it has been seen that an increase in the reinforcement ratio may also change the failure mode. While all virgin specimens have failed in ductile flexure with yielding of tensile steel before crushing of the concrete in the compression zone, FRP-plated beams have failed suddenly in a brittle manner. Due to excessive deflections which result in a moving of dial gages and in order to prevent any damage on the dial gages, the beams could not be loaded up to crushing of the concrete in the compression zone for virgin specimens. Besides, it has been seen that considerable loses in the load capacity at instant of failure and explosive de bonding mode of failure has usually occurred for CFRP-strengthened beams. Due to increasing of reinforcement ratio, crushing of concrete or/and yielding of compression steel have been detected for a single layer of two CFRP plated

beams namely, R2P2 and R3P2. This finding has coincided with the study of Ross *et al.*, [21]. It was shown that crushing of concrete in the compression zone was seen for the heavily reinforced beams (groups of 4, 5, 6) in the study of Ross *et al.*, [21].

Using load-deflection curves and moment-curvature curves another important parameter which is named as ductility can be obtained. Ductility can be defined as the ability to sustain large inelastic deformation without loss in the load carrying capacity prior to failure [23]. Ductility can give an idea to the designers about the behaviour of the performance of the structural system [19]. Two types of ductility are employed in this study namely, deflection ductility and curvature ductility. Both are calculated using curvature and deflection values at ultimate load and at the load of yielding of tension steel. The trend of curvature ductility and deflection ductility can be seen in Figure 5.26. Besides, the ductility values obtained from this study are shown in Table 5.8 as ductility ratios and ductility indices. Both deflection ductility and curvature ductility are generally increasing with respect to the reinforcement ratio. The increase is appeared clearly for the beams of P1 series. Amazingly, curvature ductility for R2 and R3 beams is smaller than R1 beam, unlike deflection ductility, but between those two beams the slope is inclined to increase anyway.

Table 5.1. Loads corresponding to limit crack width

BEAMS	Loads (kN)	Limit Crack Width (mm)
R1	49	0.4
R2	58	0.4
R3	70.5	0.4
R1P1	70.2	0.4
R2P1	80	0.4
R3P1	85	0.4
R1P2	92	0.4
R2P2	102	0.4
R3P2	107	0.4

Table 5.2. Summary of loads and deflections

LOADS AND DEFLECTIONS	BEAMS								
	R1	R2	R3	R1P1	R2P1	R3P1	R1P2	R2P2	R3P2
$P_{max\ load}$ (kN)	50.40	62.92	77.08	79.06	91.57	105.41	99.81	116.94	124.84
$P_{steel\ yields}$ (kN)	40.85	60.28	47.10	62.92	72.80	68.19	78.07	64.56	92.56
$P_{first\ crack}$ (kN)	29.00	37.00	26.00	35.00	36.00	44.00	56.00	46.00	75.00
$P_{residual}$ (kN)	****	****	****	44.14	56.66	69.17	33.93	52.38	67.53
$\delta_{steel\ yields}$ (mm)	7.6	10.9	6.2	11.4	11.2	9.2	14.5	8.1	11.6
$\delta_{for\ max\ load}$ (mm)	39.1	35.0	36.1	26.8	31.0	32.9	26.7	30.1	29.9
$\delta_{first\ crack}$ (mm)	4.5	5.9	2.7	4.7	4.4	5.3	8.1	5.4	9.0
δ_{max} (mm)	39.4	39.5	39.1	44.5	38.9	41.2	40.9	40.5	40.1

Table 5.3. Development of enhancement ratio with respect to reinforcement ratio

BEAMS	M_{max}	L_{max} for M_{max}	Average f_c'	Enhancement Ratio R_E	Area of FRP	Area of Tension Steel	Composite Ratio Afrp/As	ρ_{steel}	ρ_{fiber}
	kN-m	kN	N/mm^2		mm^2	mm^2			
R1	21.92	50.40	30		-	339		0.0094	-
R2	27.37	62.92	30		-	452		0.0125	-
R3	33.30	77.08	30		-	565		0.0156	-
R1P1	34.39	79.06	30	1.57	60	339	0.18	0.0094	0.0017
R2P1	39.83	91.57	30	1.46	60	452	0.13	0.0125	0.0017
R3P1	45.85	105.41	30	1.37	60	565	0.11	0.0156	0.0017
R1P2	43.42	99.81	30	1.98	120	339	0.35	0.0094	0.0033
R2P2	50.87	116.94	30	1.86	120	452	0.27	0.0125	0.0033
R3P2	54.31	124.84	30	1.62	120	565	0.21	0.0156	0.0033

Table 5.4. Development of compression strain with respect to reinforcement ratio

BEAMS	Moments			$\varepsilon_{top\ fiber}$ x 0.001		
	M_{max}	M@0.003	M@0.00155	ε_{max}	ε @0.003	ε @0.00155
R1	21.92	-	17.77	2.109	-	0.571
R2	27.37	-	26.22	2.258	-	0.96
R3	33.30	-	20.49	2.618	-	0.332
R1P1	34.39	-	27.37	2.871	-	1.295
R2P1	39.83	-	31.67	2.146	-	0.961
R3P1	45.85	-	29.66	2.715	-	0.968
R1P2	43.42	-	33.96	2.286	-	1.571
R2P2	50.87	50.15	28.09	3.038	3.016	0.947
R3P2	54.31	50.29	40.26	3.571	3.051	1.629

Table 5.5. Development of bottom fiber strain of concrete section with respect to reinforcement ratio

BEAMS	Moments			$\varepsilon_{bottom\ fiber}$ x 0.001		
	M_{max}	M@0.003	M@0.00155	ε_{max}	ε @0.003	ε @0.00155
R1	21.92	-	17.77	20.61	-	1.819
R2	27.37	-	26.22	19.768	-	1.97
R3	33.3	-	20.49	13.877	-	1.833
R1P1	34.39	-	27.37	4.869	-	1.931
R2P1	39.83	-	31.67	6.053	-	1.995
R3P1	45.85	-	29.66	8.164	-	1.927
R1P2	43.42	-	33.96	3.884	-	2.02
R2P2	50.87	50.15	28.09	6.911	6.656	1.951
R3P2	54.31	50.29	40.26	6.06	4.6	2.036

Table 5.6. Development of tension steel strain with respect to reinforcement ratio

BEAMS	Moments			$\varepsilon_{tension\ steel}$ x 0.001		
	M_{max}	M@0.003	M@0.00155	ε_{max}	ε @0.003	ε @0.00155
R1	21.92	-	17.77	18.131	-	1.558
R2	27.37	-	26.22	17.138	-	1.617
R3	33.3	-	20.49	11.974	-	1.583
R1P1	34.39	-	27.37	3.984	-	1.562
R2P1	39.83	-	31.67	5.08	-	1.646
R3P1	45.85	-	29.66	6.9	-	1.591
R1P2	43.42	-	33.96	3.162	-	1.6
R2P2	50.87	50.15	28.09	5.763	5.54	1.616
R3P2	54.31	50.29	40.26	4.91	3.688	1.598

Table 5.7. Development of FRP strain with respect to reinforcement ratio

BEAMS	Moments			$\varepsilon_{FRP\ fiber}$ x 0.001		
	M_{max}	M@0.003	M@0.00155	ε_{max}	ε @0.003	ε @0.00155
R1	21.92	-	17.77	-	-	-
R2	27.37	-	26.22	-	-	-
R3	33.3	-	20.49	-	-	-
R1P1	34.39	-	27.37	5.001	-	1.987
R2P1	39.83	-	31.67	6.199	-	2.05
R3P1	45.85	-	29.66	8.354	-	1.977
R1P2	43.42	-	33.96	3.992	-	2.08
R2P2	50.87	50.15	28.09	7.084	6.823	2
R3P2	54.31	50.29	40.26	6.23	4.739	2.101

Table 5.8. Ductilities of test specimens without plate end anchorages with respect to reinforcement ratio

					Deflection ductility	Curvature ductility	Relative ductility ratios	
Beams	**Δ steel yields**	**Δ for max load**	**ϕ steel yields**	**ϕ for max load**	μ_D	μ_ϕ	μ_D	μ_ϕ
R1	7.6	39.1	0.0109	0.1033	5.17	9.51	1.0	1.0
R2	10.9	35.0	0.0146	0.1096	3.23	7.53	0.6	0.8
R3	6.2	36.1	0.0104	0.0793	5.82	7.62	1.1	0.8
R1P1	11.4	26.8	0.0154	0.0369	2.34	2.4	0.5	0.3
R2P1	11.2	31.0	0.0146	0.0401	2.76	2.75	0.5	0.3
R3P1	9.2	32.9	0.0140	0.0526	3.59	3.76	0.7	0.4
R1P2	14.5	26.7	0.0175	0.0301	1.84	1.72	0.4	0.2
R2P2	8.1	30.1	0.0139	0.0478	3.71	3.43	0.7	0.4
R3P2	11.6	29.9	0.0182	0.0479	2.58	2.63	0.5	0.3

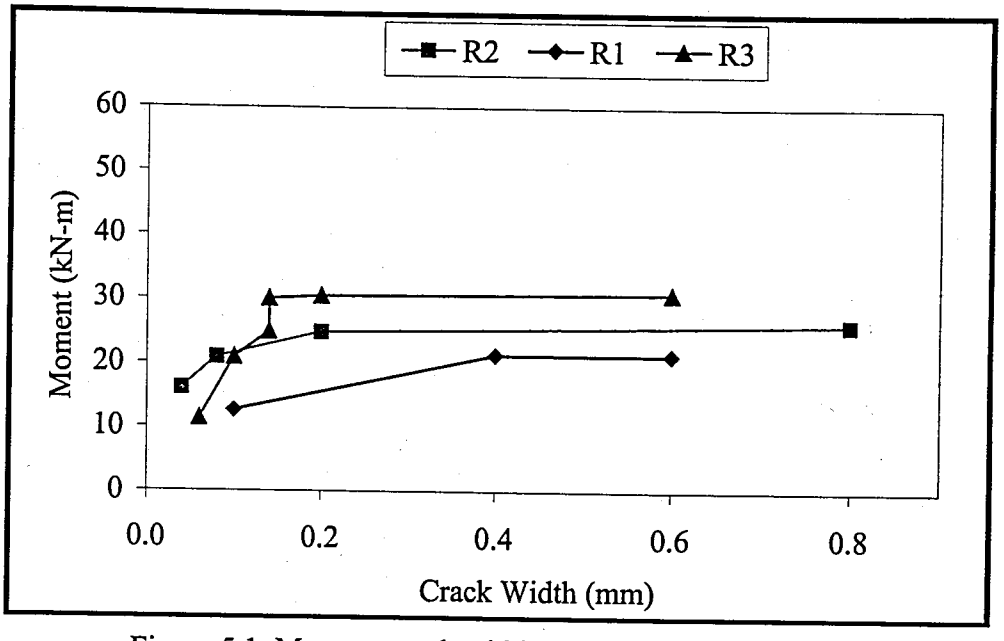

Figure 5.1. Moment crack width curves of virgin specimens

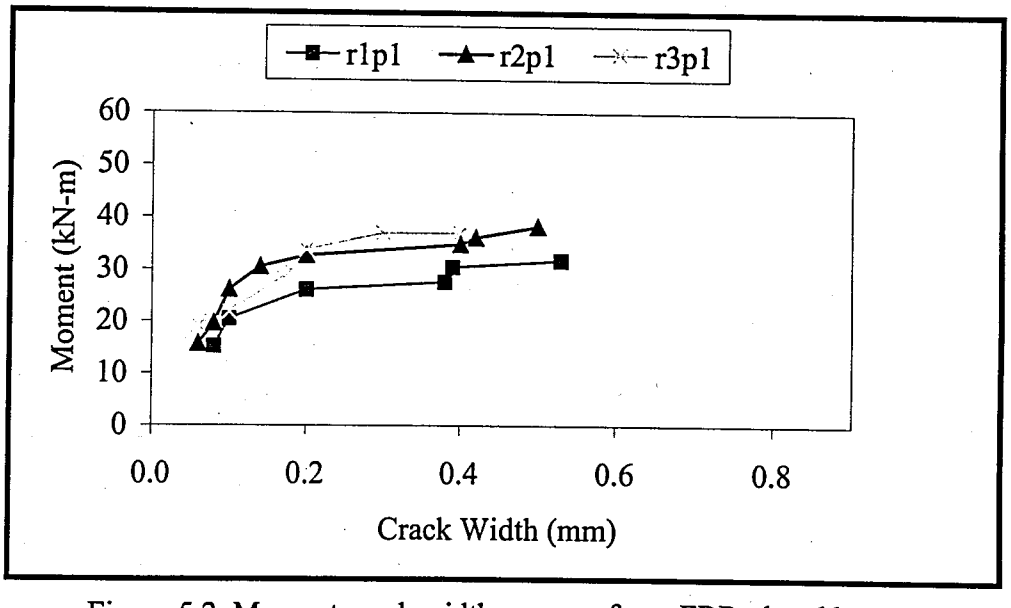

Figure 5.2. Moment crack width curves of one FRP-plated beams

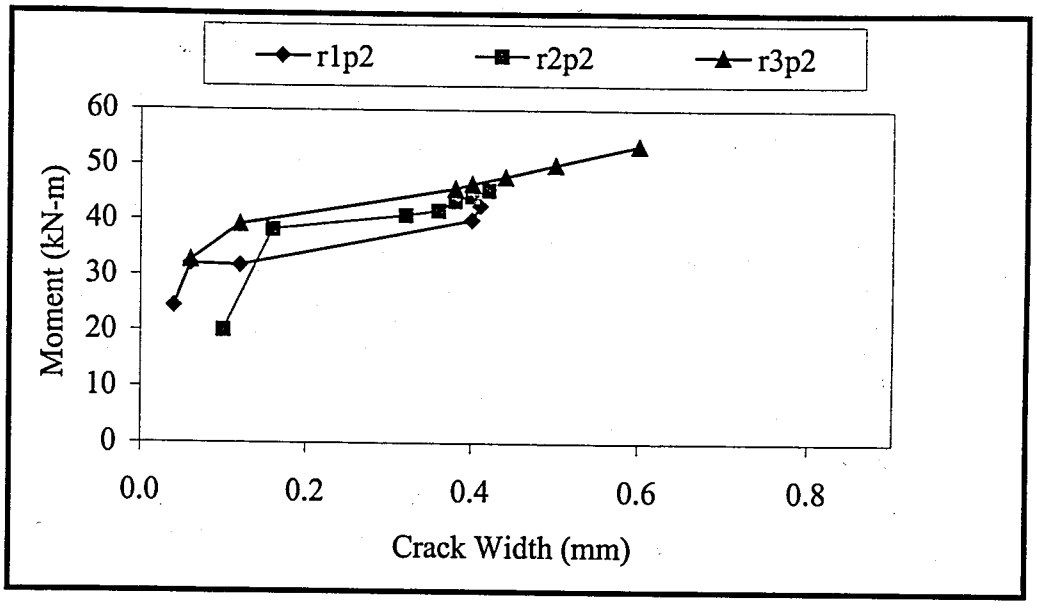

Figure 5.3. Moment crack width curves of two FRP-plated beams

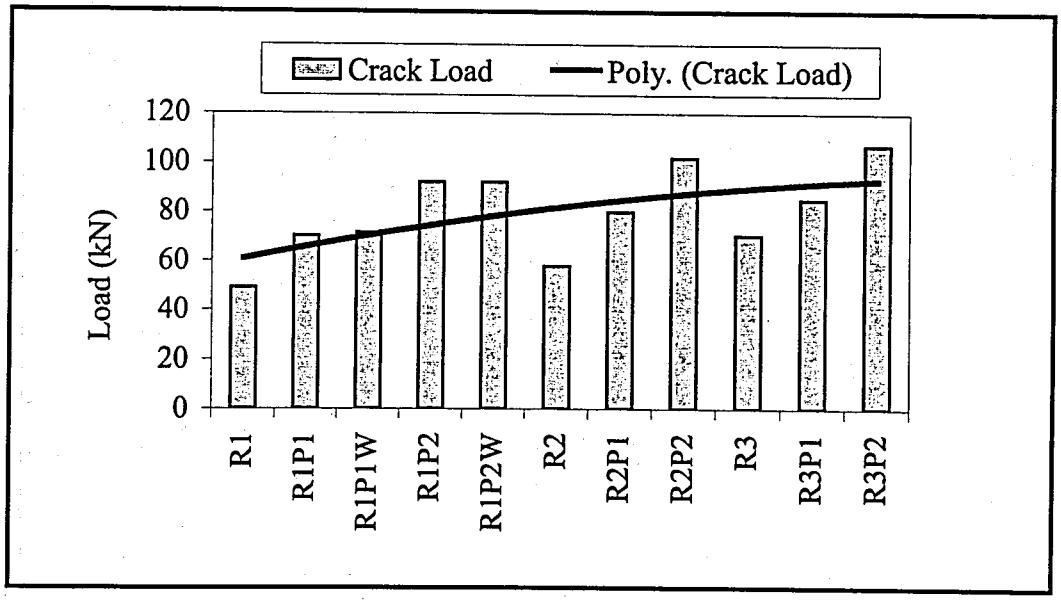

Figure 5.4. Loads at maximum crack width of 0.4 mm

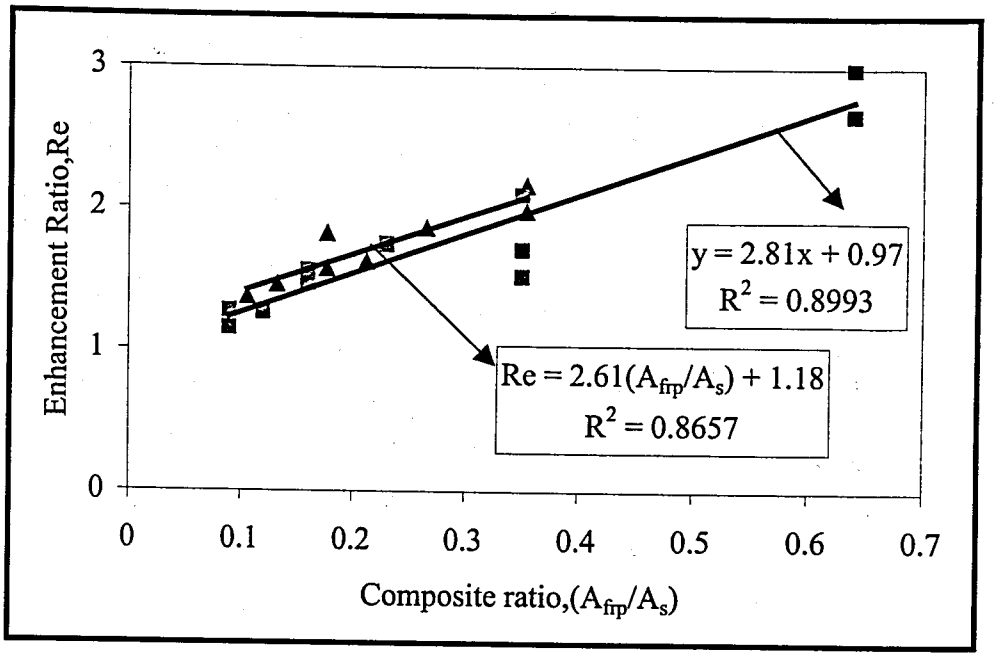

Figure 5.5. Enhancement ratio versus composite ratio diagrams

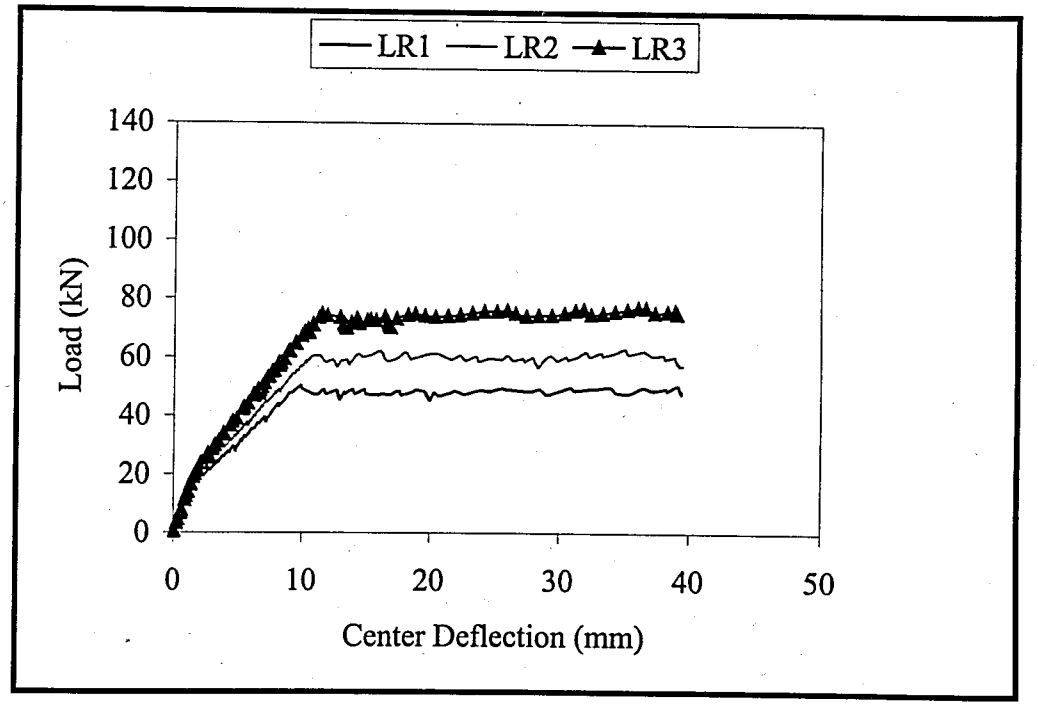

Figure 5.6. Load-center deflection diagrams of virgin specimens

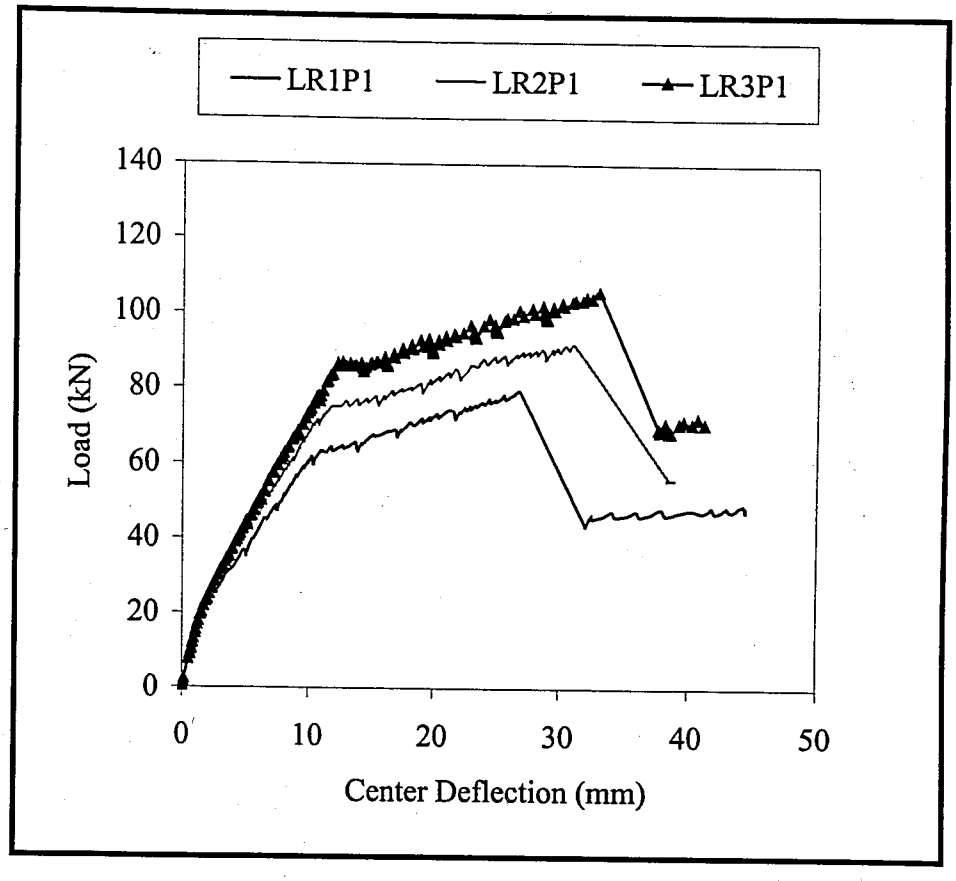

Figure 5.7. Load-center deflection diagrams of one FRP-plated beams

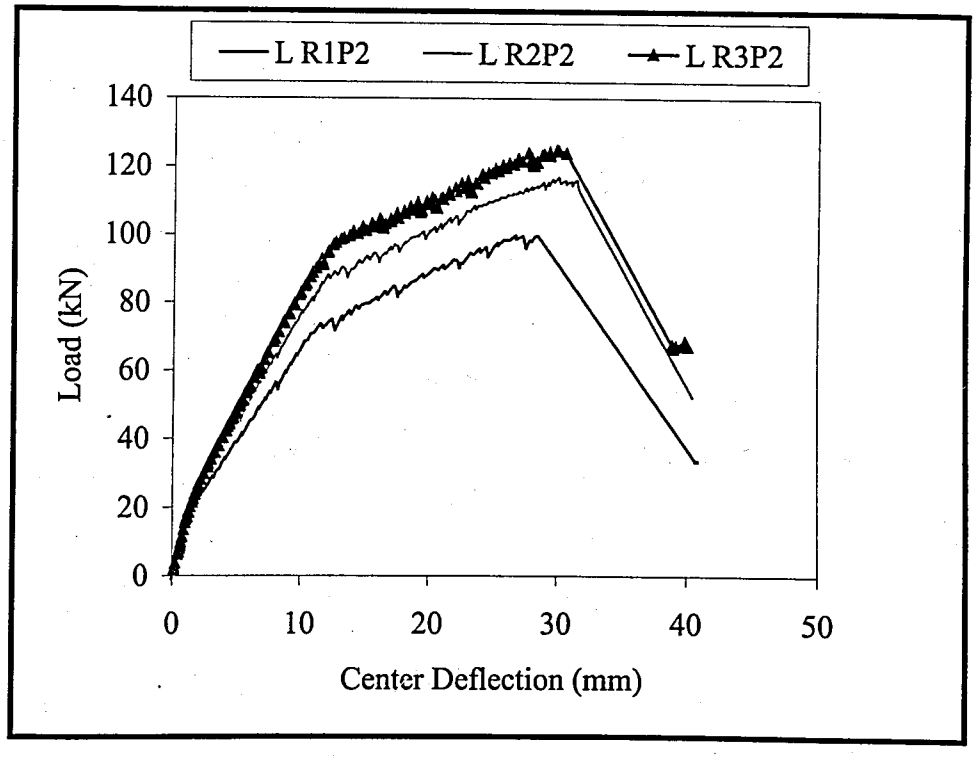

Figure 5.8. Load-center deflection diagrams of two FRP-plated beams

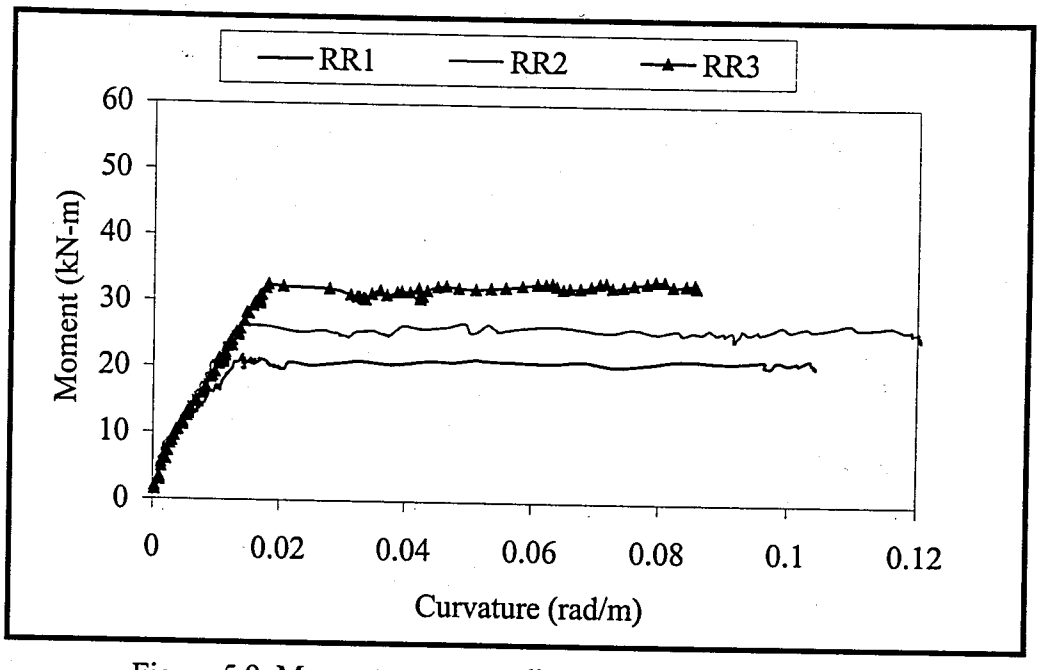

Figure 5.9. Moment-curvature diagrams of virgin specimens

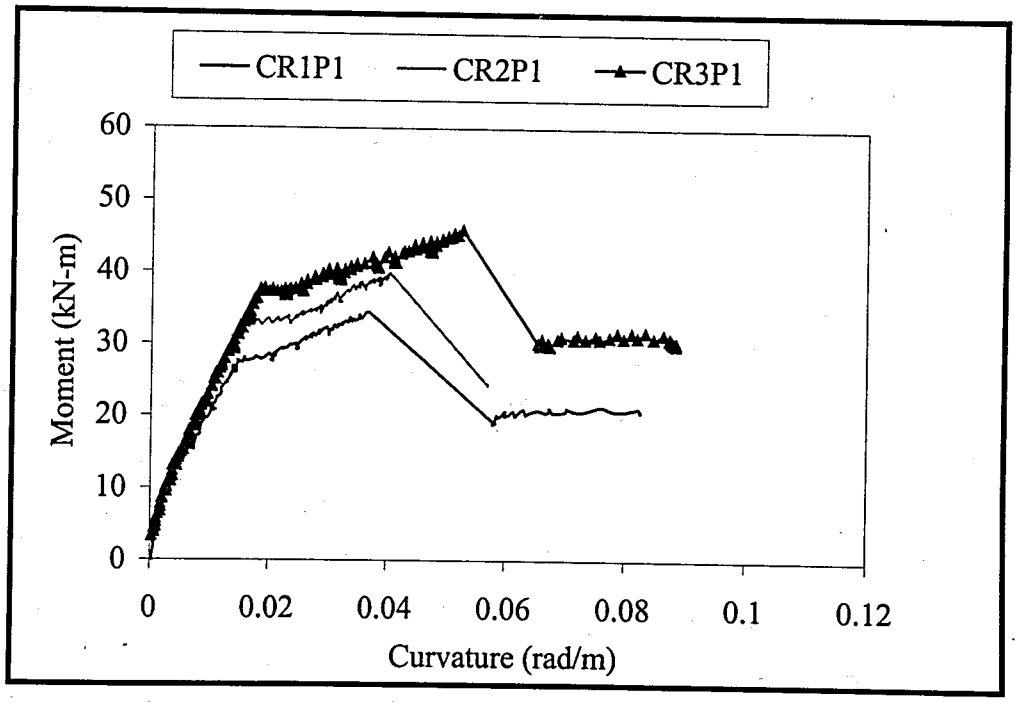

Figure 5.10. Moment-curvature diagrams of one FRP-plated specimens

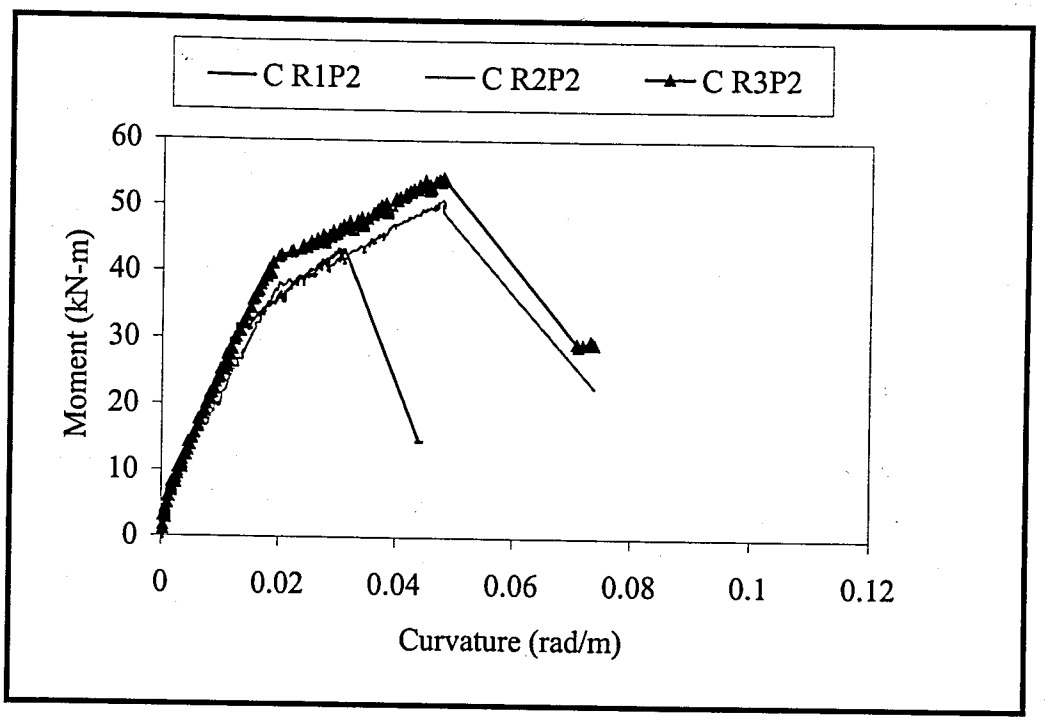

Figure 5.11. Moment-curvature diagrams of two FRP-plated specimens

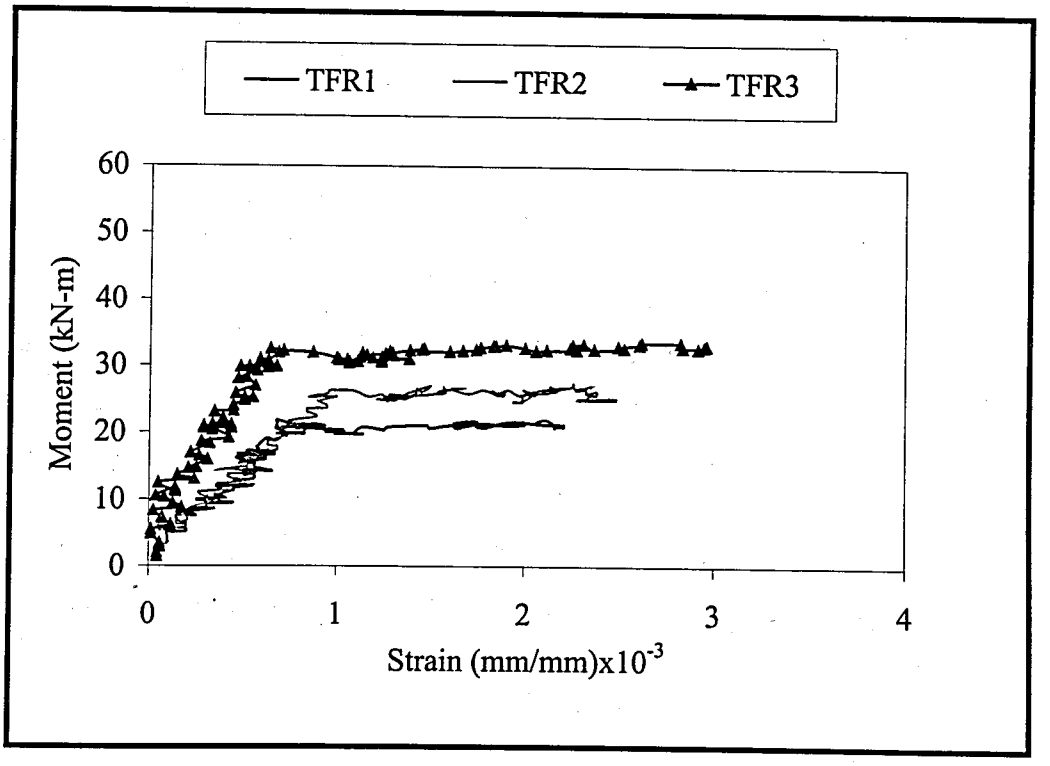

Figure 5.12. Moment-compression strain curves of virgin specimens

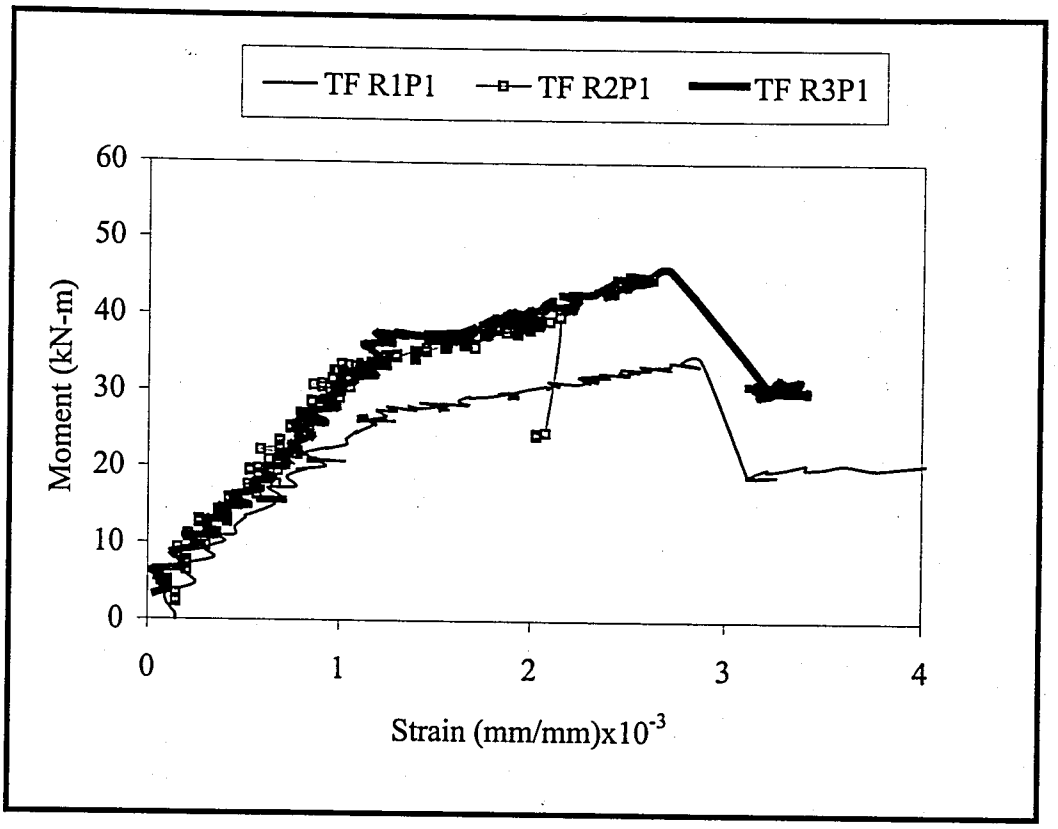

Figure 5.13. Moment-compression strain curves of one FRP-plated beams

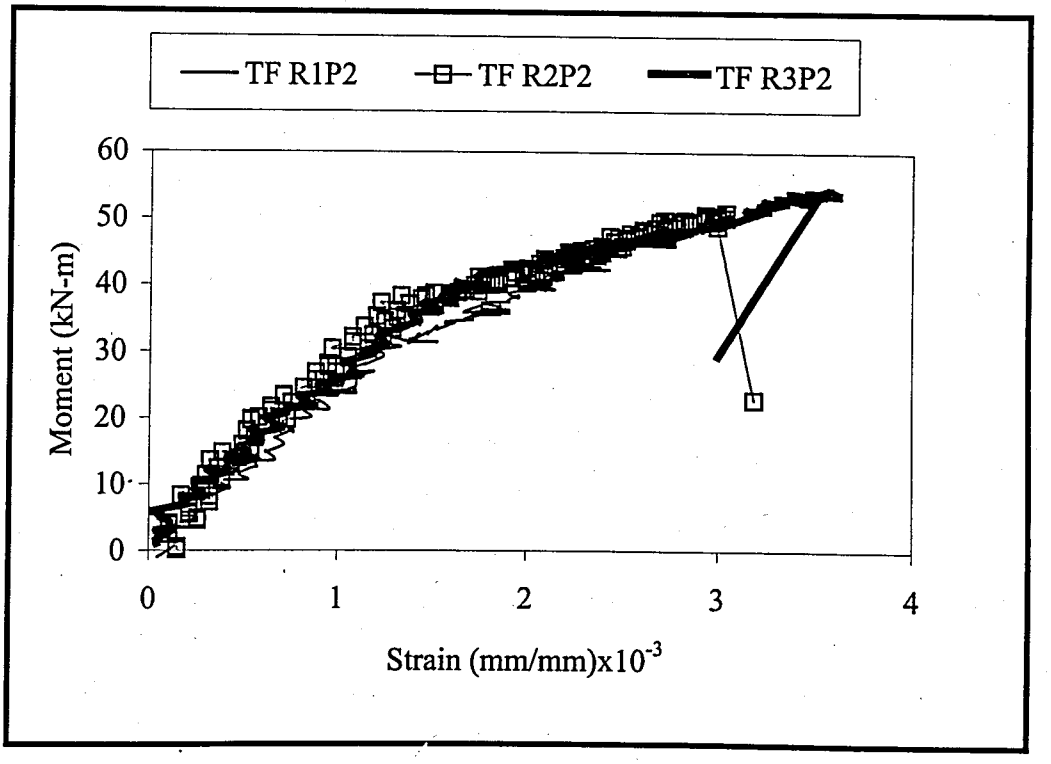

Figure 5.14. Moment-compression strain curves of two FRP-plated beams

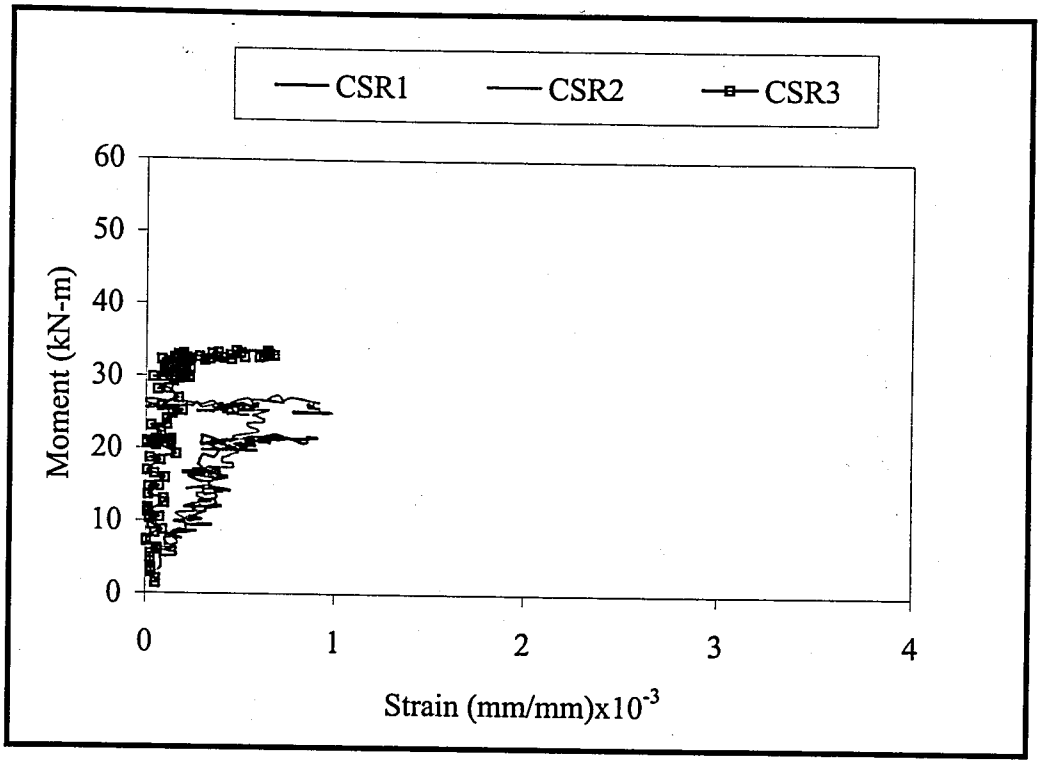

Figure 5.15. Moment- compression steel strain curves of virgin specimens

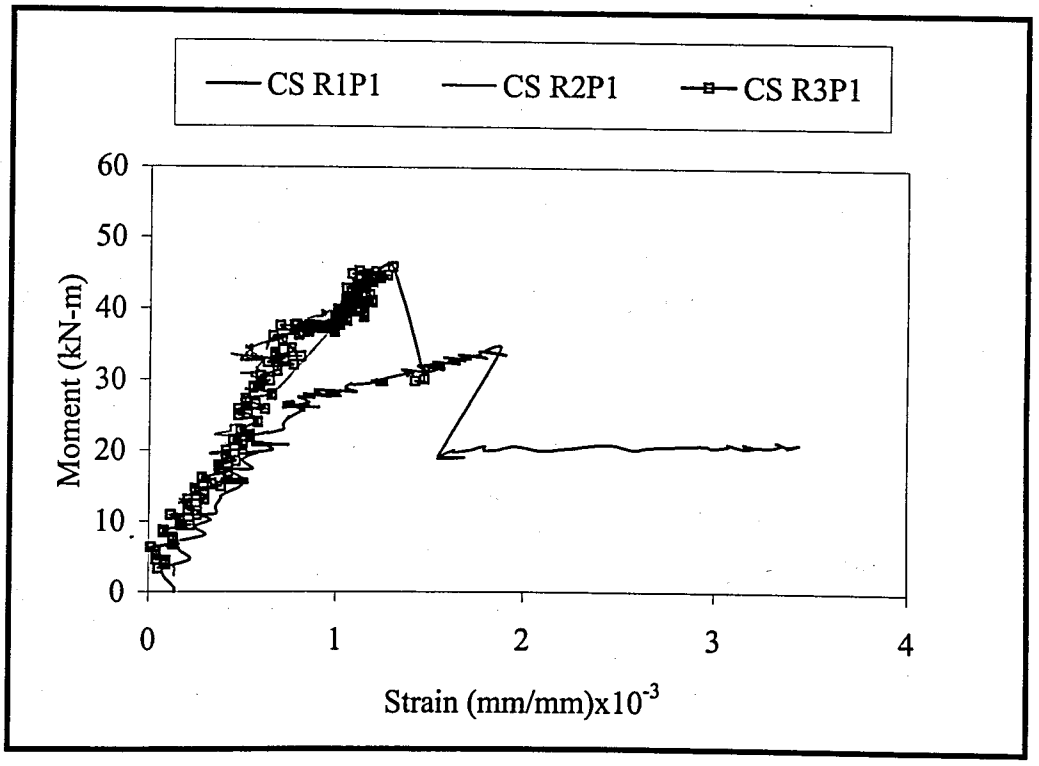

Figure 5.16. Moment- compression steel strain curves of one FRP-plated beams

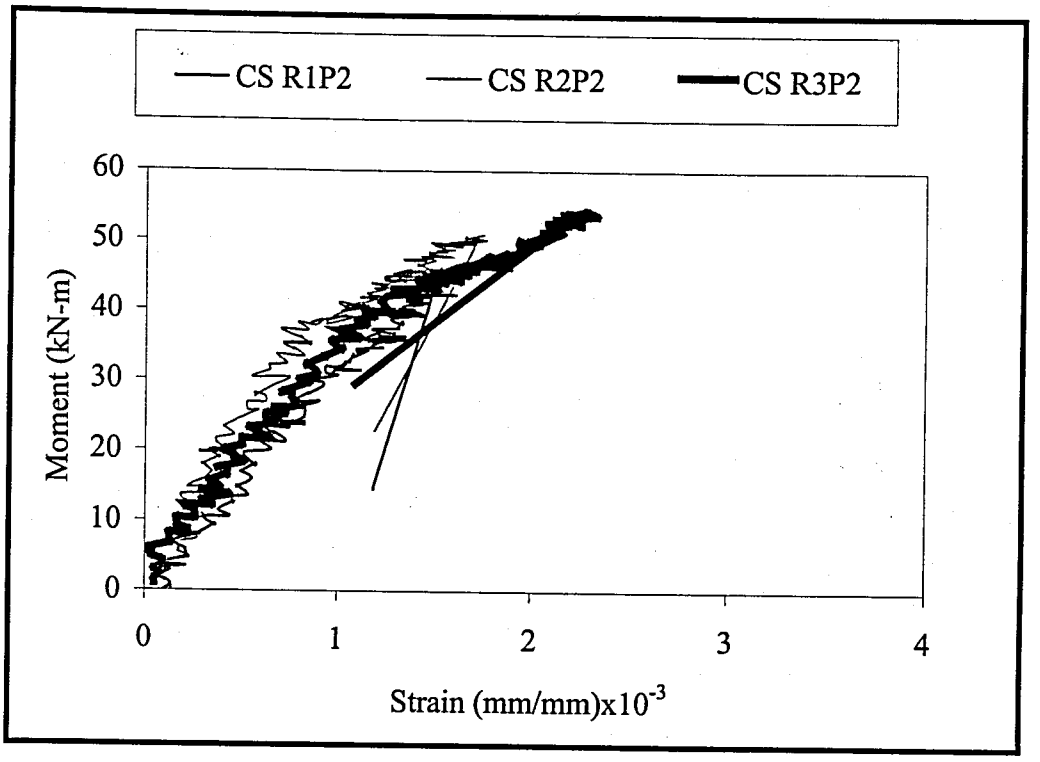

Figure 5.17. Moment-compression steel strain curves of two FRP-plated beams

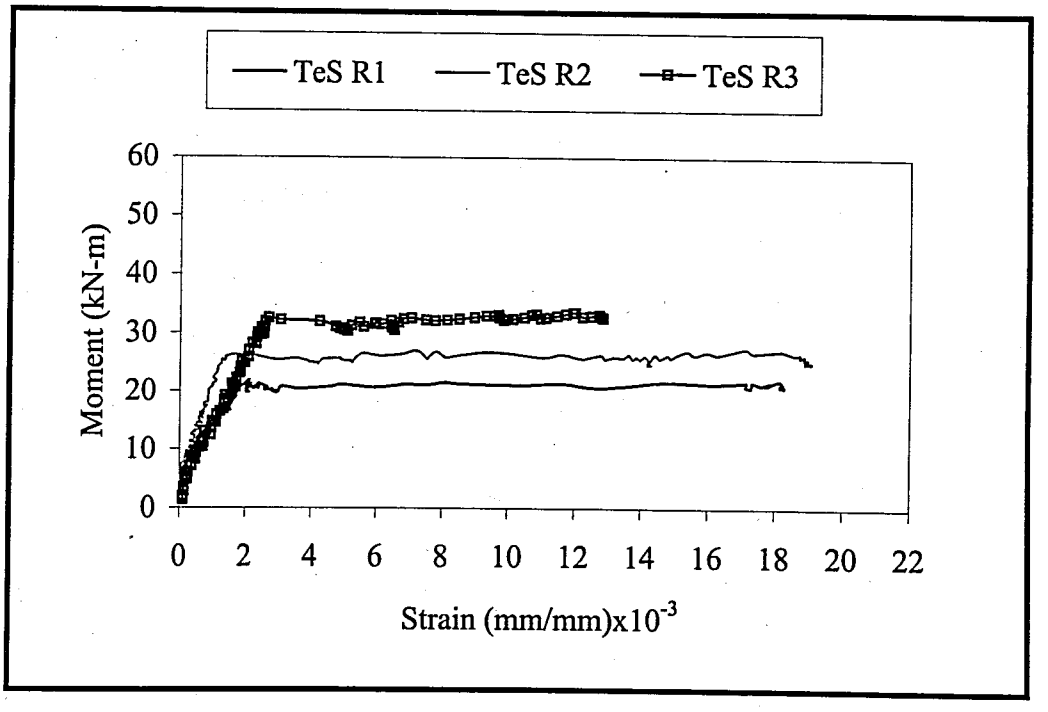

Figure 5.18. Moment-tension steel strain curves of virgin specimens

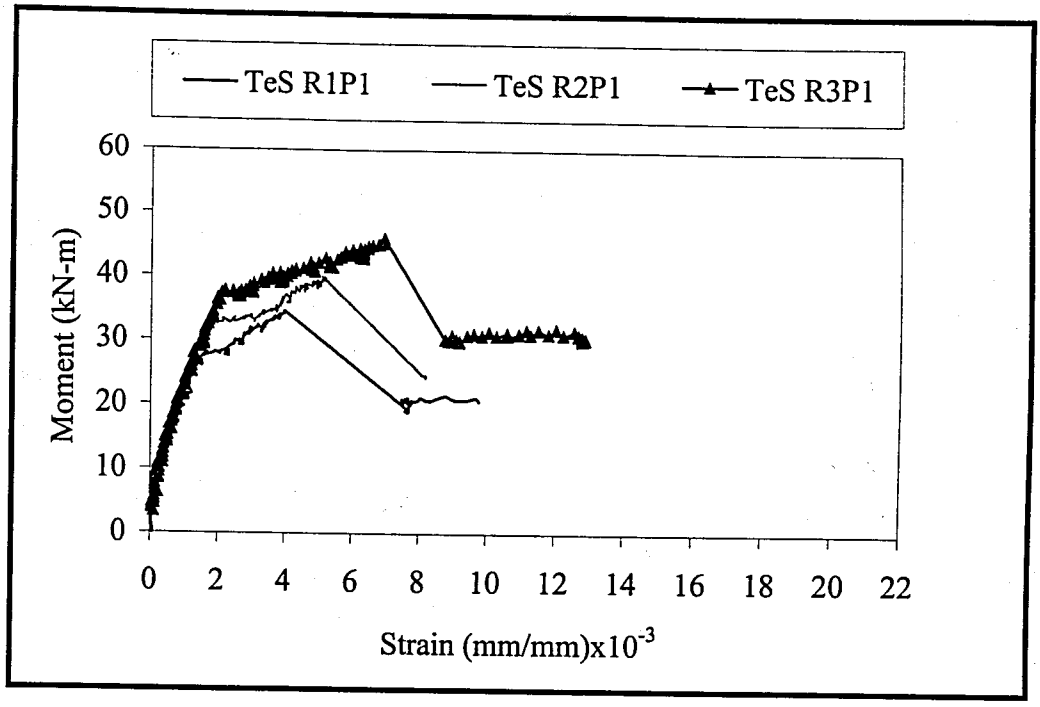

Figure 5.19. Moment-tension steel strain curves of one FRP-plated beams

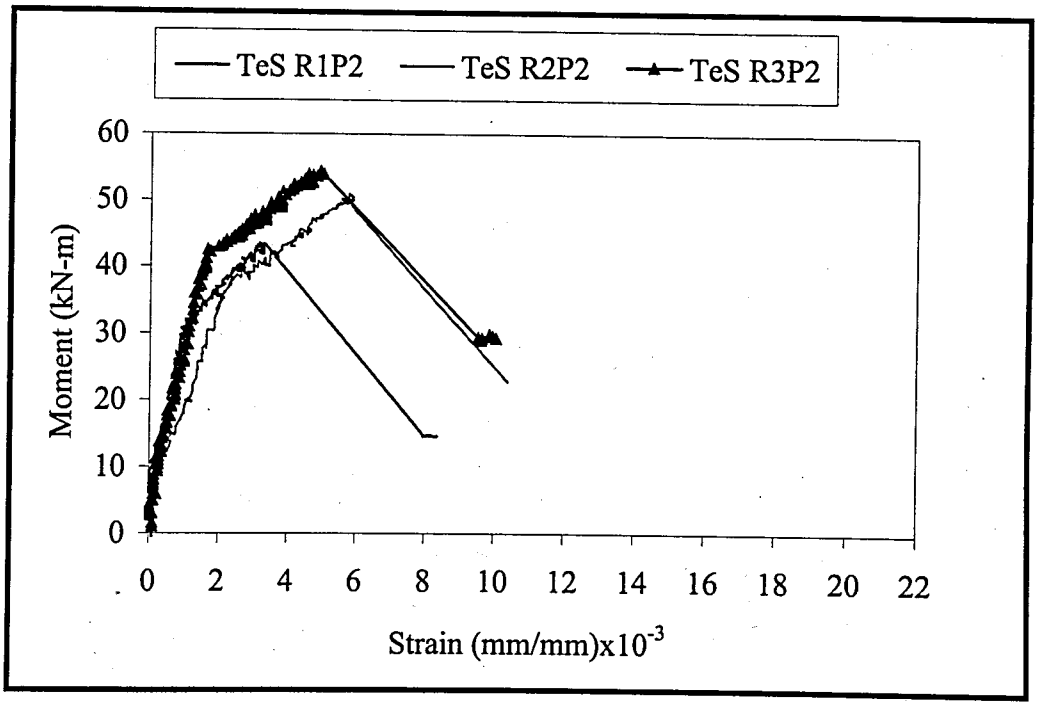

Figure 5.20. Moment-tension steel strain curves of two FRP-plated beams

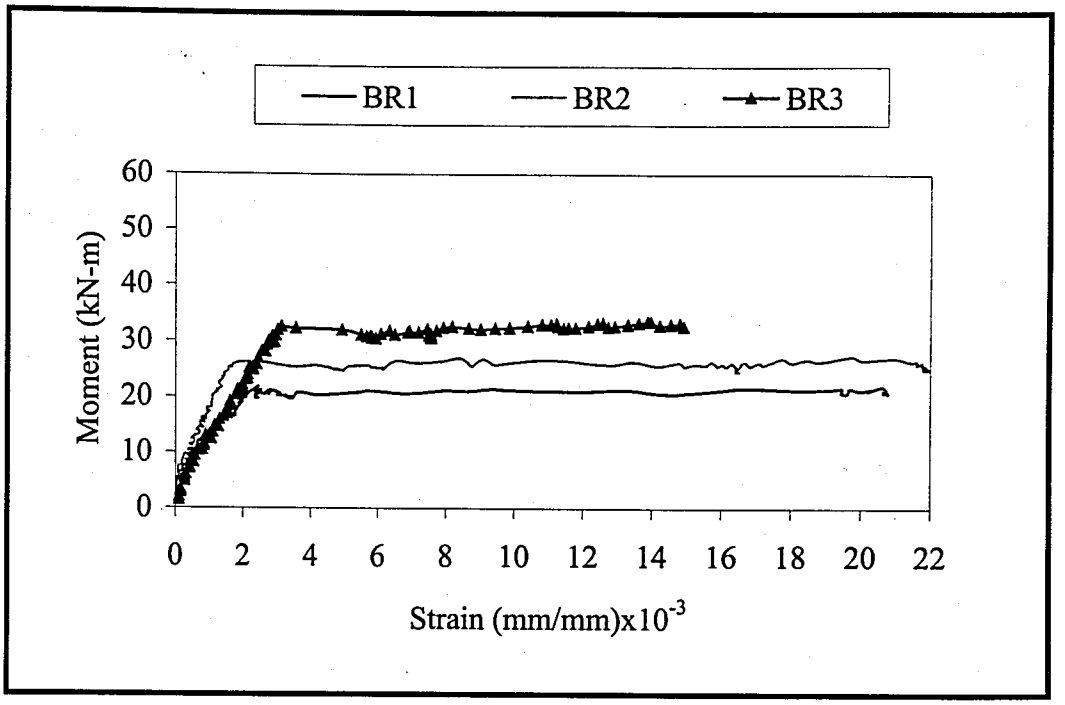

Figure 5.21. Moment-concrete strain at the bottom fiber curves of virgin specimens

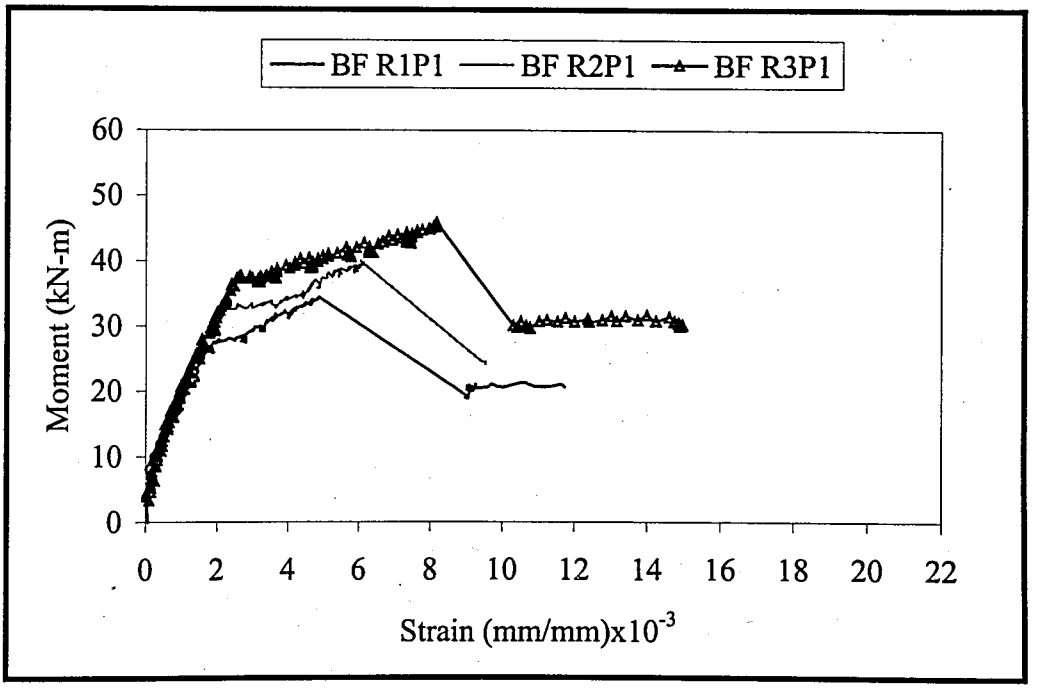

Figure 5.22. Moment-concrete strain at the bottom fiber curves of one FRP-plated beams

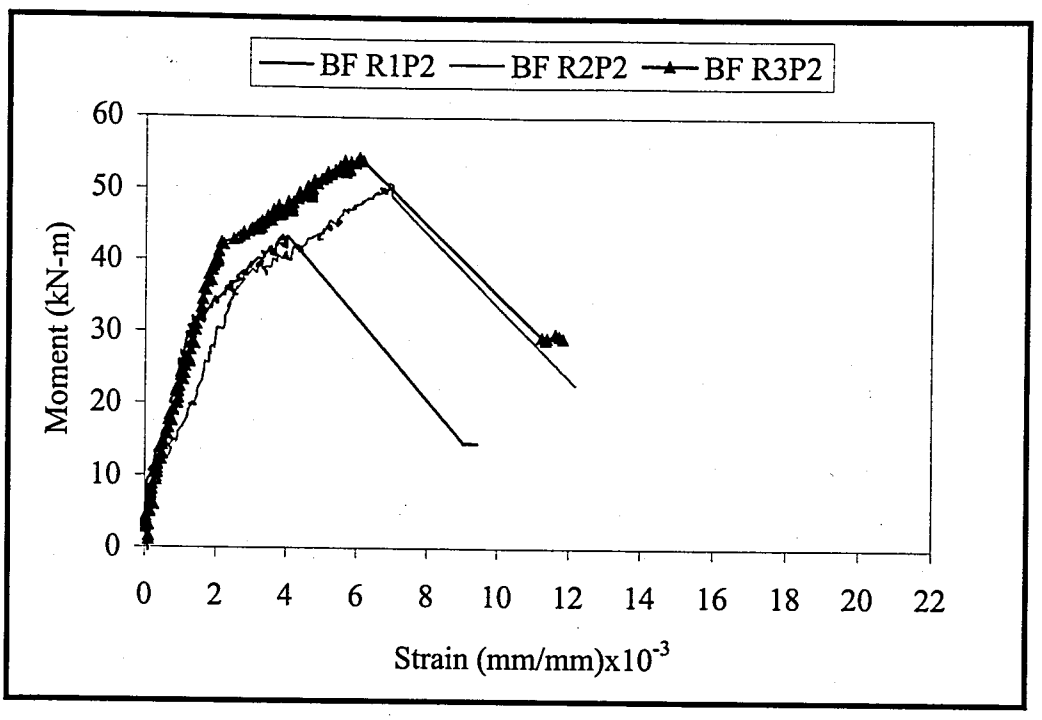

Figure 5.23. Moment-concrete strain at the bottom fiber curves of two FRP-plated beams

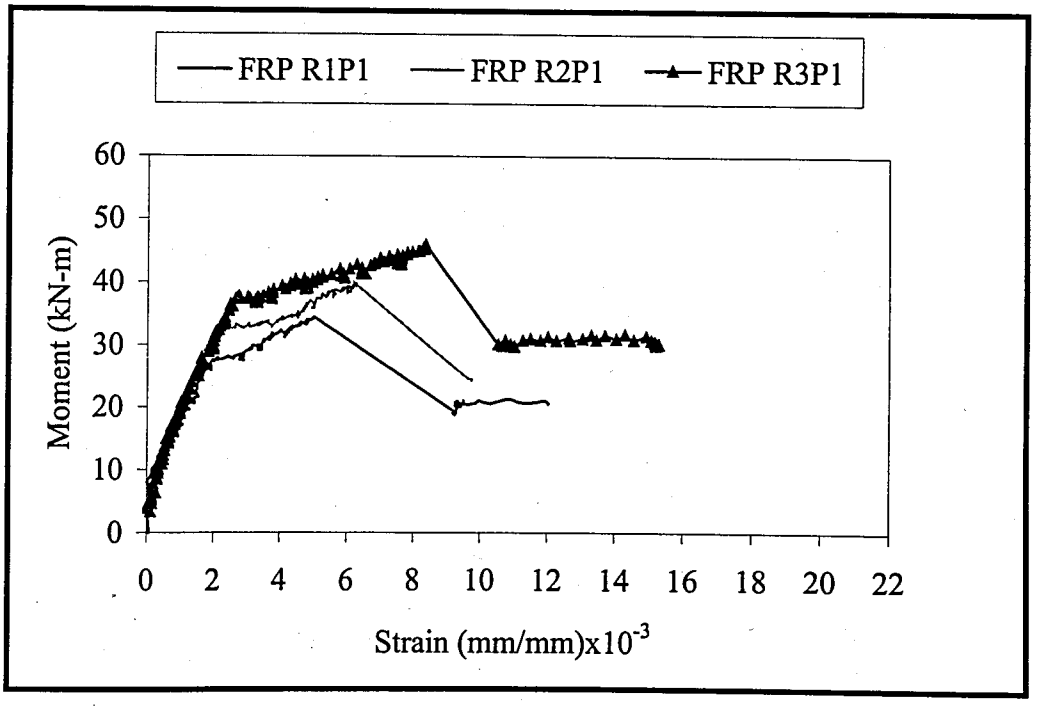

Figure 5.24 Moment-strain at the level of FRP plate curves of one FRP-plated beams

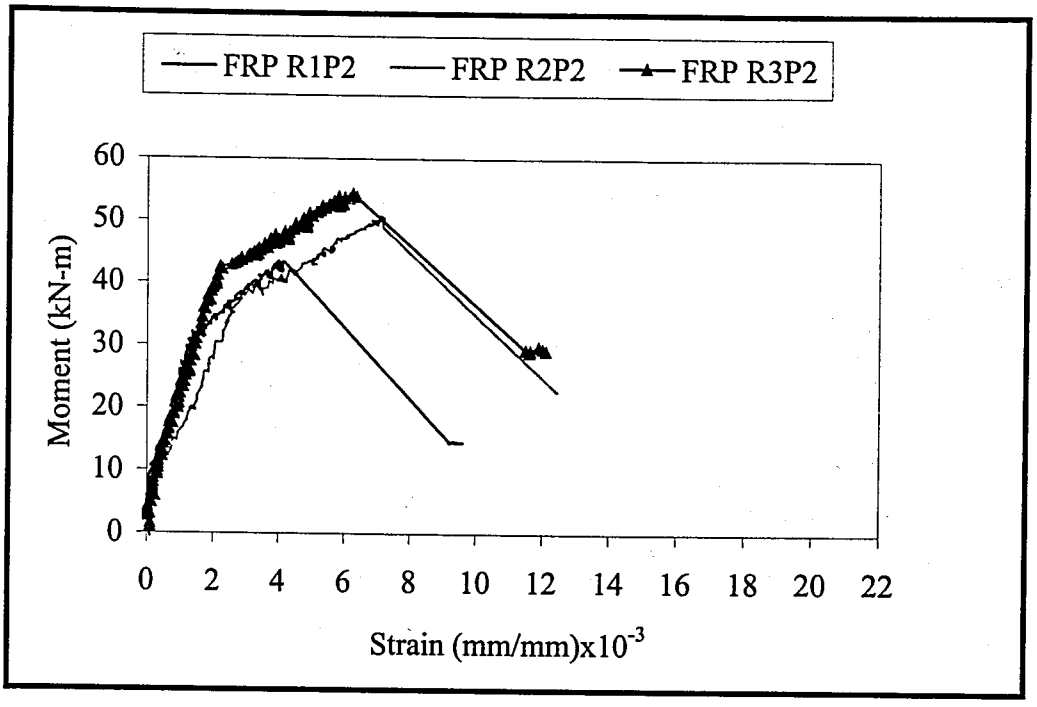

Figure 5.25. Moment-strain at the level of FRP plate curves of two FRP-plated beams

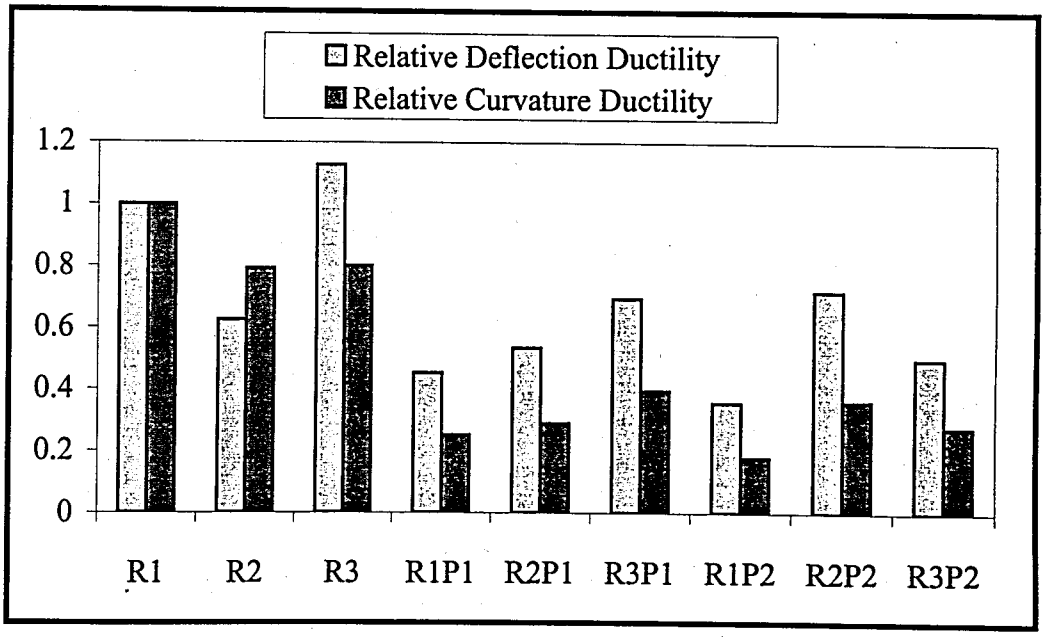

Figure 5.26. Relative ductilities of test specimens without anchorages

5.1.2. Effect of CFRP (Carbon Fiber Reinforced Plastics) Ratio

FRP (Fiber Reinforced Plastics) materials which are used for strengthening of a structural system have great effect on the behaviour of structural element or structural systems.

Cracking is one of the most important parameters that gives us information about structural elements. FRP-strengthened beams can perform an important role to reduce crack width and crack spacing. Moment versus crack width diagrams for different reinforcement ratios are shown in Figure 5.27 to 5.29 while FRP ratio is changing. As can be seen from these figures increasing FRP ratio has a positive effect so as to decrease crack width for the same moment or load values. Especially for lightly reinforced beams, effect of FRP can be seen unquestionably in Figure 5.27. These results agree with the study of Ritchie *et al.*,[30]. It has been reported that externally bonded FRP plates have altered several widely spaced and large width cracks to many more closed spaced, narrower cracks [30]. Figure 5.30 shows minimum, average and maximum crack spacing with respect to plate ratio for every beam. These values presented in Table 5.9 are obtained from the measurements done after the flexural tests of the specimens.

The closed spaced cracks and narrower cracks are important for the serviceability of the structural element. In other words, narrower cracks bring about an increase in the serviceability loads as defined in various standards and specifications. The limit crack width in TS-500 is 0.4 mm for interior beams.

The loads and deflections at the instant of yielding of tension steel, first crack and ultimate load etc. were given in Table 5.2. Test results as seen in Table 5.2 indicate that FRP-plated beams have generally greater load in which tension steel yields or first cracking occurs. Due to the restraining effect of FRP plates on tensile cracks, first cracking loads increase in FRP-plated beams in that first cracking load for FRP-plated beams can exceed the load which tension steel yields for virgin specimens [2]. Nevertheless, it has been reported that plate widths have been very important so as to enhance first cracking loads and to suppress crack opening as well [2]. Ultimate loads and ratios are given in Table 5.10. It can be noticed that strengthening effect is achieved much more for lightly

reinforced beams (R1, R1P1, R1P2). For example, while an increase in ultimate load for the beam of R1P1 is about 98 per cent with respect to virgin specimen of R1 beam, it is approximately 62 per cent for the beam of R3P2 with respect to the beam of R3. The decrease recorded in ultimate load can manifest the effectiveness of strengthening on the lightly reinforced beams.

Load-deflection curves and moment curvature curves can be depicted as the following from Figure 5.31 to Figure 5.36. Those figures indicate the effect of FRP on the behaviour of test beams while reinforcement ratio is being kept constant. Increases in strength and stiffness can be seen clearly in those figures. Behaviour of all beams are linearly elastic up to the first cracking after the first cracking stiffnesses of all beams are changing due to the shifting moment of inertia. As it can be easily understood from the following figures, FRP starts to have an effect on the behaviour of the beams after yielding of steel. The effectiveness of FRP is better realized for lightly reinforced beams. For instance, strength and stiffness increases in the series of R1 beams are much higher than the beams of R2 and R3 series.

Apart from load deflection curves and moment curvature curves, moment versus strain curves are obtained using equilibrium and compatibility equations at various levels.

Ultimate strain at the top fiber in concrete section versus moment diagrams are presented in Figure 5.37 to 5.39. In the virgin specimens, the stress in tension steel bars increases until the steel yields. After that, a large portion of any extra stress is captured by large deformations in the steel which reduces the increase in concrete compressive strain. In the FRP-strengthened beams, tensile stresses are shared between the reinforcing steel bars and FRP plates. Thus, the stress carried by steel bars generally will be less. Therefore, concrete strains at the top fiber in FRP-plated beams are usually greater than those in the control beams at the same load [23]. This is generally satisfied by the test results obtained as seen in Figure 5.37 to 5.39. Table 5.11 shows the ultimate moment and ultimate compression strain values. Ultimate compression strains and compression strain at the instant of yielding of tensile steel are generally inclined to increase.

Moment-strain curves for tension steel and bottom fiber of the concrete section demonstrate similarities to each other. These diagrams are depicted in Figure 5.40 to 5.45. Increases in yield loads are better visualized for the lightly reinforced beams (Figure 5.40) due to decreasing of the stresses in the tension steel. Since the stresses in the tension steel are shifted by FRP plates, yield loads increase. Strain values calculated by using compatibility equations are illustrated in Table 5.12 and Table 5.13. In FRP-plated beams strains in compression steel are inclined to enhance like concrete compressive strains. Moment-strain at compression steel diagrams are exhibited in Figure 5.46 to 5.48. These figures also show that ultimate strains are generally much higher than those of virgin specimens in that compression steel reaches its yield strain in FRP plated beams of R3 series.

Strains at the level of FRP are calculated using compatibility equations as well. Table 5.14 illustrates the FRP strains at max load and at the instant of yielding of steel. After yielding of tension steel, strains in FRP increase more rapidly showing that FRP plates carry on extra stresses of the tensile component in the concrete section. In addition, moment versus strains at FRP curves are shown in Figure 5.49 to 5.51. Whilst FRP plate ratio increases, strain at FRP generally tends to decrease at the same load and at the peak load. As the decrease in R1 series is being 25 per cent with respect to R1P1, in R3 series it is approximately 34 per cent with respect to R3P1. However, ultimate strains in FRP in the R2 series at failure tend to increase amazingly.

Ultimate loads of the beams and modes of failure of the test specimens can be summarized in Table 5.15. As indicated in Table 5.15, virgin specimens have failed in conventional ductile flexure with yielding of tension steel. Crushing of concrete in compression zone could not be observed. However, it is believed that yielding of tension steel would be followed by crushing of concrete in compression zone if flexural tests of virgin specimens have been continued. In virgin specimens, shear cracks have not occurred significantly because all beams were reinforced in shear to preclude premature shear failure. Strengthening of RC beams with FRP has changed the mode of failure from ductile, conventional flexural manner into a brittle manner with sudden drop of the load. In all FRP-plated beams, FRP plates have separated from concrete beam in one of the shear spans with a layer of concrete which still bonded to the FRP plate. The thickness of this

concrete layer changes associated with plate ratio. Besides, for a single layer of two FRP plated beams, concrete layer between FRP plate and steel reinforcement bars is generally separated around mid-span. For almost all beams except R1P1W and R2P1, separation has become at the side of right support. At all beams de-bonding type of failure are observed due to peeling off of the FRP plate. For the more heavily beams with respect to FRP ratio and reinforcement ratio crushing of concrete in compression zone has recorded such as R2P2 and R3P2. This situation brings about that the beams could not transfer load to FRP plate. So, FRP plates could not be used effectively. Thus, the situation of existing structure should be checked before application and then strengthening should be applied. Otherwise, optimum solution would not be found. FRP-plated beams with plate end anchorages have shown slow slippage of the FRP laminate. However, failure was due to peeling off of the FRP plate accomplished by tearing away of CFRP sheet at tension face of the beam. Besides, wrapping of shear span of the beam has postponed the failure and has resulted in preceding warning signs such as snapping sounds.

Although strengthening of the RC beams with FRP increases stiffness and strength of the structural element, it reduces crack width and results in fine distributed cracks, ductility of FRP-plated beams somewhat decreases as well. Ductility can be described as the capacity of structural element or structural system to put up with large inelastic deformations prior to total collapse. Measures of ductility are associated with structural parameters such as curvature or deflection. Ductility can be stated as an index which is the ratio between the curvature/deflection at the instant of ultimate load and the curvature /deflection at the instant of yielding of steel. Since FRP-plated beams have no definite yield region, structural ductility of FRP plated beams are very low [19]. The structural ductility decreases up to 18 per cent based on curvature ductility and 36 per cent based on deflection ductility with respect to R1 beam. These low values agree with the available results obtained by other researchers. Curvature ductility and deflection ductility values of the test specimens are listed in Table 5.16. As FRP ratio changes at constant reinforcement ratio, curvature ductility and deflection ductility are also shown in Figure 5.52. As shown in Figure 5.52, structural ductility generally decreases quickly while FRP ratio increases.

Table 5.9. Crack spacing values of the test specimens

BEAMS	Crack Spacing (cm)		
	a_{min}	a_{max}	$a_{average}$
R1	5.5	17.0	11.1
R1P1	3.0	14.3	7.9
R1P1W	4.8	12.2	7.3
R1P2	2.8	11.2	7.4
R1P2W	4.5	12.3	9.0
R2	2.6	22.0	13.0
R2P1	7.6	14.5	10.6
R2P2	2.2	15.6	8.1
R3	6.0	23.7	13.5
R3P1	5.2	17.3	9.6
R3P2	3.5	14.0	9.2

Table 5.10. Ultimate loads and ratios with respect to virgin specimens of each batch

BEAMS	M_{max}	L_{max} for M_{max}	(P_{FRP}/P_{virgin})-1 ratios
	kN-m	kN	
R1	21.92	50.40	
R1P1	34.39	79.06	0.57
R1P1W	39.83	91.57	0.82
R1P2	43.417	99.81	0.98
R1P2W	47.429	109.03	1.16
R2	27.368	62.92	
R2P1	39.83	91.57	0.46
R2P2	50.87	116.94	0.86
R3	33.3	77.08	
R3P1	45.85	105.41	0.37
R3P2	54.307	124.84	0.62

Table 5.11. Development of compression strain with respect to FRP ratio

BEAMS	Moments			$\varepsilon_{top\ fiber}$ x 0.001		
	M_{max}	M @0.003	M @0.00155	ε_{max}	ε @0.003	ε @0.00155
R1	21.92	-	17.77	2.109	-	0.571
R1P1	34.39	-	27.37	2.871	-	1.295
R1P2	43.42	-	33.96	2.286	-	1.571
R2	27.37	-	26.22	2.2585	-	0.96
R2P1	39.83	-	31.67	2.146	-	0.961
R2P2	50.87	50.15	28.09	3.038	3.016	0.947
R3	33.3	-	20.49	2.618	-	0.332
R3P1	45.85	-	29.66	2.715	-	0.968
R3P2	54.31	50.29	40.26	3.571	3.051	1.6296

Table 5.12. Development of tension steel strain with respect to FRP ratio

BEAMS	Moments			$\varepsilon_{tension\ steel}$ x 0.001		
	M_{max}	M @0.003	M @0.00155	ε_{max}	ε @0.003	ε @0.00155
R1	21.92	-	17.77	18.131	-	1.5579
R1P1	34.39	-	27.37	3.984	-	1.562
R1P2	43.42	-	33.96	3.162	-	1.6
R2	27.37	-	26.22	17.138	-	1.617
R2P1	39.83	-	31.67	5.08	-	1.646
R2P2	50.87	50.15	28.09	5.763	5.54	1.616
R3	33.3	-	20.49	11.974	-	1.583
R3P1	45.85	-	29.66	6.9	-	1.591
R3P2	54.31	50.29	40.26	4.91	3.688	1.598

Table 5.13. Development of bottom fiber strain of concrete section wrt. FRP ratio

BEAMS	Moments			$\varepsilon_{bottom\ fiber}$ x 0.001		
	M_{max}	M @0.003	M @0.00155	ε_{max}	ε @0.003	ε @0.00155
R1	21.92	-	17.77	20.61	-	1.819
R1P1	34.39	-	27.37	4.869	-	1.931
R1P2	43.42	-	33.96	3.884	-	2.02
R2	27.37	-	26.22	19.768	-	1.97
R2P1	39.83	-	31.67	6.053	-	1.995
R2P2	50.87	50.15	28.09	6.911	6.656	1.951
R3	33.3	-	20.49	13.877	-	1.833
R3P1	45.85	-	29.66	8.164	-	1.927
R3P2	54.31	50.29	40.26	6.06	4.6	2.036

Table 5.14. Development of FRP strain with respect to FRP ratio

BEAMS	Moments			$\varepsilon_{FRP\ fiber}$ x 0.001		
	M_{max}	M @0.003	M @0.00155	ε_{max}	ε @0.003	ε @0.00155
R1	21.92	-	17.77	-	-	-
R1P1	34.39	-	27.37	5.001	-	1.987
R1P2	43.42	-	33.96	3.992	-	2.08
R2	27.37	-	26.22	-	-	-
R2P1	39.83	-	31.67	6.199	-	2.05
R2P2	50.87	50.15	28.09	7.084	6.823	2
R3	33.3	-	20.49	-	-	-
R3P1	45.85	-	29.66	8.354	-	1.977
R3P2	54.31	50.29	40.26	6.23	4.739	2.101

Table 5.15. Summary of ultimate loads and modes of failure

BEAMS	ULTIMATE LOADS (kN)	MODES OF FAILURE
R1	50.40	Yielding of tension steel
R1P1	79.06	De-bonding of CFRP plate due to peeling off
R1P1W	91.57	De-bonding of CFRP plate due to peeling off, slow slippage
R1P2	99.81	De-bonding of CFRP plate due to peeling off
R1P2W	109.03	De-bonding of CFRP plate due to peeling off, slow slippage
R2	62.92	Yielding of tension steel
R2P1	91.57	De-bonding of CFRP plate due to peeling off
R2P2	116.94	De-bonding of CFRP plate due to peeling off, crushing of concrete
R3	77.08	Yielding of tension steel
R3P1	105.41	De-bonding of CFRP plate due to peeling off
R3P2	124.84	De-bonding of CFRP plate due to peeling off, crushing of concrete

Table 5.16. Ductilities of test specimens without plate end anchorages with respect to FRP ratio

					Deflection ductility	Curvature ductility	Relative ductility ratios	
BEAMS	**Δ steel yields**	**Δ for max load**	**ϕ steel yields**	**ϕ for max load**	μ_D	μ_ϕ	μ_D	μ_ϕ
R1	7.6	39.1	0.0109	0.1033	5.17	9.51	1.0	1.0
R1P1	11.4	26.8	0.0154	0.0369	2.34	2.40	0.5	0.3
R1P2	14.5	26.7	0.0175	0.0301	1.84	1.72	0.4	0.2
R2	10.9	35.0	0.0146	0.1096	3.23	7.53	0.6	0.8
R2P1	11.2	31.0	0.0146	0.0401	2.76	2.75	0.5	0.3
R2P2	8.1	30.1	0.0139	0.0478	3.71	3.43	0.7	0.4
R3	6.2	36.1	0.0104	0.0793	5.82	7.62	1.1	0.8
R3P1	9.2	32.9	0.0140	0.0526	3.59	3.76	0.7	0.4
R3P2	11.6	29.9	0.0182	0.0479	2.58	2.63	0.5	0.3

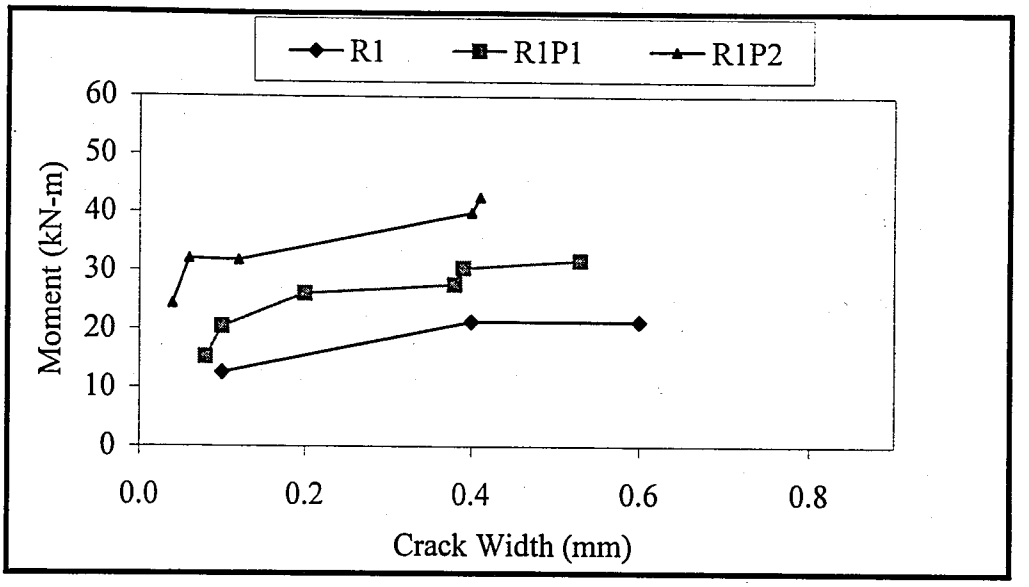

Figure 5.27. Moment crack width curves of the batch of R1 beams without anchorages

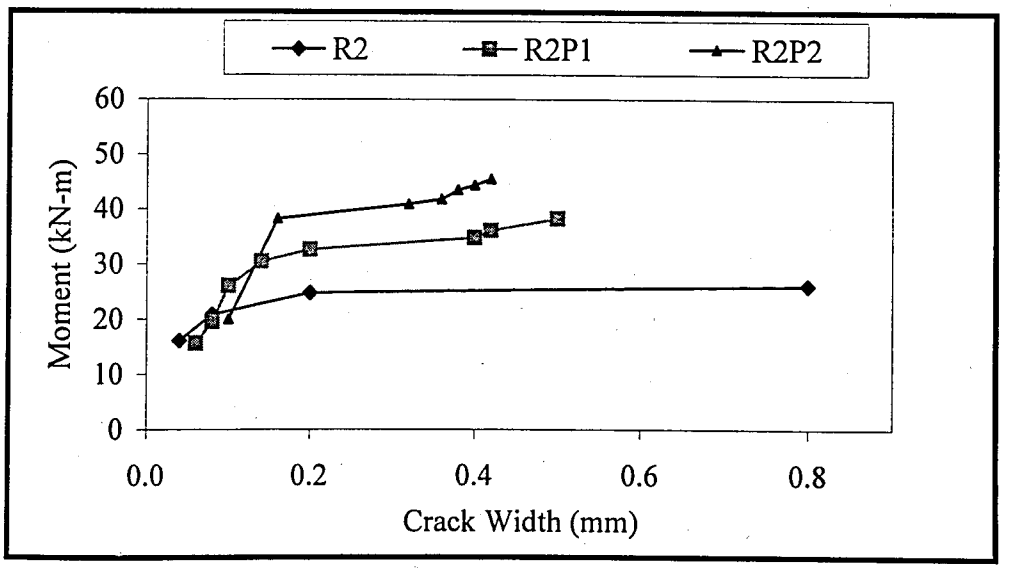

Figure 5.28. Moment crack width curves of the batch of R2 beams

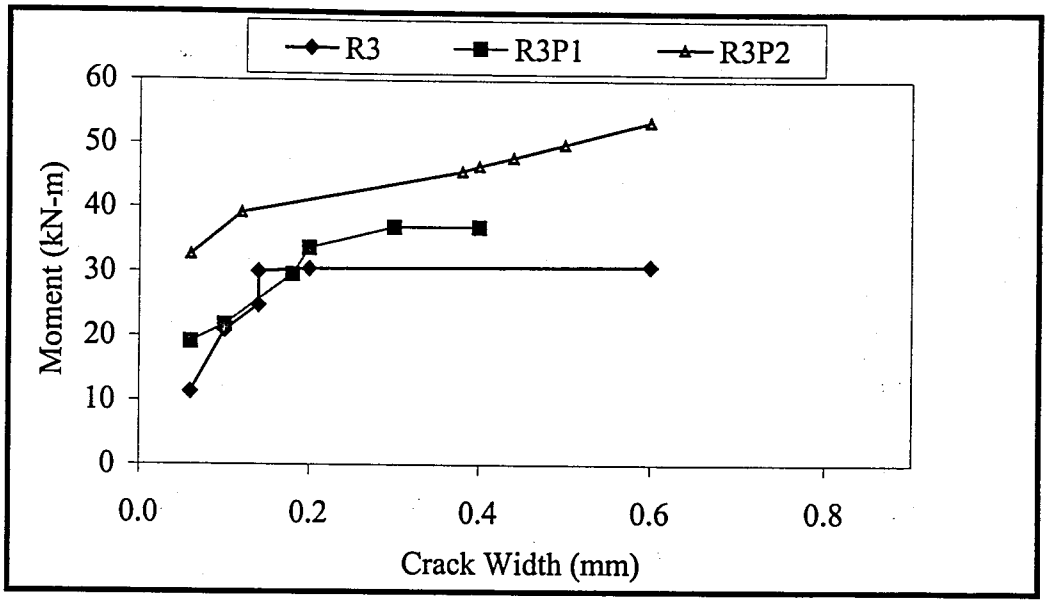

Figure 5.29. Moment crack width curves of the group of R3 beams

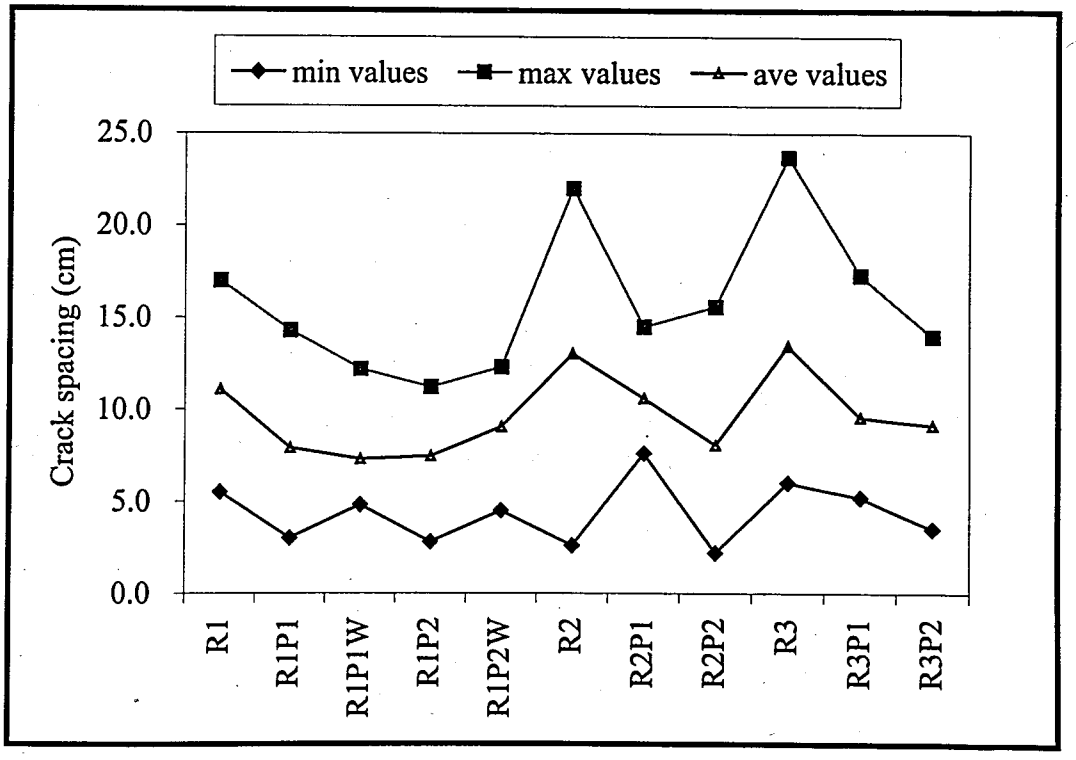

Figure 5.30. Crack spacing values of test specimens

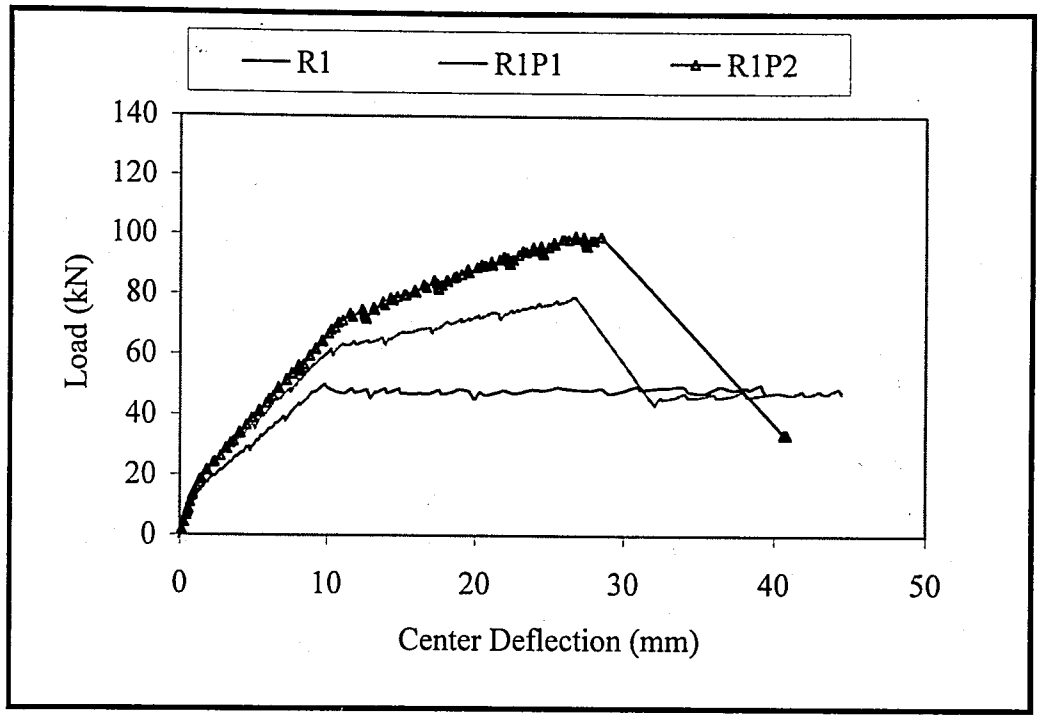

Figure 5.31. Load-center deflection curves of R1 series without anchorages wrt. FRP ratio

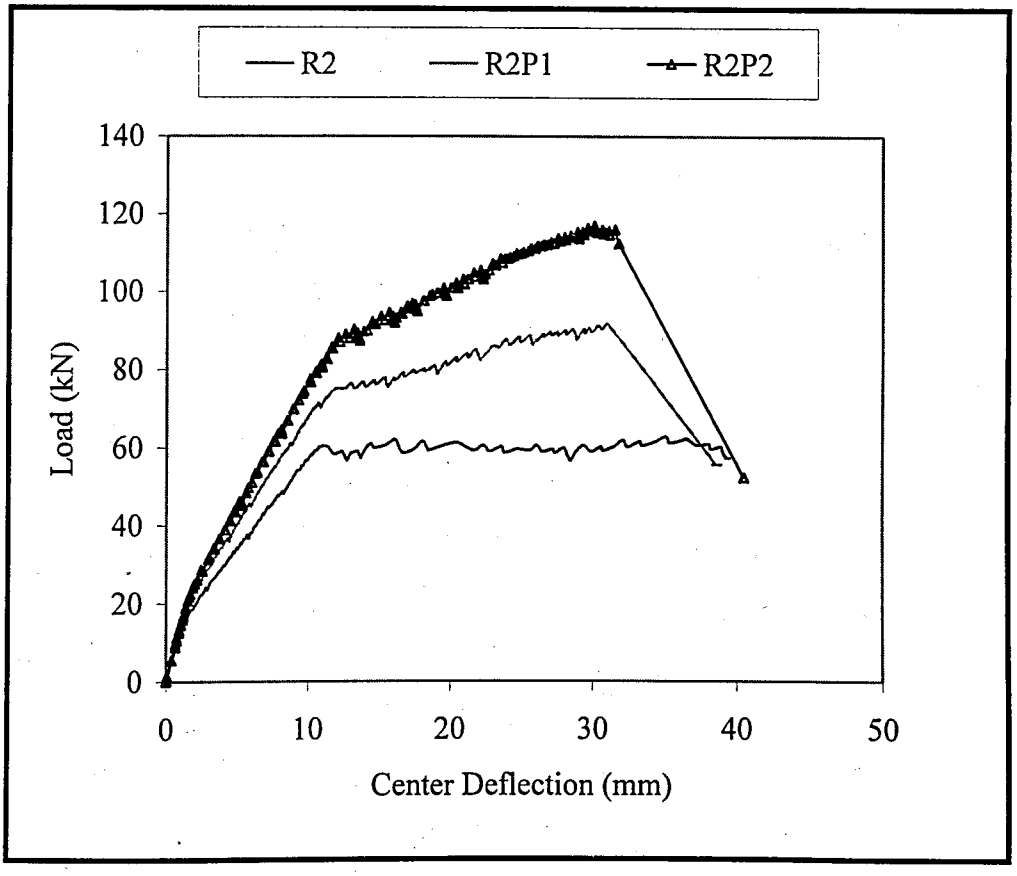

Figure 5.32. Load-center deflection curves of R2 series wrt. FRP ratio

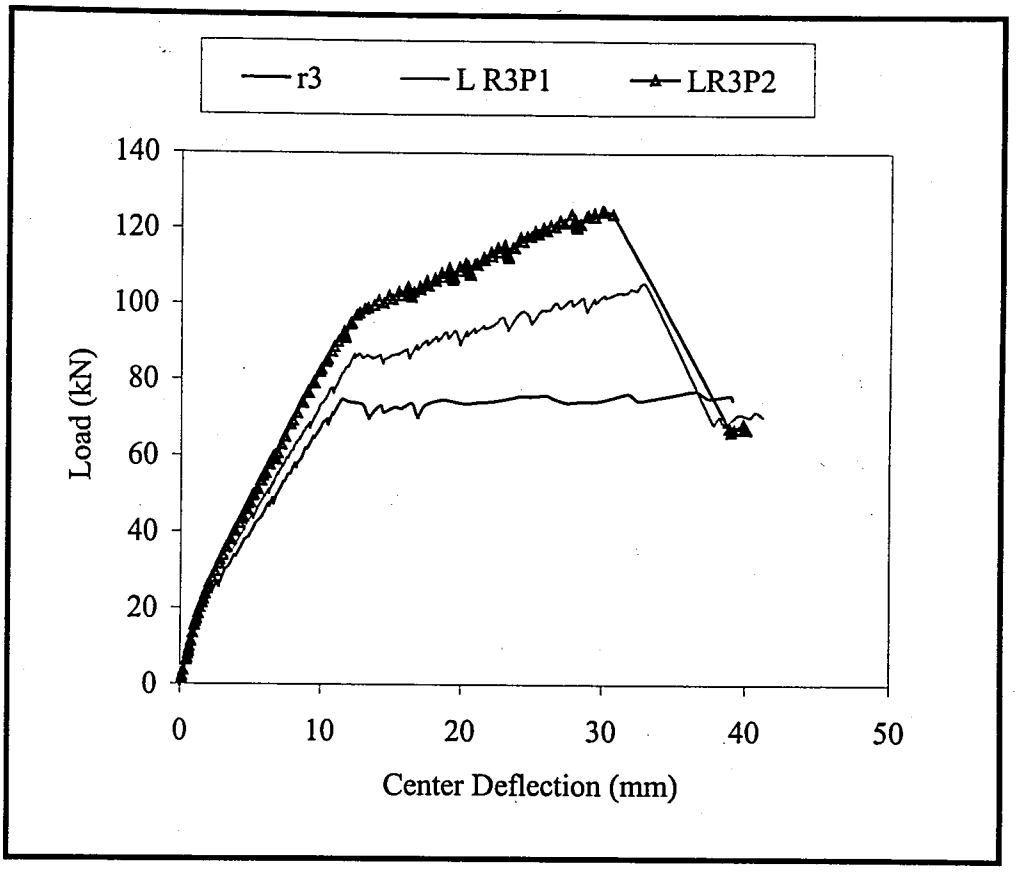

Figure 5.33. Load-center deflection curves of R3 series wrt. FRP ratio

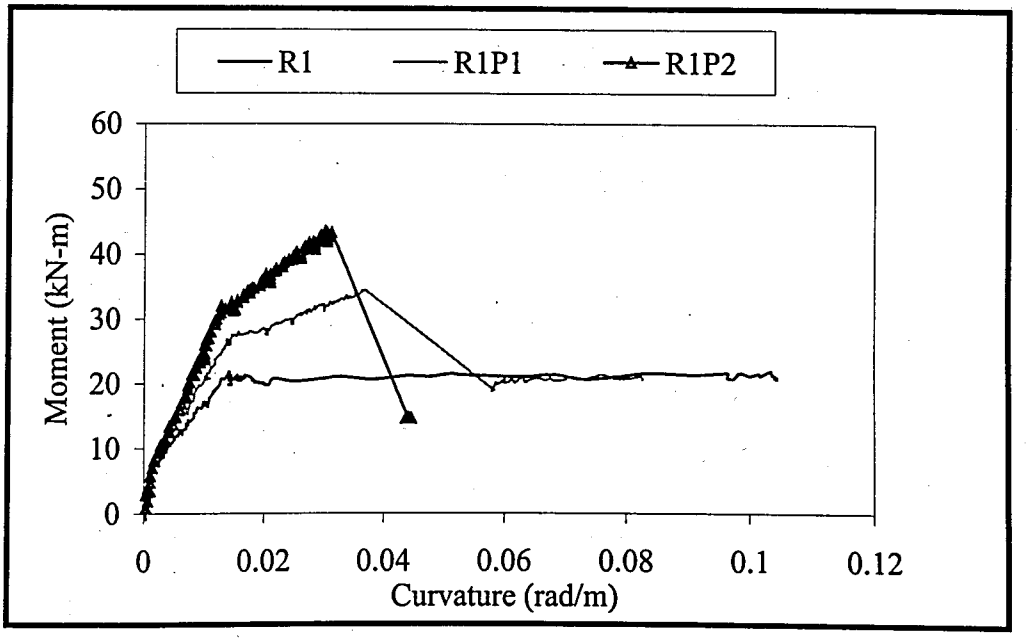

Figure 5.34. Moment-curvature curves of R1 series without anchorages wrt. FRP ratio

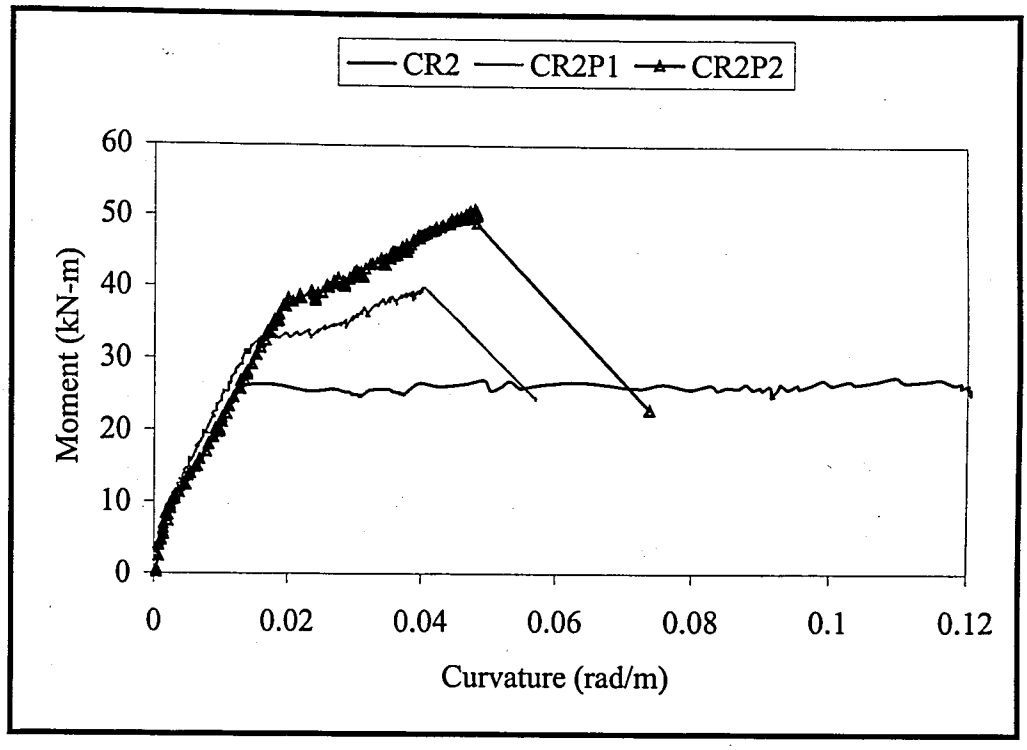

Figure 5.35. Moment-curvature curves of R2 series wrt. FRP ratio

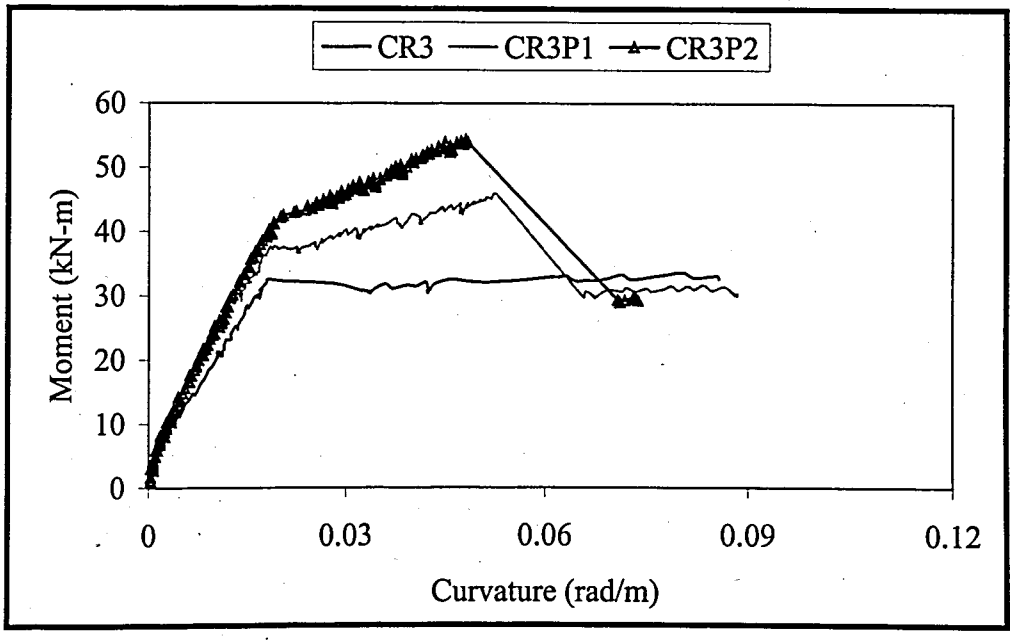

Figure 5.36. Moment-curvature curves of R3 series wrt. FRP ratio

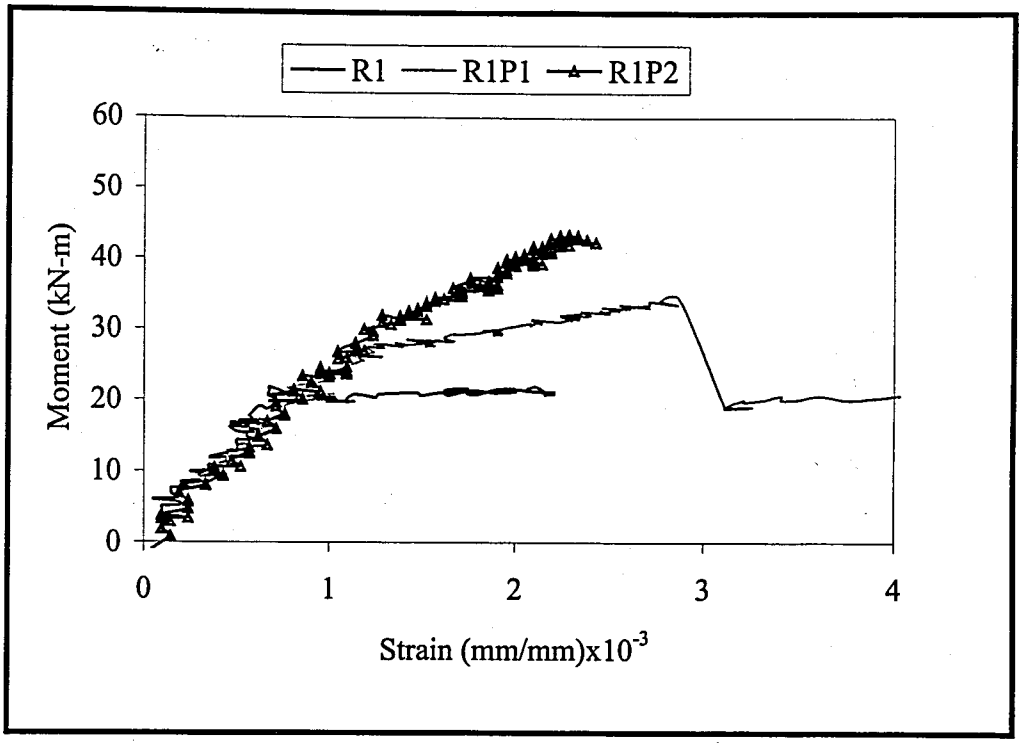

Figure 5.37. Moment-compression strain curves of the group of R1 beams without anchorages wrt. FRP ratio

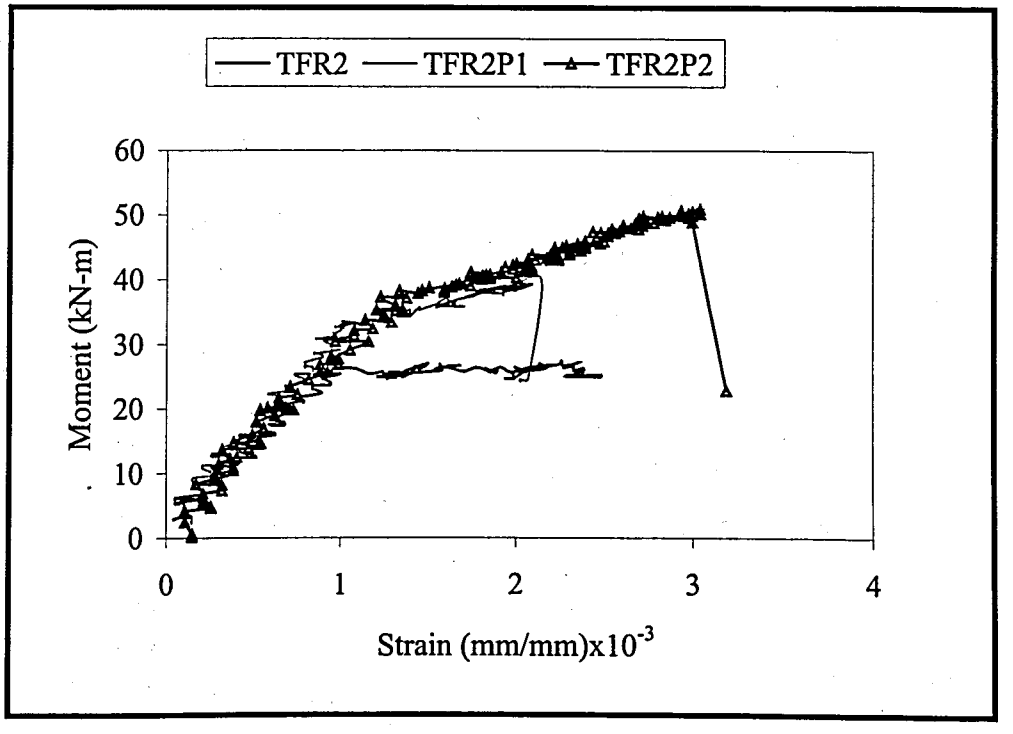

Figure 5.38. Moment-compression strain curves of the group of R2 beams wrt. FRP ratio

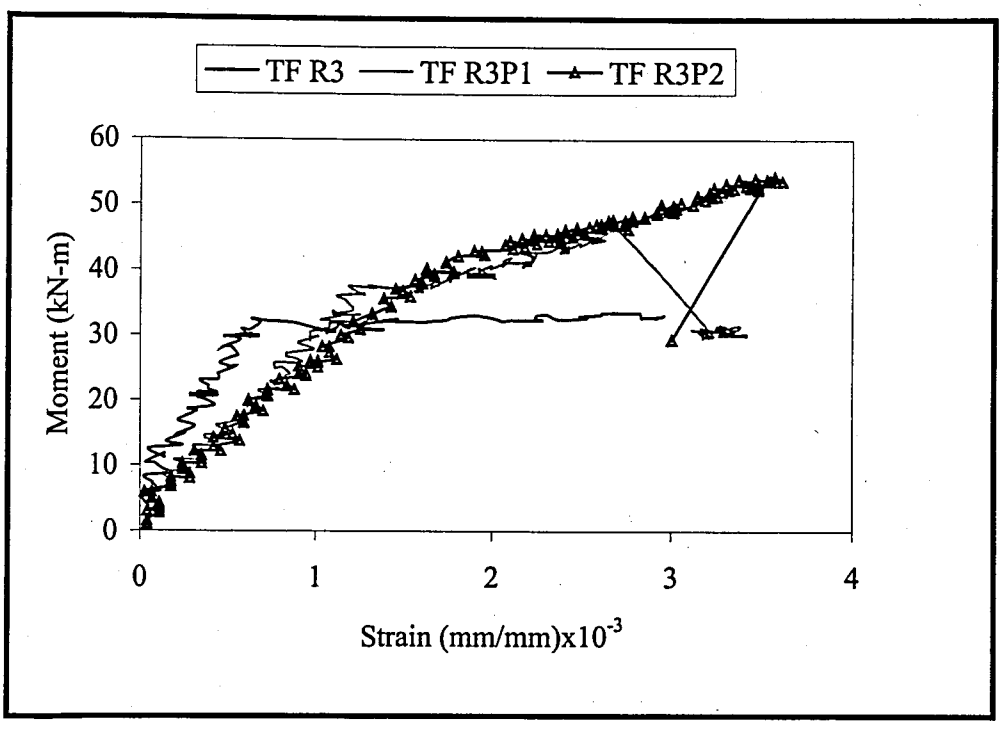

Figure 5.39. Moment-compression strain curves of the group of R3 beams wrt. FRP ratio

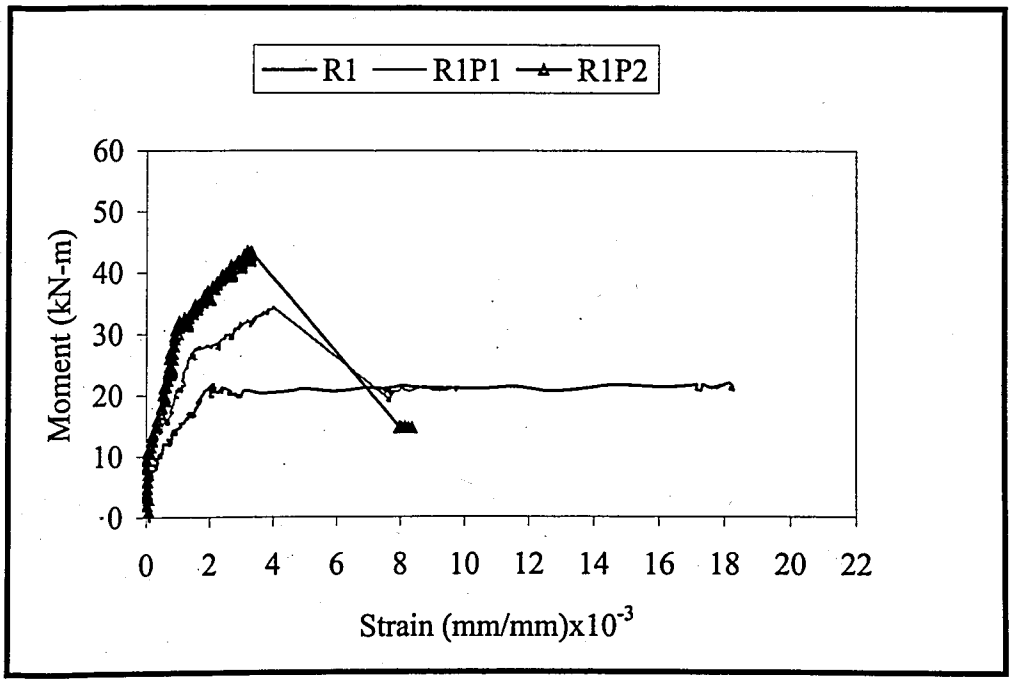

Figure 5.40. Moment-tension steel strain curves of the group of R1 beams without anchorages wrt. FRP ratio

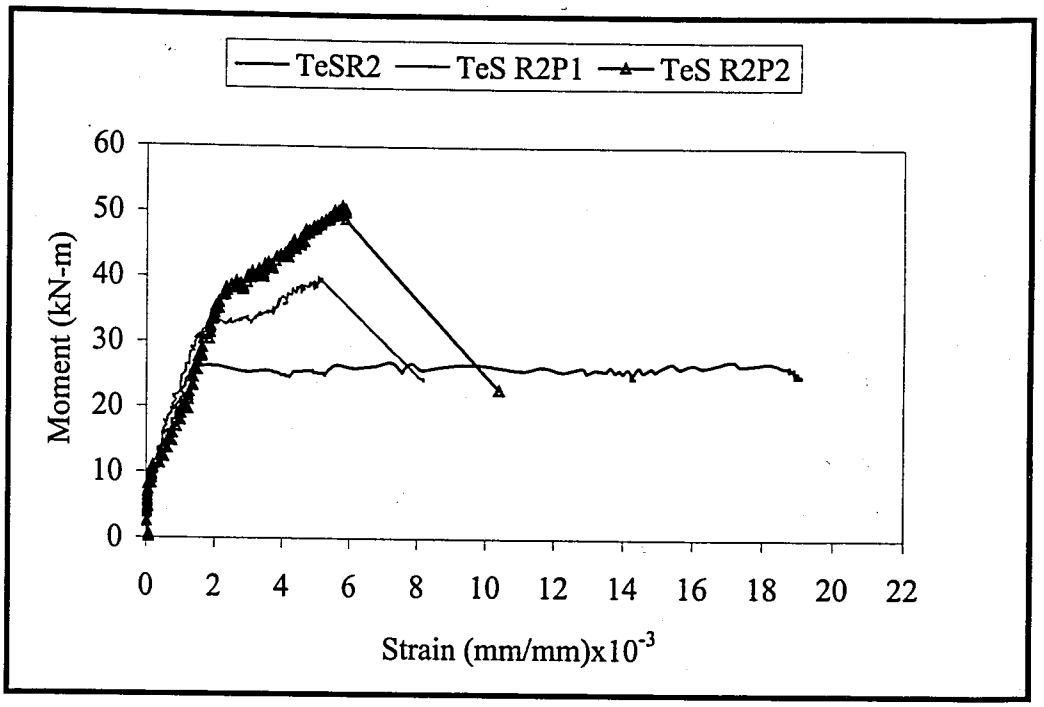

Figure 5.41. Moment-tension steel strain curves of the group of R2 beams wrt. FRP ratio

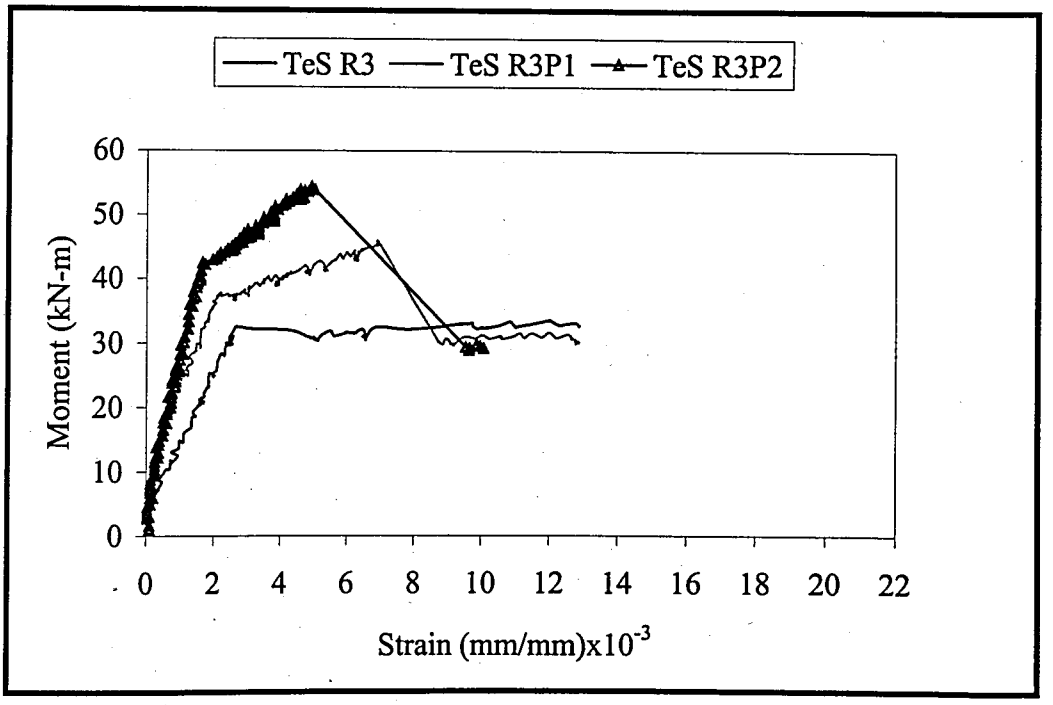

Figure 5.42. Moment-tension steel strain curves of the group of R3 beams wrt. FRP ratio

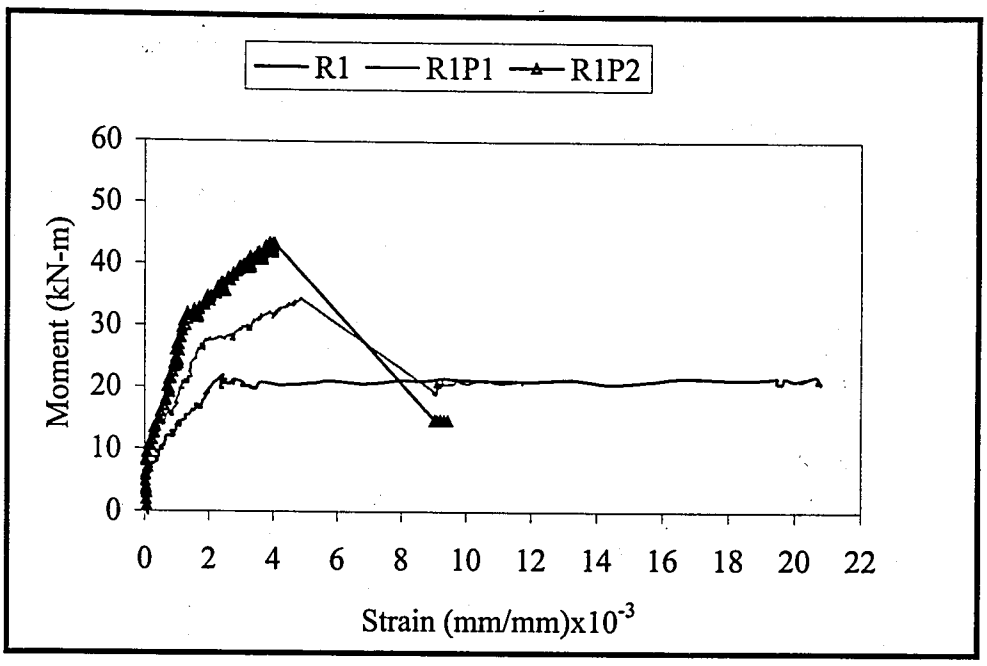

Figure 5.43. Moment-concrete strain at the bottom fiber curves of the group of R1 beams without anchorages wrt. FRP ratio

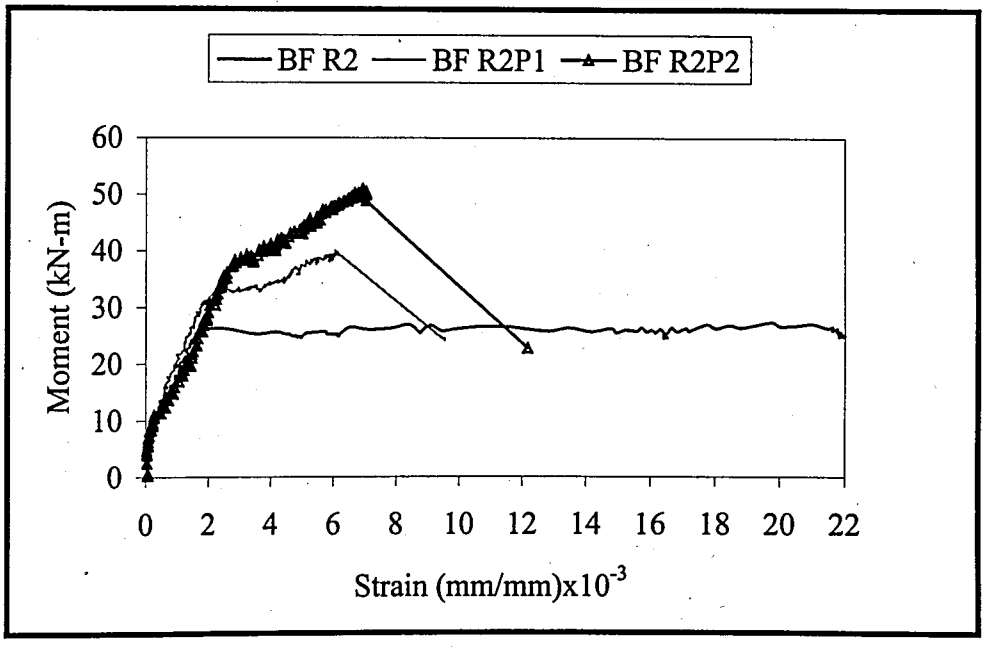

Figure 5.44. Moment-concrete strain at the bottom fiber curves of the group of R2 beams wrt. FRP ratio

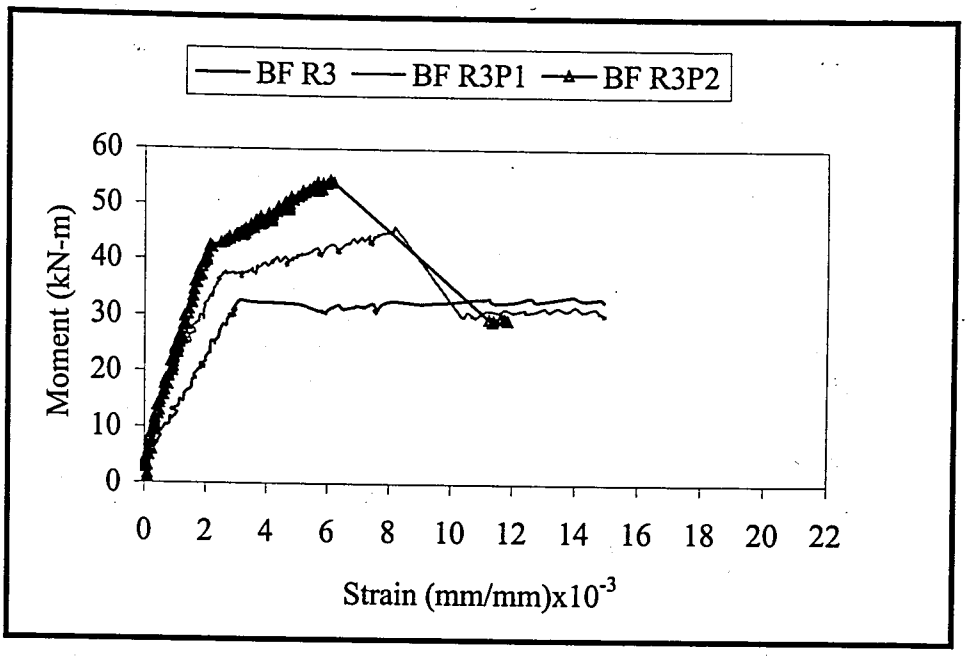

Figure 5.45. Moment-concrete strain at the bottom fiber curves of the group of R3 beams wrt. FRP ratio

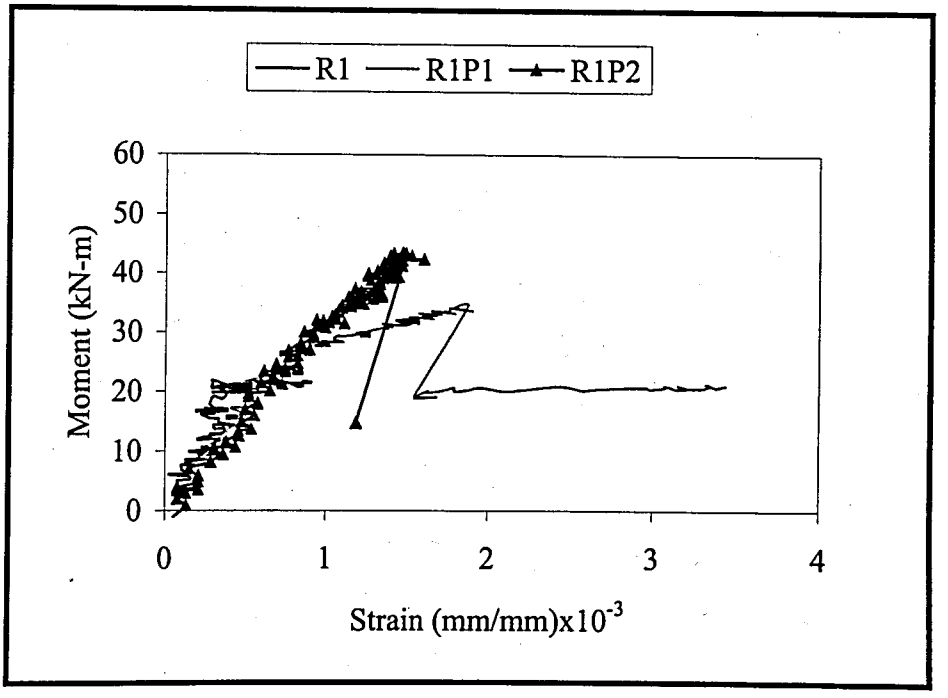

Figure 5.46. Moment-compression steel strain curves of the group of R1 beams without anchorages wrt. FRP ratio

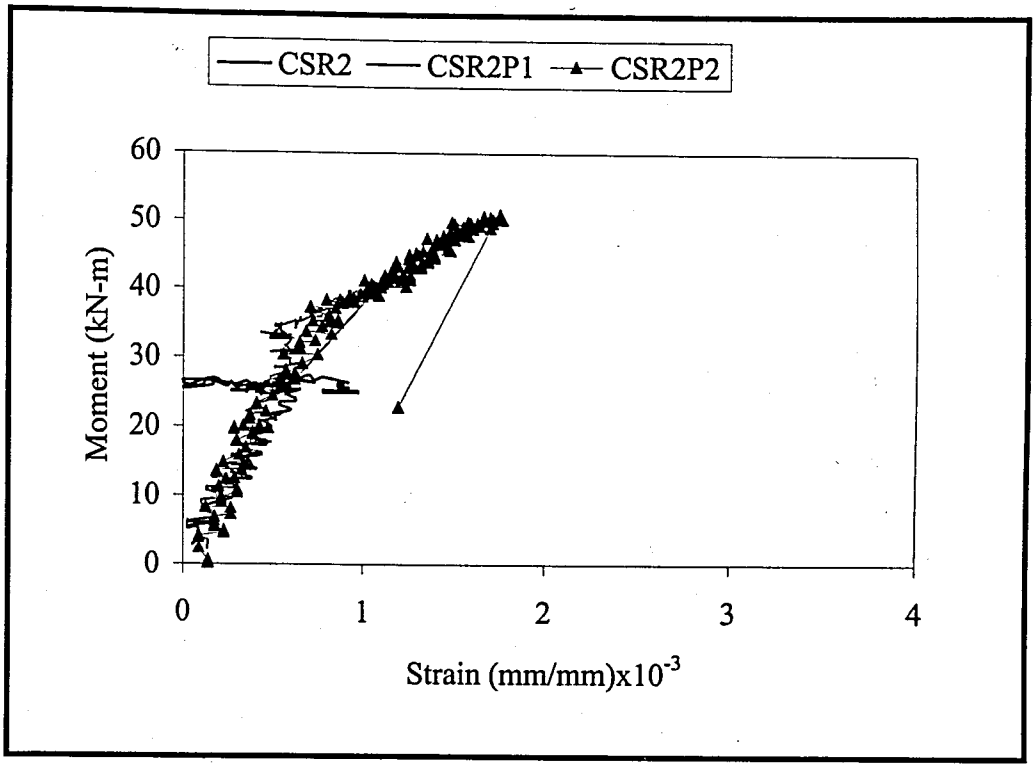

Figure 5.47. Moment-compression steel strain curves of the group of R2 beams wrt. FRP ratio

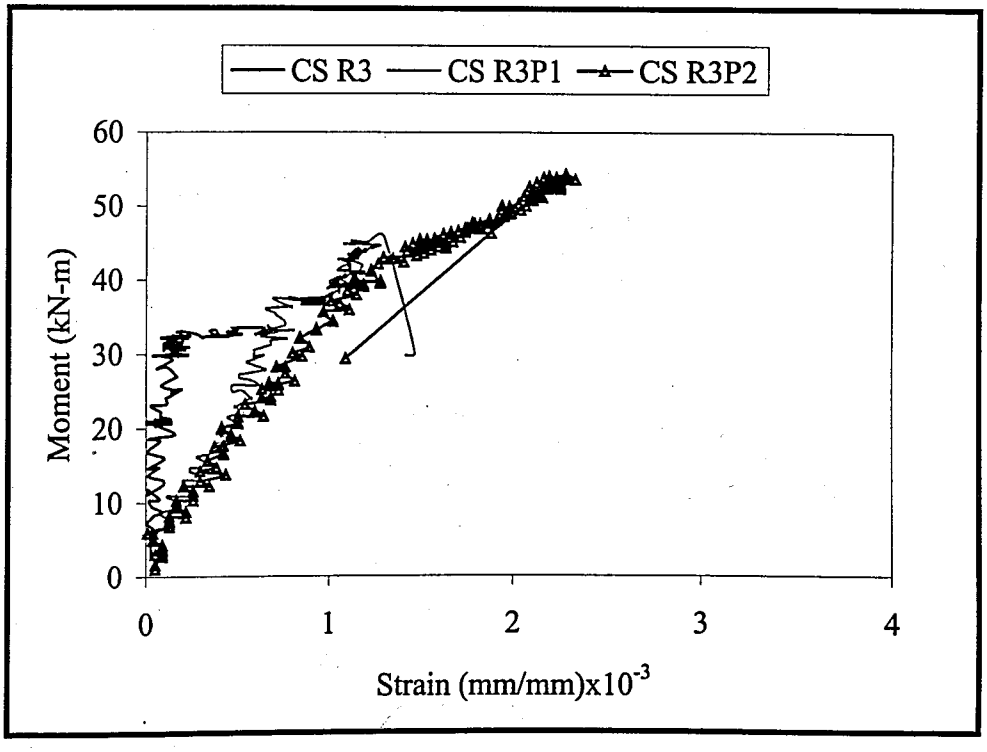

Figure 5.48. Moment-compression steel strain curves of the group of R3 beams wrt. FRP ratio

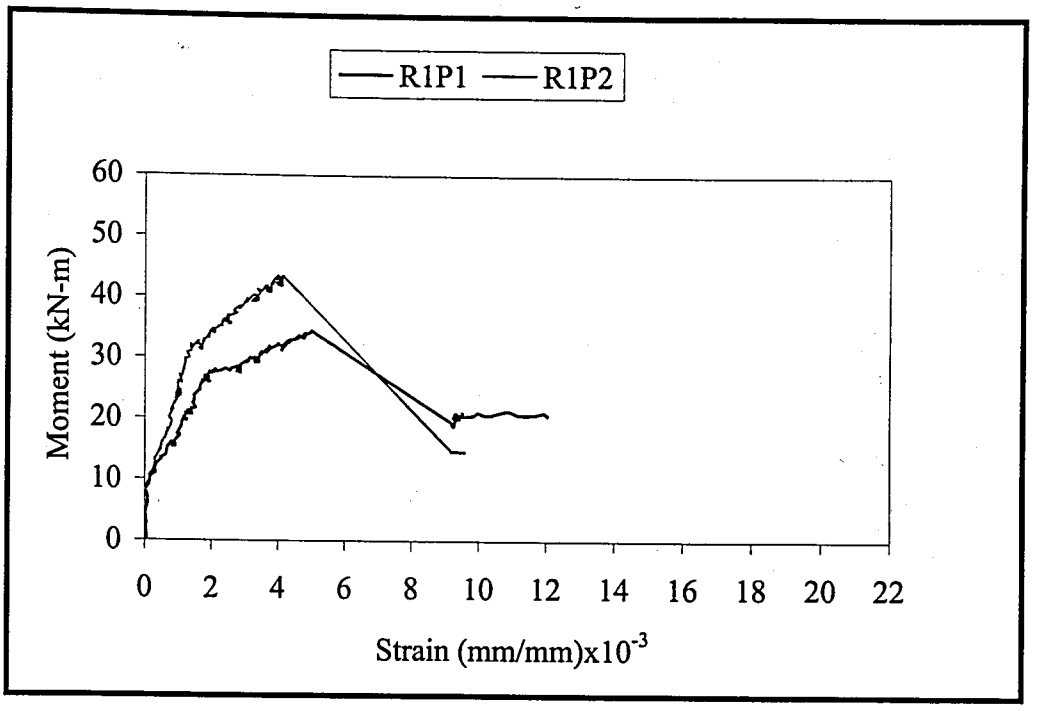

Figure 5.49. Moment-FRP strain curves of the group of R1 beams without anchorages wrt. FRP ratio

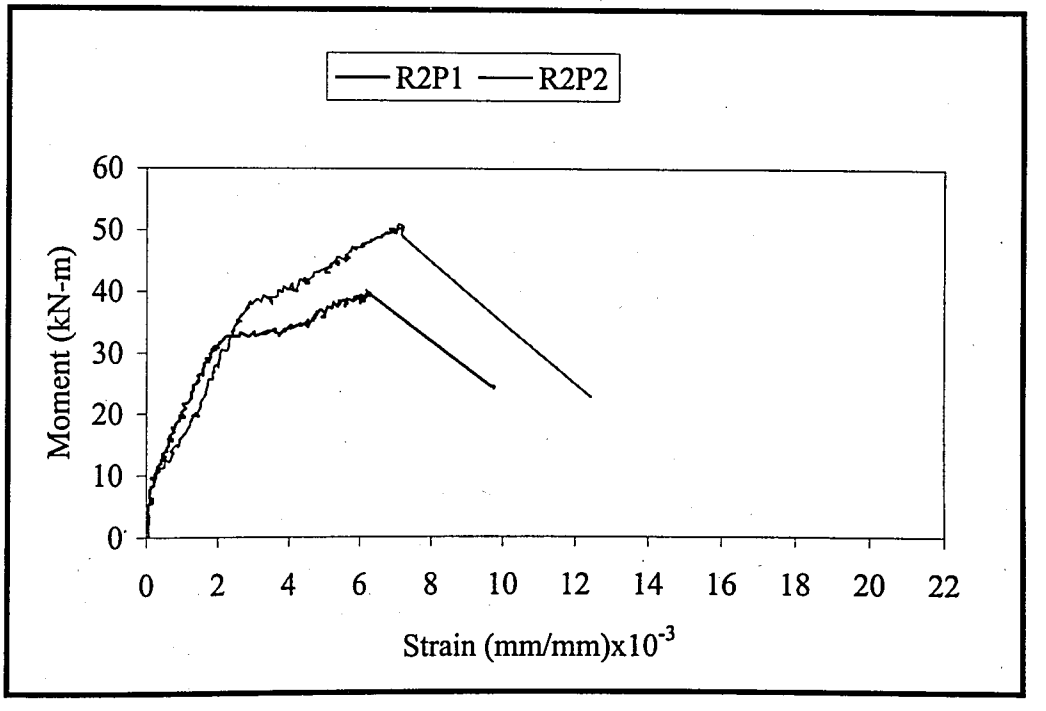

Figure 5.50. Moment-FRP strain curves of the group of R2 beams wrt. FRP ratio

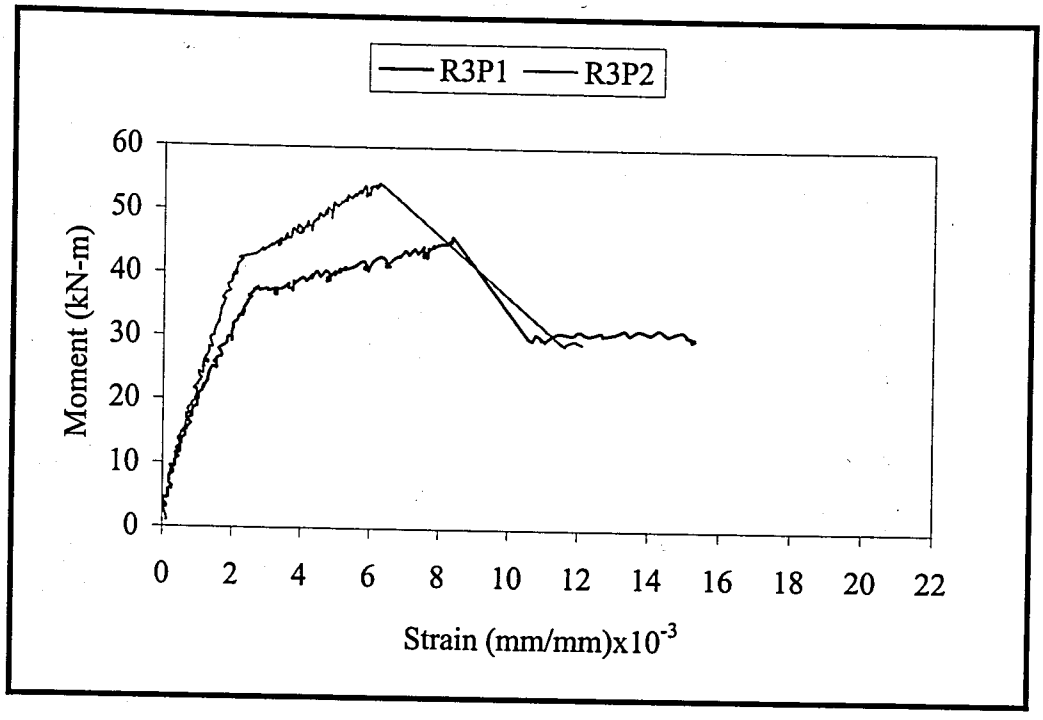

Figure 5.51. Moment-FRP strain curves of the group of R3 beams wrt. FRP ratio

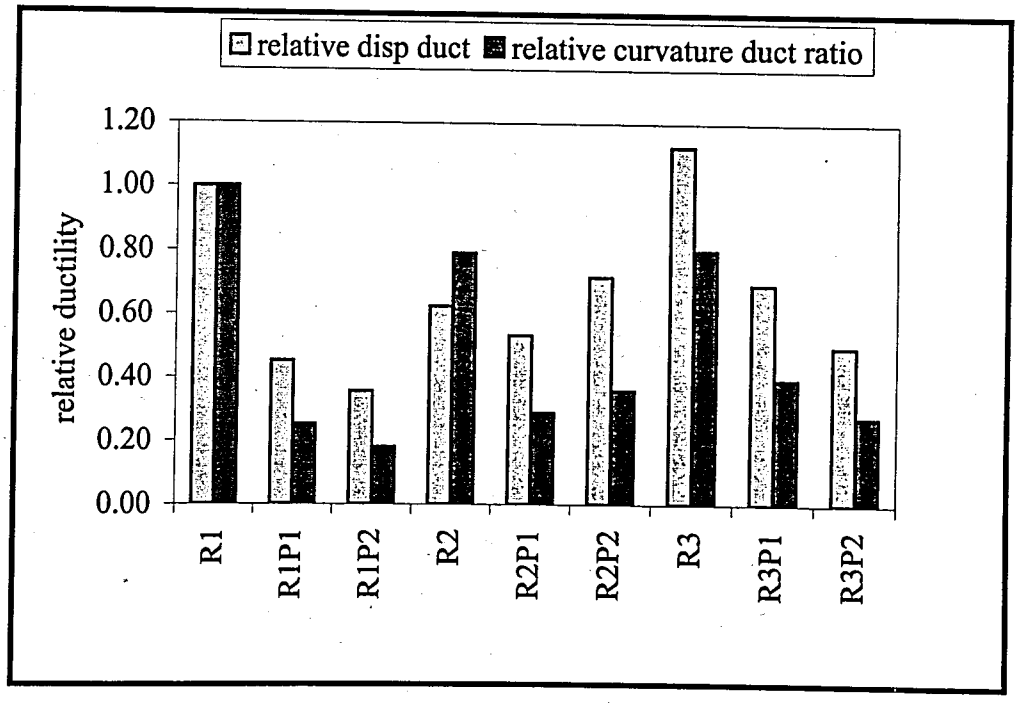

Figure 5.52. Relative ductilities of test specimens without anchorages wrt. FRP ratios

5.1.3. Effect of Anchorage

It may be necessary to apply an anchorage system to the plate so that the full capacity of FRP is developed and plate separation (de-bonding) is precluded [21]. Carefully designed external anchorages generally are inclined to increase the effectiveness of CFRP plates. In this study, only the beams of R1 series have included external anchorages obtained by wrapping of the curtailment zone of FRP at both sides.

The presence of the anchorages has a tendency to decrease crack width for the same load with respect to the virgin specimen significantly. Moment crack width diagrams for R1 series are shown in Figure 5.53. Besides, wrapping of shear span in this study has shown that crack width decreases at the same load in R1P1W with respect to R1P1 up to the crack width of 0.40 mm which is the limit crack width in TS-500 for interior beams. For R1P2W beam, while crack width is greater than R1P2 at the same load in the beginning of crack opening, the difference between crack widths decreases rapidly in that the same crack width values are encountered after approximately 0.24 mm up to the crack width of 0.40 mm. If anchorage length of R1P2W had increased, crack width values probably would have been inclined to decrease in the same load for R1P2W with respect to R1P2.

Wrapping of shear span, however, has not increased the load corresponded to the limit crack width of 0.4 mm in TS-500. The load values obtained corresponding to the limit crack width of 0.4 mm in TS-500 are 70.2 kN, 71.5 kN, 92 kN and 92 kN for R1P1, R1P1W, R1P2 and R1P2W respectively. In addition to crack width, while presence of anchorage in the beam of R1P1W has decreased crack spacing from 7.9 mm to 7.3 mm with respect to R1P1, it was not observed that crack width has decreased in the beam of R1P2W with respect to R1P2. This probably occurred due to inadequate anchorage length for the beam of R1P2W

Loads and deflections values at the instant of first cracking, yielding of tension steel and at the instant of ultimate are illustrated in Table 5.17. As indicated in Table 5.17, FRP plated beams without plate end anchorage have a bit higher yield loads. Ultimate loads, however, increase 82 per cent for R1P1W and 116 per cent for R1P2W with respect to R1

beam. Besides, First cracking loads are also higher than plated beams without end anchorages. This implies that FRP strip end anchorages increase the effectiveness of FRP plates and plate end anchorages have also an effect to postpone forming of the first cracking.

Presence of plate end anchorages results in a decrease in the bond slip action between FRP plates and concrete to maintain the stress transfer mechanism throughout the loading range up to failure [31]. Reducing slip between FRP and concrete brings about the extension of the composite action of the FRP bonded beam up to as near failure as possible [17]. Since composite action of the FRP plated beams with plate end anchorage continues longer time, the beams with plate end anchorages, R1P1W and R1P2W, as far as enhancement ratios are considered carry on approximately 25 per cent higher load with respect to R1P1 and 18 per cent higher load with respect to R1P2 respectively. These values also show the importance of carefully designed anchorages since anchorage length and placing are not changed while FRP ratio increases. As a result, the effectiveness of anchorages decreases 7 per cent as far as enhancement ratios are considered while plate ratio increases with constant steel ratio.

Load deflection and moment curvature curves are illustrated in Figure 5.54 and Figure 5.55. As indicated in these figures, changes in stiffness become insignificant before cracking. Stiffness of the beams start to change beyond cracking. After yielding of tension steel, end anchorages become more effective but changes in stiffness of the beams which have end anchorages retain insignificant with respect to FRP plated beams without anchorage. Presence of plate end anchorages increases ultimate deflection values with respect to the plated beams without anchorage as shown in Figure 5.54. As indicated in Figure 5.55, plate end anchorages are inclined to enhance rotation capacity as well. However, increase ratio in rotation capacity for the beam of R1P1W with respect to R1P1 is greater than that of R1P2W with respect to R1P2. It can be clearly seen in Figure 5.55 that composite action with no-bond slip or minimum bond-slip is satisfied with plate end anchorage frankly.

What's more, in order to investigate effect of plate end anchorages on the behaviour of test specimens, moment versus strain diagrams at various levels are shown in Figure

5.56 to 5.60. These strain values are calculated using compatibility equations at various levels.

Ultimate strains at the top fiber of concrete section, compression steel, tension steel, lower bottom fiber of concrete section and at the level of FRP, strains at the instant of yielding of tension steel and at the instant of crushing of concrete are shown in Table 5.18. The strains at the top fiber of concrete section are inclined to decrease for the wrapped beams with respect to plated beams without anchorage. The ultimate strain values at the top fiber of concrete section for R1P1W and R1P2W beams decrease, in turn, 35 per cent and 31 per cent with respect to that of R1P1 and R1P2. As indicated in Figure 5.56 strain values at the top fiber of concrete section for R1P1W and R1P2W are inclined to decrease at the same load values with respect to plated beams without anchorage prior to failure.

Like concrete compression strain, strain at the compression steel has a tendency to decrease at the same load with respect to plated beams without anchorage. Moment versus strain at compression steel diagram is shown in Figure 5.57. As indicated in this figure, the slope for the wrapped beams is steeper than the beams without anchorage. In addition to that, strains at ultimate and at the instant of yielding of tension steel are smaller than strains values of the beams without anchorage as illustrated in Table 5.19.

Moment–strain at the level of tension steel and moment versus strain at the lower bottom fiber of concrete section are shown in Figure 5.58 and Figure 5.59. These two figures exhibit some similarities as seen. Although strain values for R1P1W and R1P2W are smaller than that of virgin specimen at the same load, those values are higher than those of plated beams without anchorage at the same load. Nonetheless, ultimate strains in R1P1W and R1P2W are greater than R1P1 and R1P2 correspondingly. Strain values corresponding to the ultimate strain, the ultimate concrete compression strain at the top fiber of concrete section and tension steel yield strain at the level of lower bottom fiber of concrete and at the level of tension steel are summarized in Table 5.20 and Table 5.21.

Moment versus FRP strain diagram are shown in Figure 5.60. As indicated, up to first cracking the beams have similar stiffness. After cracking, the stiffness begins to change. R1P1W and R1P2W have a bit smaller stiffness than those of plated beams

without anchorage. In other words, FRP-strain of the beams with plate end anchorages is higher than that of the beams of R1P1 and R1P2 at the same load. However, ultimate strains of the beams of R1P1W and R1P2W are much more than the beams without anchorage. This result indicates that FRP is used efficiently with plate end anchorages. Besides, increase rate of ultimate strain of R1P1W with respect to R1P1 is greater than that of the beam of R1P2W with respect to R1P2. Those values can be summarized in Table 5.22. Interestingly, FRP strains at which tension steel yields are closer to each other for the beams with and without plate end anchorages as seen in Table 5.22.

Carefully designed external anchorages are inclined to enhance structural ductility based on curvature ductility and deflection ductility. An increase in structural ductility with external anchorages can be clearly seen in Figure 5.61. As indicated in Figure 5.61, increase ratio is approximately 47 per cent for R1P1W with respect to R1P1 and 22 per cent for R1P2W with respect to R1P2 based on deflection ductility. It can be concluded that while external anchorages extend composite action, they are very useful to increase structural ductility. Nevertheless, plate end anchorages should be designed as FRP ratio is taken into account. Therefore, it can be concluded that while FRP ratio increases with constant external anchorages, ductility increase rate decreases.

Carrying higher loads, greater ductility, slow slippage of CFRP and extending composite action can emphasize the effectiveness of plate end anchorages [19].

Table 5.17. Loads and deflections of the beams of R1 series

LOADS AND DEFLECTIONS	BEAMS				
	R1	R1P1	R1P1W	R1P2	R1P2W
$P_{max\ load}$ (kN)	50.40	79.06	91.57	99.81	109.03
$P_{steel\ yields}$ (kN)	40.85	62.92	56.66	78.07	75.10
$P_{first\ crack}$ (kN)	29.00	35.00	48.40	56.00	63.00
$P_{residual}$ (kN)	****	44.14	45.79	33.93	35.91
$\delta_{steel\ yields}$ (mm)	7.6	11.4	9.3	14.5	11.7
$\delta_{for\ max\ load}$ (mm)	39.1	26.8	44.1	26.7	35.4
$\delta_{first\ crack}$ (mm)	4.5	4.7	7.5	8.1	9.2
δ_{max} (mm)	39.4	44.5	44.9	40.9	46.1

Table 5.18. Development of compression strain at the top fiber of concrete of R1 series

BEAMS	Moments			$\varepsilon_{top\ fiber}$ x 0.001		
	M_{max}	M@0.003	M@0.00155	ε_{max}	ε @0.003	ε @0.00155
R1	21.92	-	17.77	2.1097	-	0.571
R1P1	34.39	-	27.37	2.871	-	1.295
R1P1W	39.83	-	24.65	2.125	-	0.889
R1P2	43.42	-	33.96	2.286	-	1.571
R1P2W	47.43	-	32.67	1.746	-	1.012

Table 5.19. Development of compression steel strain of R1 series

BEAMS	Moments			$\varepsilon_{compression\ steel}$ x 0.001		
	M_{max}	M@0.003	M@0.00155	ε_{max}	ε @0.003	ε @0.00155
R1	21.92	-	17.77	0.5998	-	0.278
R1P1	34.39	-	27.37	1.876	-	0.881
R1P1W	39.83	-	24.65	0.589	-	0.523
R1P2	43.42	-	33.96	1.473	-	1.098
R1P2W	47.43	-	32.67	0.537	-	0.614

Table 5.20. Development of tension steel strain of R1 series

BEAMS	Moments			$\varepsilon_{tension\ steel}$ x 0.001		
	M_{max}	M@0.003	M@0.00155	ε_{max}	ε @0.003	ε @0.00155
R1	21.92	-	17.77	18.131	-	1.558
R1P1	34.39	-	27.37	3.984	-	1.562
R1P1W	39.83	-	24.65	8.172	-	1.561
R1P2	43.42	-	33.96	3.162	-	1.6
R1P2W	47.43	-	32.67	6.134	-	1.582

Table 5.21. Development of strain at the bottom fiber of concrete of R1 series

BEAMS	Moments			$\varepsilon_{bottom\ fiber}$ x 0.001		
	M_{max}	M@0.003	M@0.00155	ε_{max}	ε @0.003	ε @0.00155
R1	21.92	-	17.77	20.61	-	1.819
R1P1	34.39	-	27.37	4.869	-	1.931
R1P1W	39.83	-	24.65	9.538	-	1.885
R1P2	43.42	-	33.96	3.884	-	2.02
R1P2W	47.43	-	32.67	7.209	-	1.935

Table 5.22. Development of FRP strain of R1 series

BEAMS	Moments			$\varepsilon_{FRP\ fiber}$ x 0.001		
	M_{max}	M@0.003	M@0.00155	ε_{max}	ε @0.003	ε @0.00155
R1	21.92	-	17.77	-	-	-
R1P1	34.39	-	27.37	5.001	-	1.987
R1P1W	39.83	-	24.65	9.74	-	1.934
R1P2	43.42	-	33.96	3.992	-	2.08
R1P2W	47.43	-	32.67	7.37	-	1.989

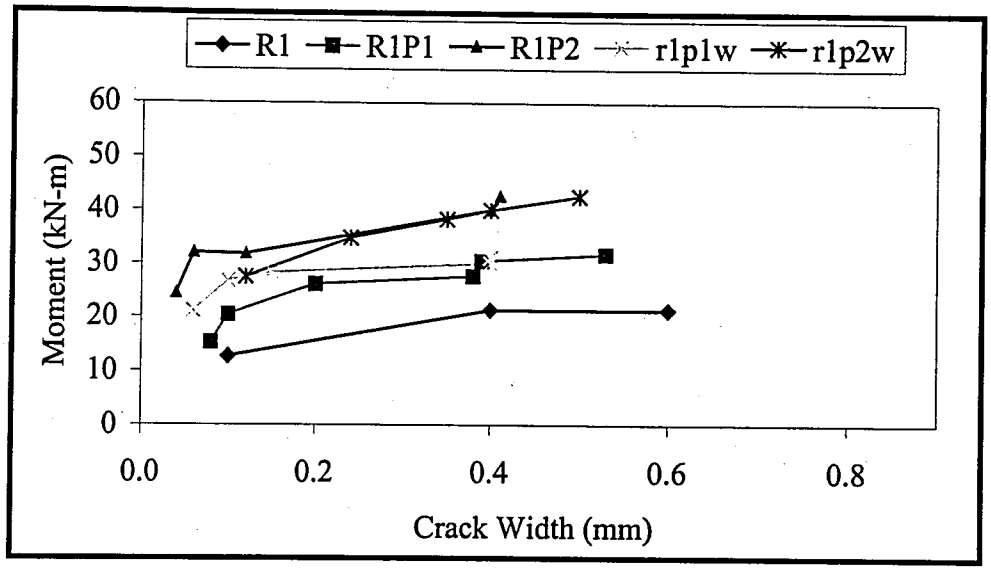

Figure 5.53. Moment crack width diagrams of the batch of R1 beams

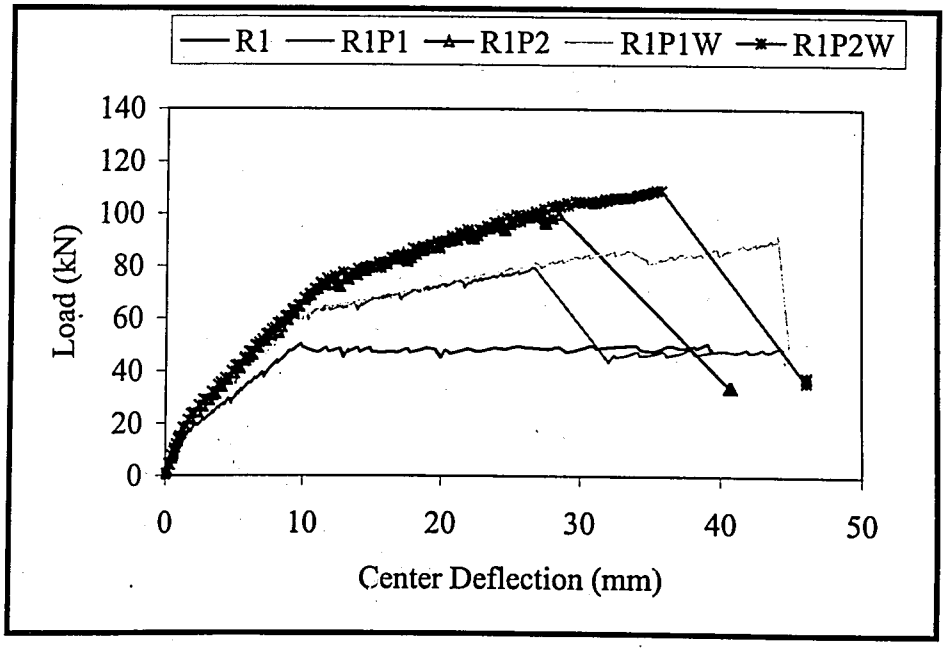

Figure 5.54. Load center deflection diagrams of the batch of R1 beams

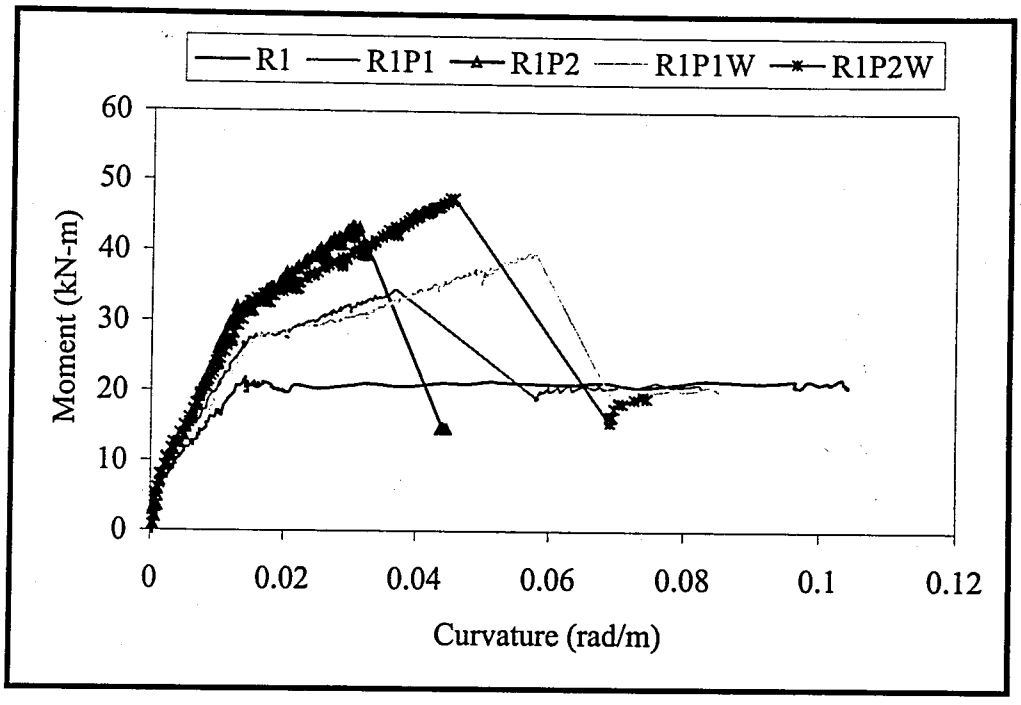

Figure 5.55. Moment curvature diagrams of the batch of R1 beams

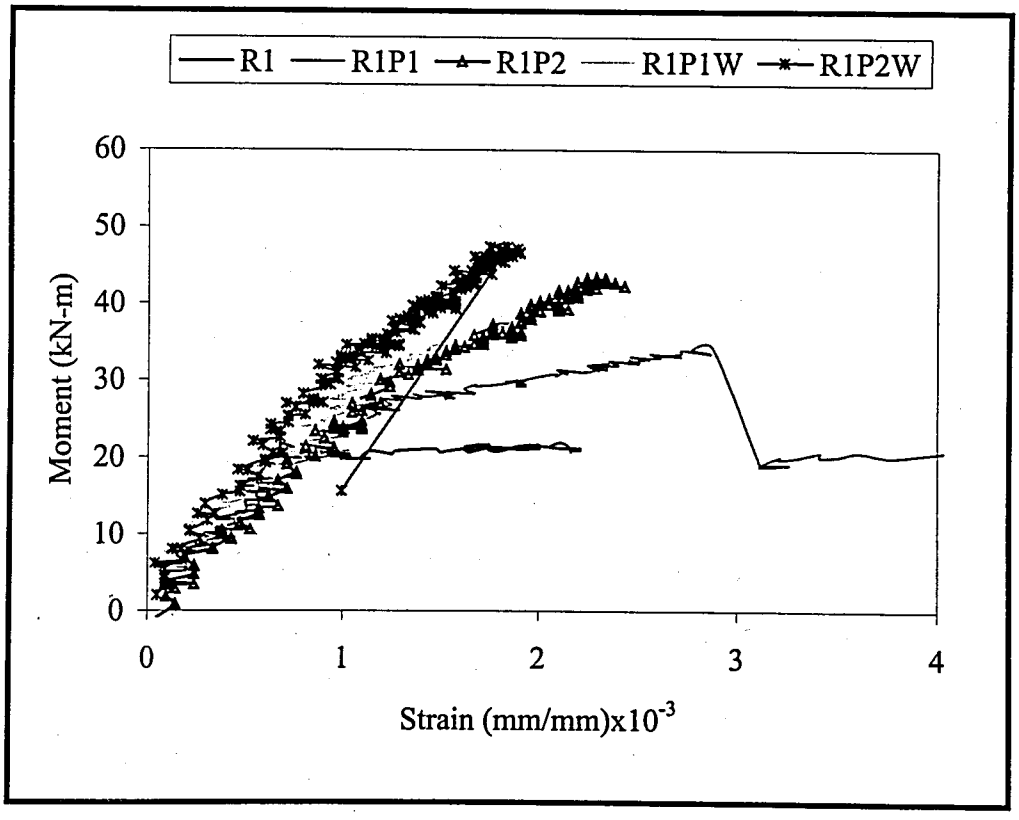

Figure 5.56. Moment strain at the top fiber of concrete diagrams of the batch of R1 series

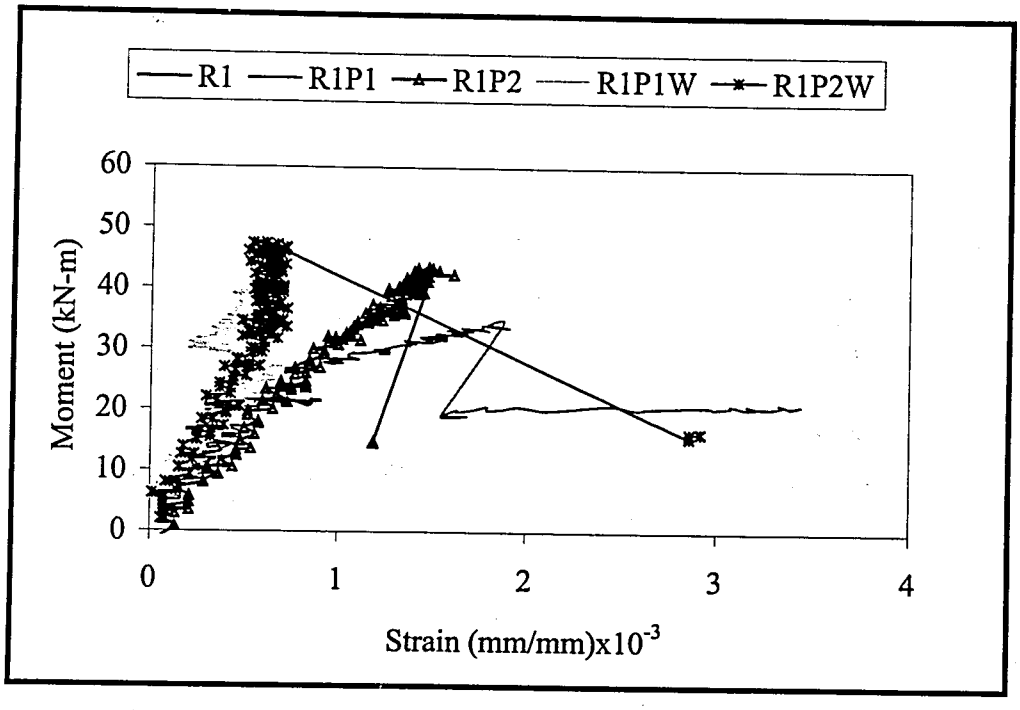

Figure 5.57. Moment compression steel strain diagrams of the batch of R1 series

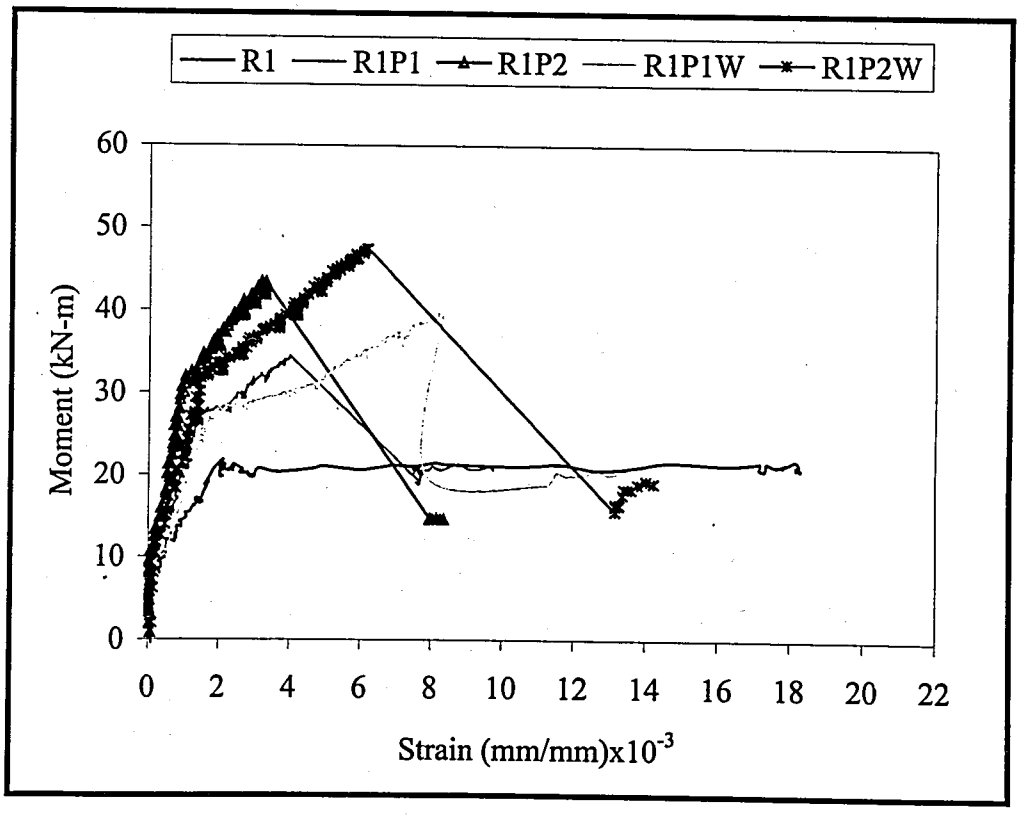

Figure 5.58. Moment tension steel strain diagrams of the batch of R1 series

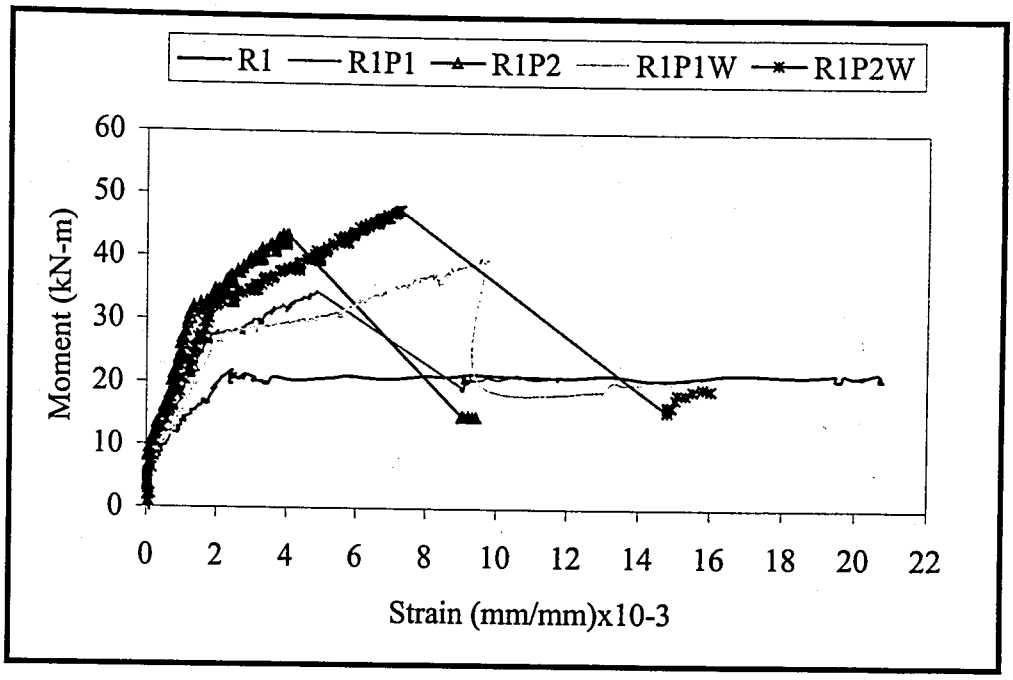

Figure 5.59. Moment strain at bottom fiber of concrete diagrams of the batch of R1 series

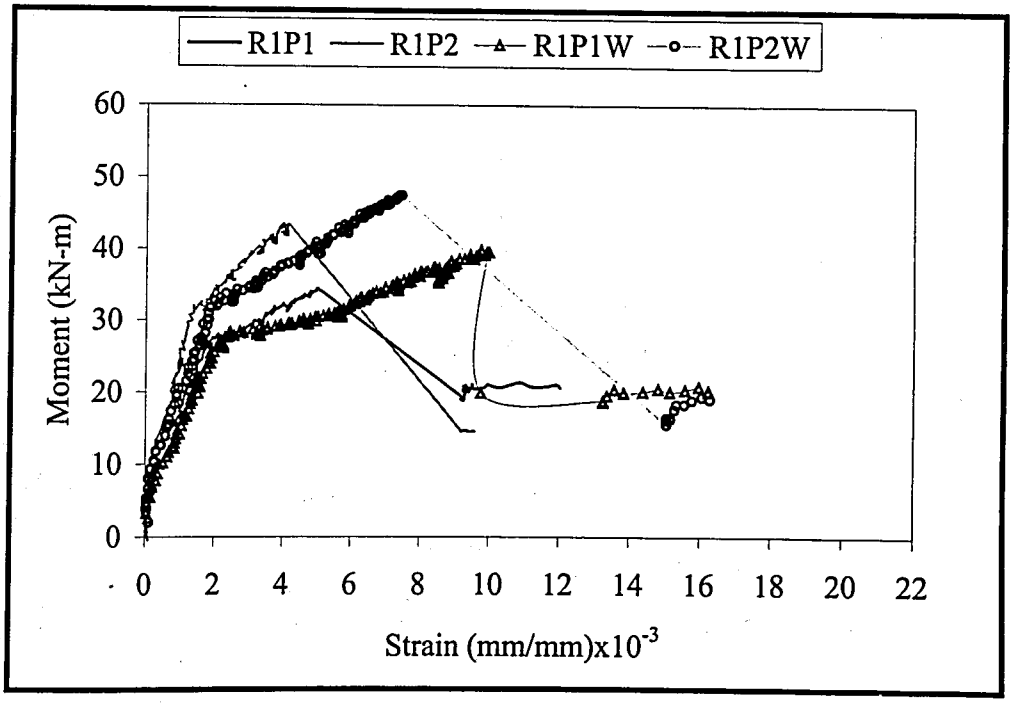

Figure 5.60. Moment FRP strain diagrams of the batch of R1 series

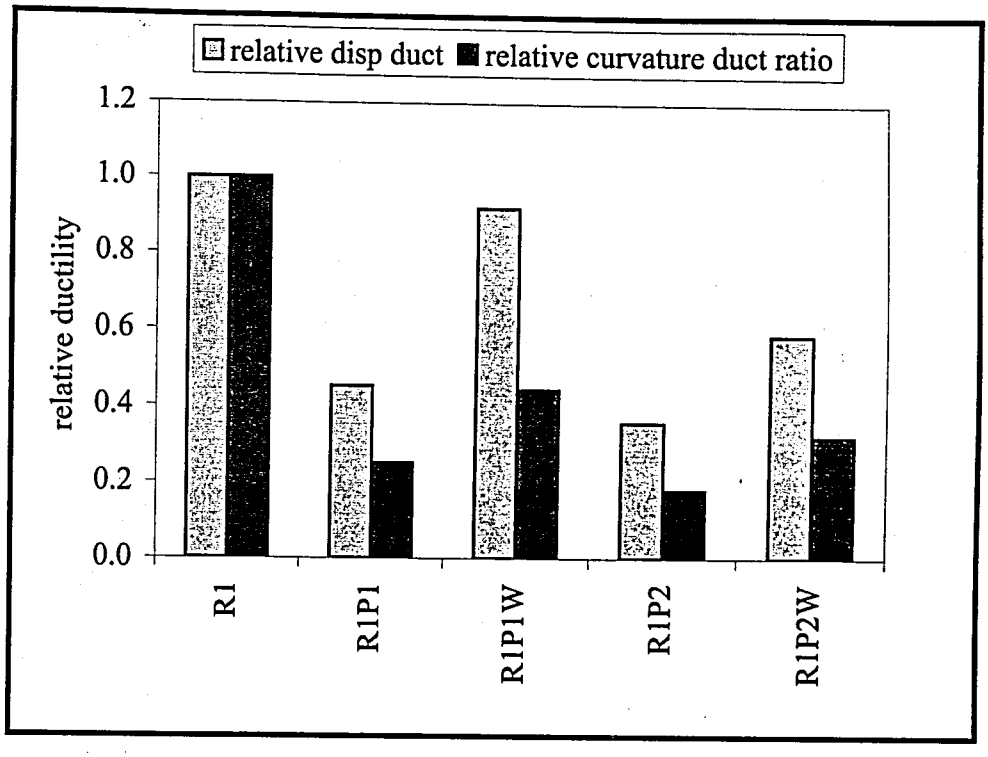

Figure 5.61. Relative ductilities of the batch of R1 series

5.2. Section Analysis for Rectangular Cross-Sections Strengthened with FRP

In order to investigate the behaviour of the beams strengthened with FRP analytical calculations developed by An *et al.*, [22] are used as well as experimental study. In the present analysis, compatibility equations and equilibrium equations are employed to determine moment curvature values. Some failure modes can not be included so as to use given formulations below. In order to satisfy the failure modes which are preferable, several limitations should be employed.

Those are summarized as follows:

- The cross-sectional area of FRP is chosen smaller than maximum cross-sectional area of FRP in order to avoid compression failure which is the mode of crushing of concrete before yielding of tension steel,
- Unevenness of concrete surface, shear reinforcement and epoxy bonding are assumed to be designed properly so as to avoid anchorage failure of the concrete layer between FRP plate and tension steel, shear failure which occurs if shear

capacity of the section is exceeded and de-bonding failure or peeling-off failure which results from crack opening in the section.

Thus, failure mode will be either tension failure or FRP rupture with the above assumptions [25]. In other words, failure occurs either concrete strain reaches crushing strain of 0.003 or FRP plate reaches its ultimate strain [22]. In addition to the previous work, further assumptions made by An *et al.*, [22] are summarized in the following in order to facilitate the section analysis of the beams strengthened with FRP plates.

- Linear strain distribution in the cross-section is employed up to failure,
- Plane sections before bending remain plane after bending,
- No-slip among FRP plate, longitudinal steel reinforcing bars and concrete (Perfect bond),
- Tensile strength of concrete can be negligible,
- Deformations due to shear forces are neglected,
- Strain in the bottom fiber of concrete section is assumed zero when FRP is bonded ($\varepsilon_{first}=0$).

Stress strain relationships of the materials which are FRP, tension steel, compression steel and concrete are illustrated in Figure 5.63 to 5.66. Besides, a typically reinforced concrete section strengthened with FRP plate and forces acting in the section are shown in Figure 5.62.

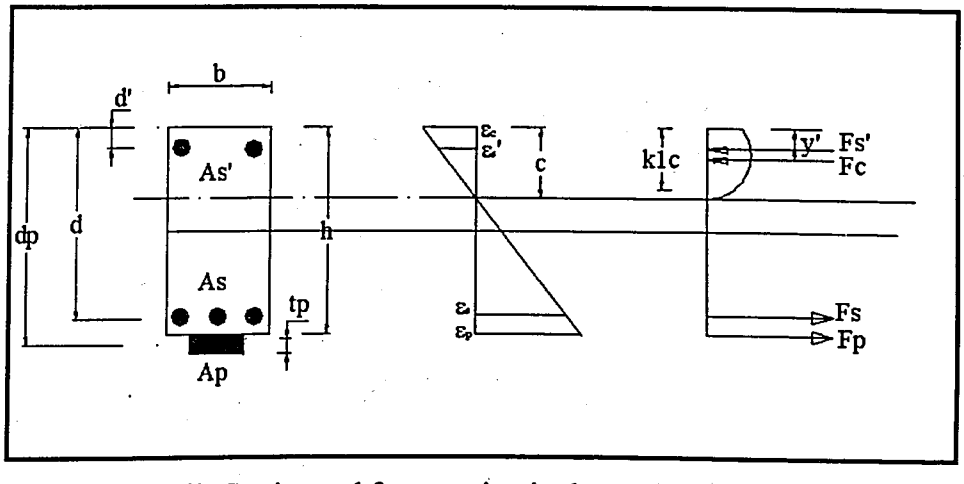

Figure 5.62. Strains and forces using in the analytical calculations

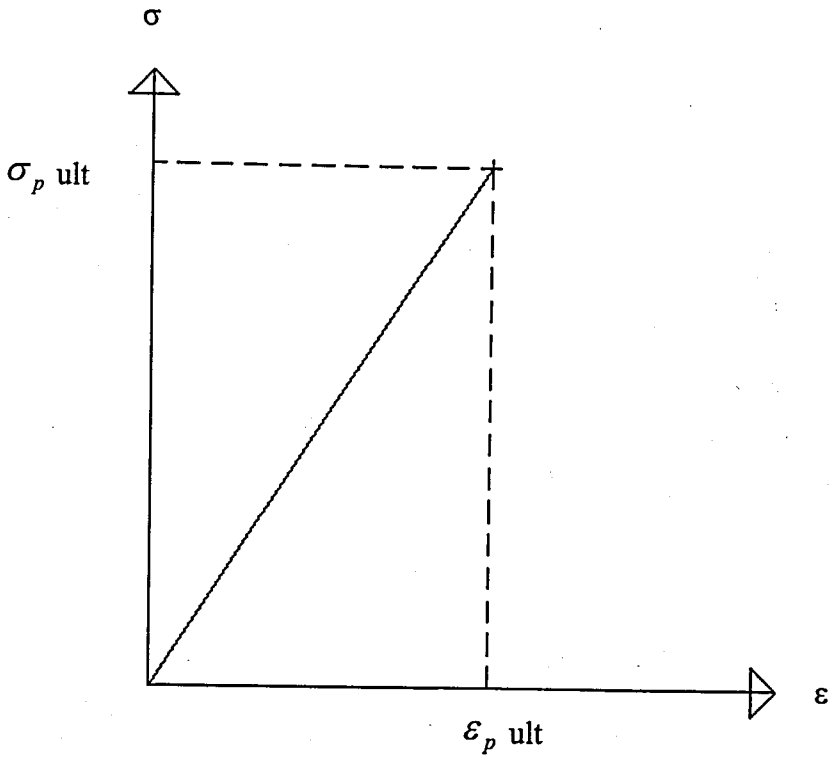

Figure 5.63. Stress-strain relationship of FRP

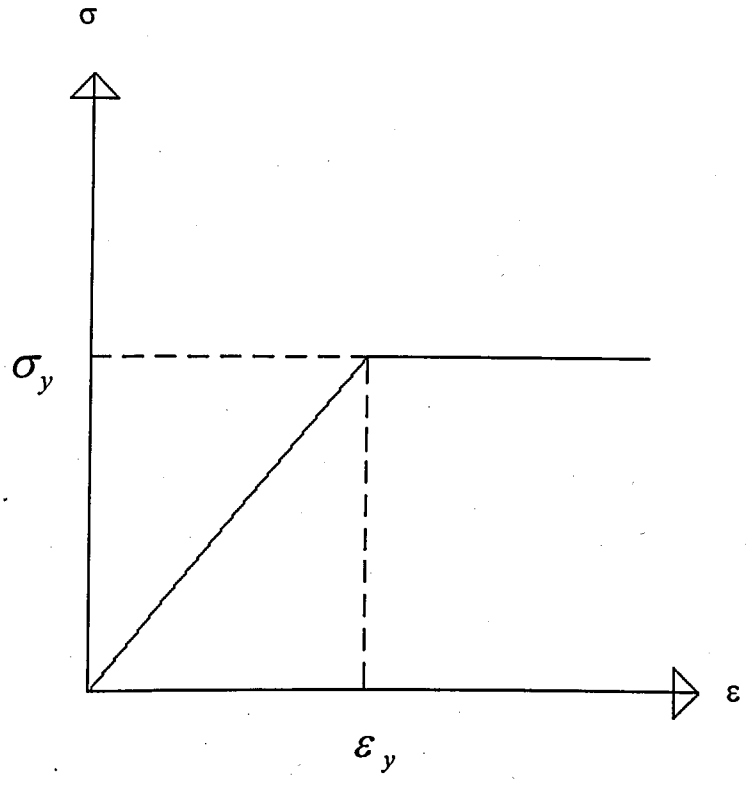

Figure 5.64. Stress-strain relationship of tension steel

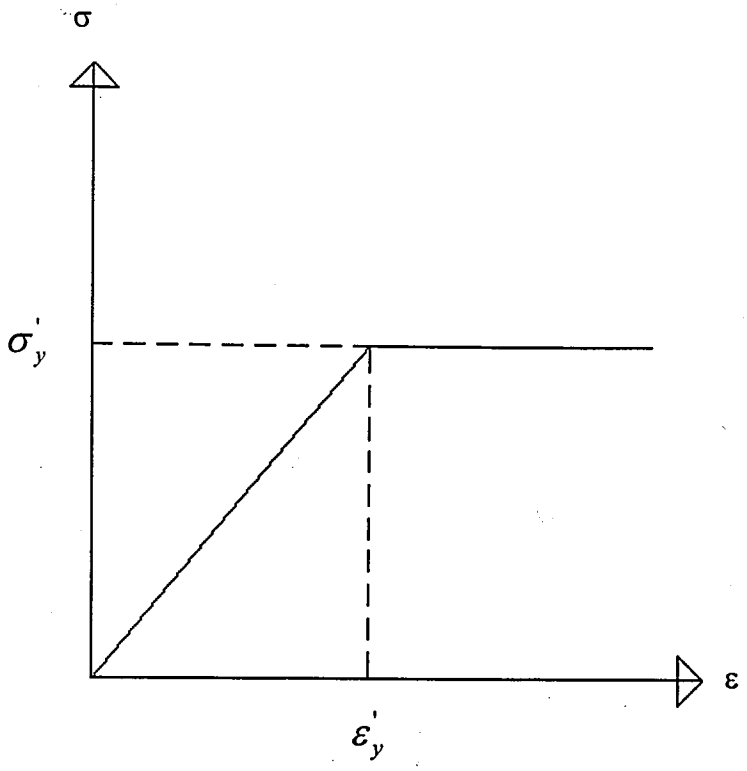

Figure 5.65. Stress-strain relationship of compression steel

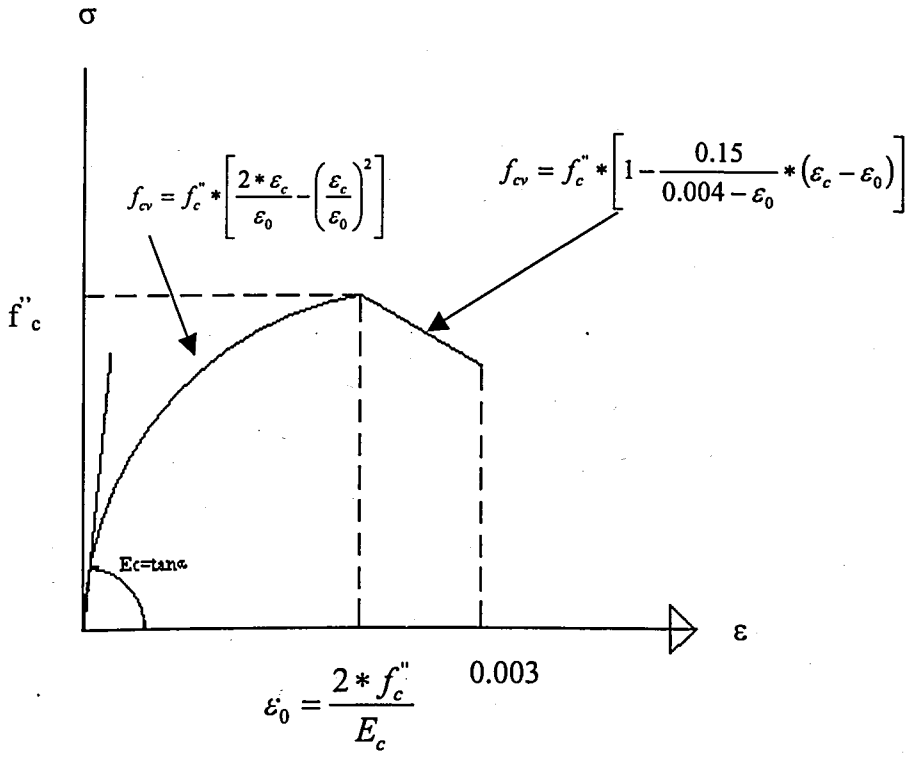

Figure 5.66. Idealized stress-strain diagram for concrete in uniaxial compression [22]

The formulations mentioned before are presented as follows:

$$\varepsilon_s = \varepsilon_c * \frac{(d-c)}{c} \tag{5.1}$$

$$\varepsilon_s^{'} = \varepsilon_c * \frac{(c-d')}{c} \tag{5.2}$$

$$\varepsilon_p = \varepsilon_c * \frac{(d_p-c)}{c} \tag{5.3}$$

After calculating strain values, stresses and forces for steel and FRP plate can be calculated as the following:

$$f_s = E_s * \varepsilon_s, \quad \text{if } \varepsilon_s \leq \varepsilon_y \tag{5.4}$$

$$f_s = f_y, \quad \text{if } \varepsilon_s \rangle \varepsilon_y \tag{5.5}$$

$$f_s^{'} = E_s^{'} * \varepsilon_s^{'}, \quad \text{if } \varepsilon_s^{'} \leq \varepsilon_y^{'} \tag{5.6}$$

$$f_s^{'} = f_y^{'}, \quad \text{if } \varepsilon_s^{'} \rangle \varepsilon_y^{'} \tag{5.7}$$

$$f_p = E_p * \varepsilon_p \tag{5.8}$$

$$F_s = f_s * A_s \tag{5.9}$$

$$F_s^{'} = f_s^{'} * A_s^{'} \tag{5.10}$$

$$F_P = f_P * A_P \tag{5.11}$$

The distribution of concrete stresses in compression zone can be stated as follows with respect to concrete strain in the extreme fiber in the compression zone.

$$f_{cv} = f_c'' * \left[2 * \frac{\varepsilon_c}{\varepsilon_0} - \left(\frac{\varepsilon_c}{\varepsilon_0} \right)^2 \right], \qquad \text{if } 0 \le \varepsilon_c \langle \varepsilon_0 \tag{5.12}$$

$$f_{cv} = f_c'' * \left[1 - \frac{0.15}{0.004 - \varepsilon_0} * (\varepsilon_c - \varepsilon_0) \right] \qquad \text{if } \varepsilon_0 \le \varepsilon_c \le 0.003 \tag{5.13}$$

$$F_c = \alpha * f_c'' * b * c \tag{5.14}$$

The parameter α which is mean stress factor can be used to convert non-linear stress-strain relationship of the concrete into an equivalent rectangular stress-strain curve. Area under stress-strain curve of concrete can be calculated as integrating the curve seen in Figure 5.66.

$$A = \int_0^{\varepsilon_c} f_{cv} * d\varepsilon_c = \alpha * f_c'' * \varepsilon_c \tag{5.15}$$

$$\alpha = \frac{\int_0^{\varepsilon_c} f_{cv} * d\varepsilon_{cv}}{f_c'' * \varepsilon_c} \tag{5.16}$$

$$\alpha = \frac{\varepsilon_c}{\varepsilon_0} - \frac{\varepsilon_c^2}{3 * \varepsilon_0^2} \qquad \text{if } 0 \le \varepsilon_c \langle \varepsilon_0 \tag{5.17}$$

$$\alpha = 1 + \frac{\varepsilon_c}{\varepsilon_0} * \left(1 - \frac{\varepsilon_c}{3 * \varepsilon_0} - \frac{\varepsilon_0^2}{\varepsilon_c^2} \right) - \frac{0.15}{0.004 - \varepsilon_0} * \left(\frac{\varepsilon_c}{2} - \varepsilon_0 \right) - \frac{0.075}{0.004 - \varepsilon_0} * \left(\frac{\varepsilon_0^2}{\varepsilon_c} \right)$$

$$\text{if } \varepsilon_0 \le \varepsilon_c \le 0.003 \tag{5.18}$$

Using the parameter of γ which is centroid factor, the distance of concrete compressive force from the top fiber of the concrete can be determined.

$$y' = \gamma * c \tag{5.19}$$

$$Q = \int_0^{\varepsilon_c} f_{cv} * \varepsilon_{cv} * d\varepsilon_{cv} = \ddot{\varepsilon}_c * A \tag{5.20}$$

$$\ddot{\varepsilon}_c = (1-\gamma) * \varepsilon_c \tag{5.21}$$

Where,

Q: The first moment of area under the stress-strain curve about the origin,

$\ddot{\varepsilon}_c$: strain at centroid of area under concrete stress-strain diagram

$$Q = (1-\gamma) * \varepsilon_c * \int_0^{\varepsilon_c} f_{cv} * \varepsilon_{cv} * d\varepsilon_{cv} = \ddot{\varepsilon}_c * A \tag{5.22}$$

$$\gamma = 1 - \frac{\int_0^{\varepsilon_c} \varepsilon_{cv} * f_{cv} * d\varepsilon_{cv}}{\varepsilon_c * \int_0^{\varepsilon_c} f_{cv} * d\varepsilon_{cv}} \tag{5.23}$$

$$\gamma = \frac{\frac{1}{3} - \frac{\varepsilon_c}{12 * \varepsilon_0}}{1 - \frac{\varepsilon_c}{3 * \varepsilon_0}} \qquad \text{if } 0 \le \varepsilon_c \langle \varepsilon_0 \tag{5.24}$$

$$\gamma = 1 - \frac{(\varepsilon_c^3 - 5.1 * \varepsilon_0 * \varepsilon_c^2 - 0.004 * \varepsilon_0^2 + 0.024 * \varepsilon_c^2)}{\varepsilon_c * (3.925 * \varepsilon_0^2 - 10.2 * \varepsilon_0 * \varepsilon_c - 0.9 * \varepsilon_c^2 - 0.016 * \varepsilon_0 + 0.048 * \varepsilon_c)}$$

$$\text{if } \varepsilon_0 \le \varepsilon_c \langle 0.003 \tag{5.25}$$

Neutral axis depth can be obtained form the equilibrium of internal forces calculated by previous formulations. This equilibrium can be solved iteratively until the equation is satisfied.

$$\sum F = F_c + F_s + F_s^{'} + F_p = 0 \tag{5.26}$$

$$\sum F = \alpha * f_c^{''} * b * c + \sum_{i=1}^{n} f_{si} * A_{si} + f_p * A_p = 0 \tag{5.27}$$

The internal moment is obtained by summing the moments of the internal forces about an axis.

$$M = f_s^{'} * A_s^{'} * (\gamma * c - d^{'}) + f_s * A_s * (d - \gamma * c) + f_p * A_p * (d_p - \gamma * c) \tag{5.28}$$

$$\phi = \frac{\varepsilon_c}{c} \tag{5.29}$$

Using the above formulations based on strain compatibility and equilibrium equations, moment versus curvature diagrams of FRP-strengthened beams without plate end anchorage can be are presented as the following from Figure 5.67 to Figure 5.72. It can be easily seen that moment curvature diagrams drawn analytically coincide with moment curvature diagrams drawn by using experimental data better while reinforcement ratio increases. In addition, analytical method based on equilibrium and strain compatibility equations can approximately predict the behaviour of the beams. Since analytical calculations do not consider peeling-off failure which is seen commonly ultimate moment and curvature values obtained by analytically are greater than experimental values. The difference between those values can show slippage of the FRP.

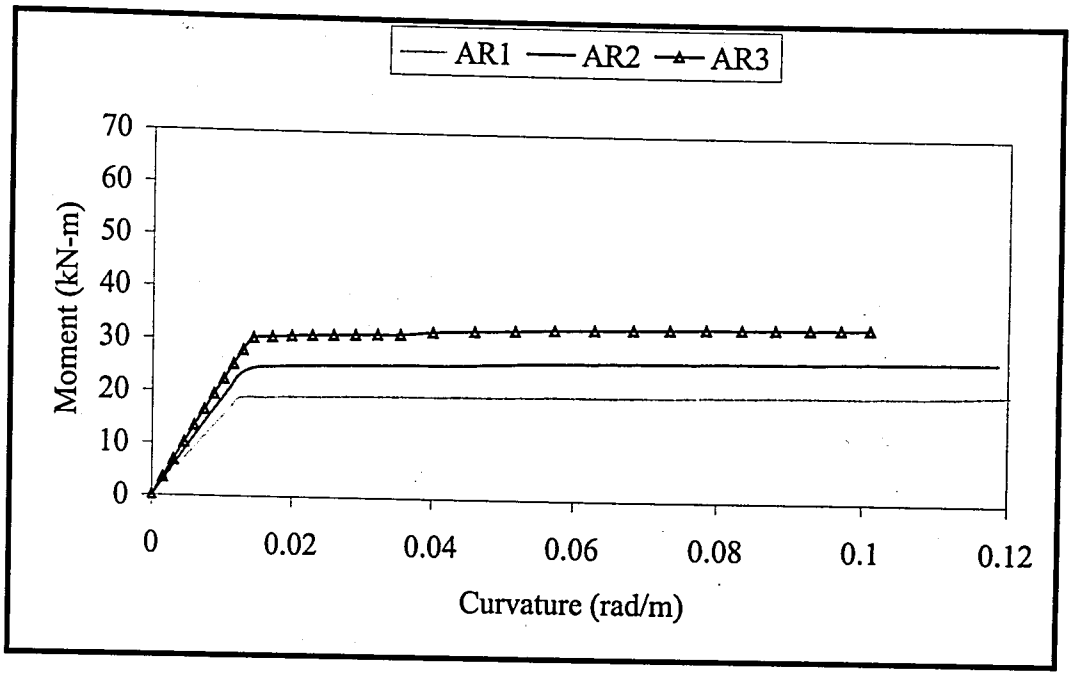

Figure 5.67. Moment curvature curves of virgin specimens obtained by analytically

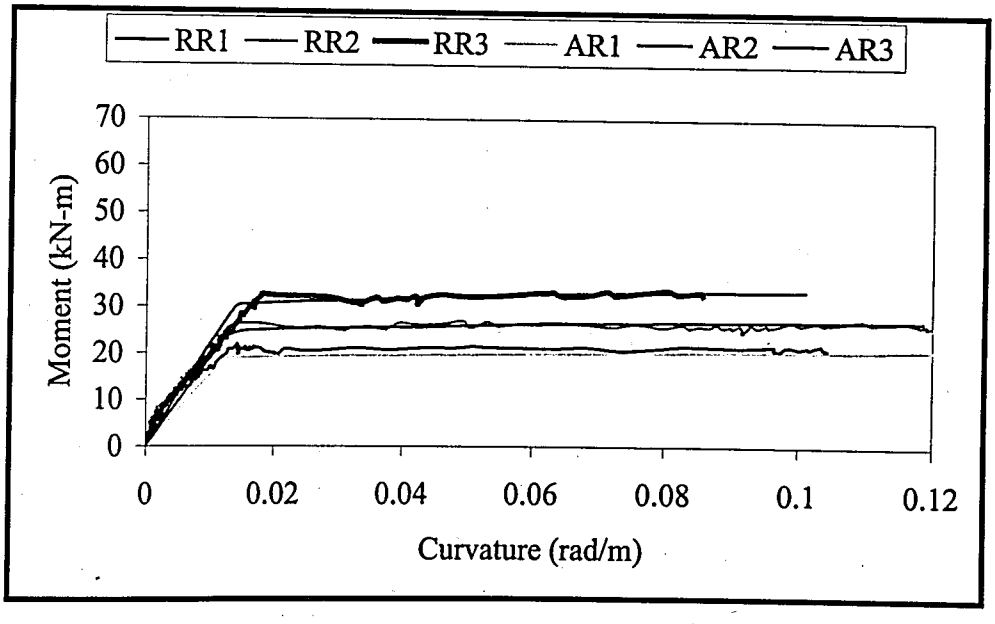

Figure 5.68. Moment curvature curves of virgin specimens obtained by analytically and experimentally

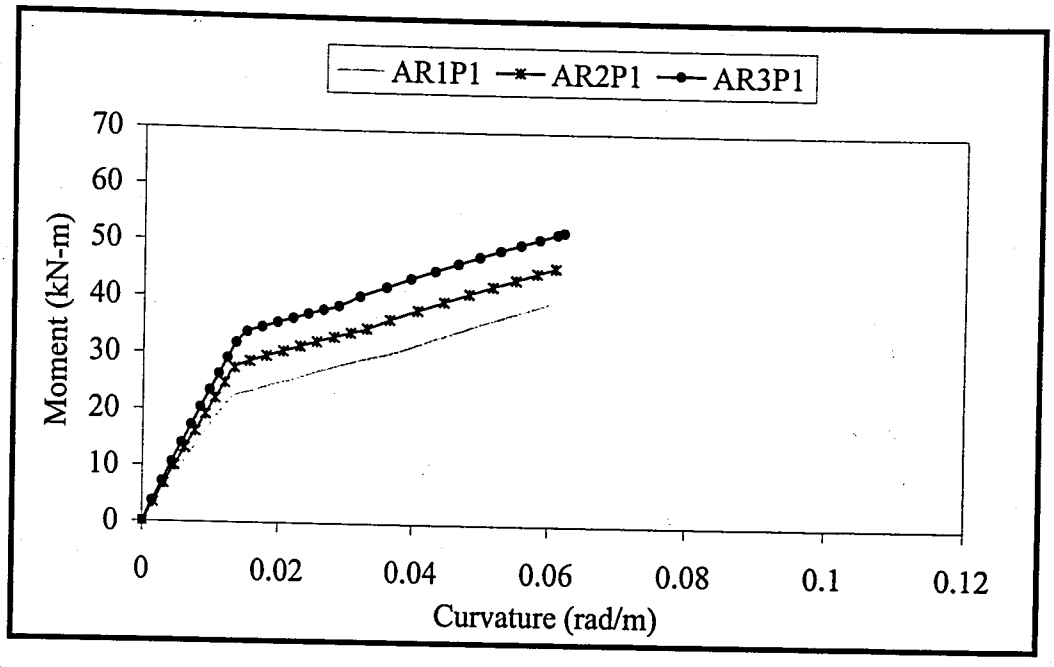

Figure 5.69. Moment curvature curves of one FRP-plated beams obtained by analytically

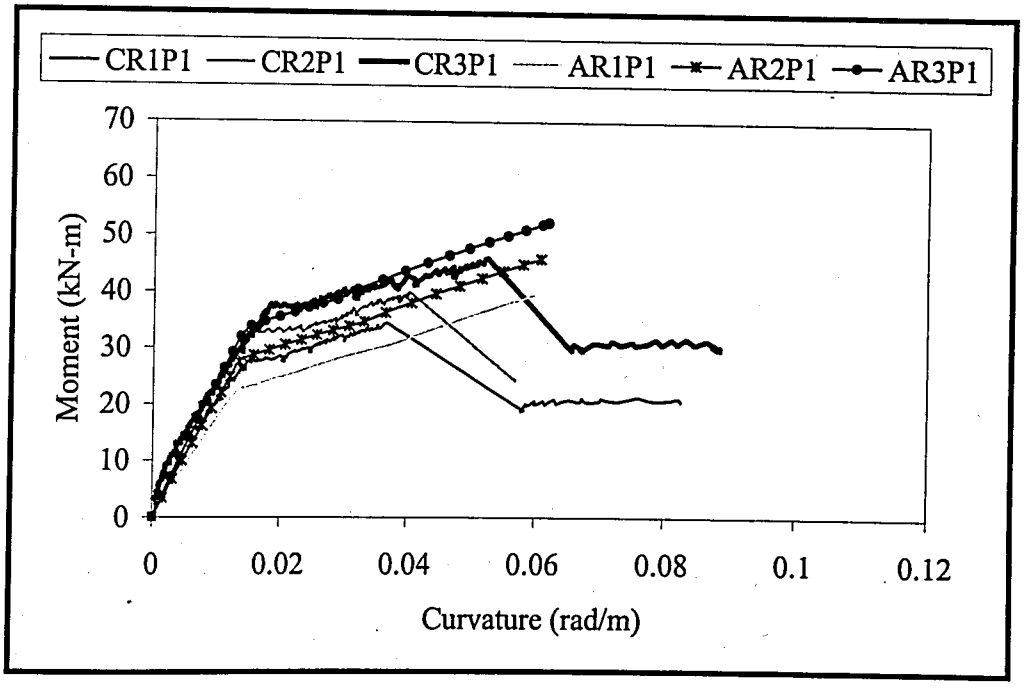

Figure 5.70. Moment curvature curves of one FRP-plated beams obtained by analytically and experimentally

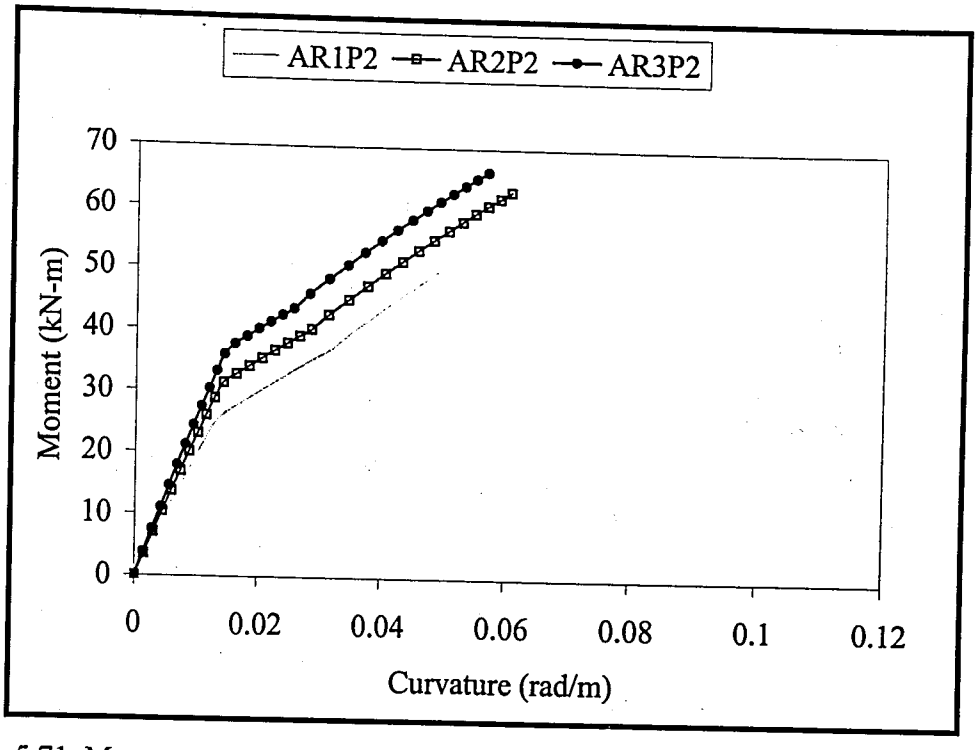

Figure 5.71. Moment curvature curves of two FRP-plated beams obtained by analytically

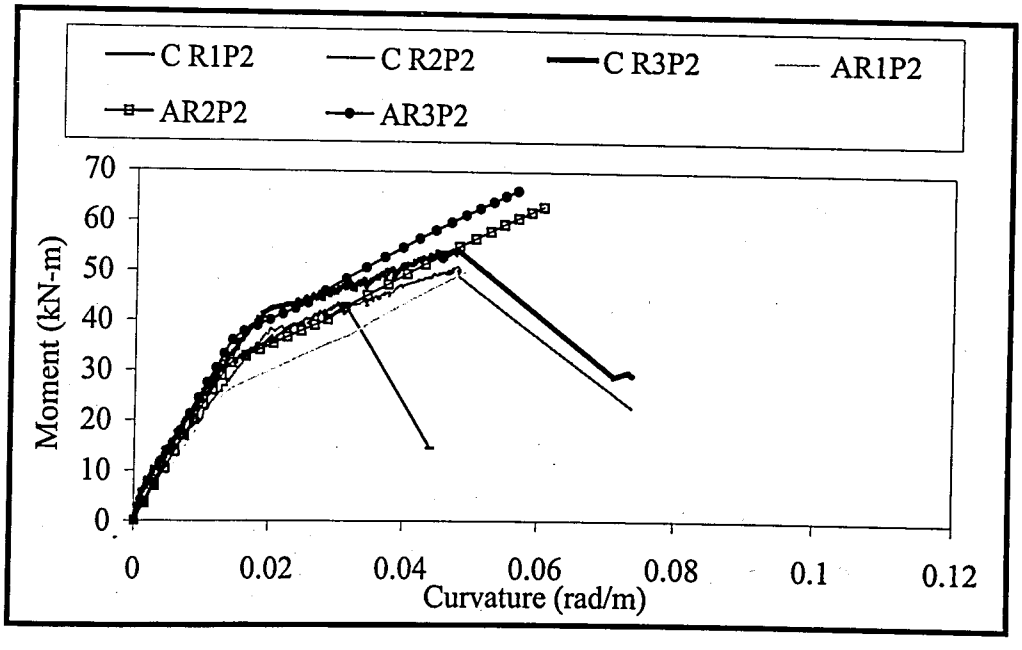

Figure 5.72. Moment curvature curves of two FRP-plated beams obtained by analytically and experimentally

6. CONCLUSIONS AND RECOMMENDATIONS

The following conclusions may be drawn from the results of the current study:

- While virgin specimens have shown a ductile behaviour, FRP-strengthened beams have shown a brittle behaviour. Moreover, strengthened beams with FRP plates have failed suddenly with a significant loss of load capacity at the instant of failure.
- Presence of external anchorages influences the overall behaviour of the FRP-strengthened beams favorably. It tends to increase the load carrying capacity, moment bearing capacity and strength of the beams. Besides, external anchorages generally supply greater ductility with respect to FRP-plated beams without anchorages and slow slippage since they usually increase ultimate load and curvature values.
- It has been observed that external anchorages have failed by tearing away and they have postponed the de-bonding failure.
- Unless external anchorages should be designed carefully, they would not be used efficiently. In order to use full capacity of FRP applying an anchorage system may be necessary.
- Crack width and crack spacing are generally inclined to decrease with an increase in FRP ratio. This brings about an increase in serviceability loads.
- Preparing of surfaces of FRP plate and substrate, producing a homogeneous adhesive thickness, adjusting temperature and humidity conditions are very important stages to maintain maximum benefit from the composite structure formed by FRP laminate, epoxy adhesive and concrete. That's why, special attention should be paid for the application.
- Load at first crack generally increases with enhancing FRP ratio. This increase mostly results from the added stiffness of the flexural FRP plate and reaches up to 188 per cent.
- Externally bonded FRP plates increased the failure load up to 120 per cent and this increase in the capacity can be seen clearly in lightly reinforced beams.

- The rupture of FRP plates has not occurred in any of the tests, but de-bonding type of failure has been dominant. Besides, externally bonded FRP plates have generally changed the failure modes from flexural yielding of steel to de-bonding failure.
- Strengthening of R.C. beams with externally bonded FRP plates results in a considerable decrease in ductility up to 64 per cent with respect to virgin specimens. However, wrapping of shear span usually increases ductility of the FRP-plated beams.
- The contribution of FRP plates can also be seen in moment curvature and load deflection diagrams clearly. Presence of FRP plates has increased ultimate loads and ultimate moments.
- Since analytical calculations used can predict the behaviour of the FRP-plated beams roughly, analytical calculations which include different failure loads like local failures should become widespread and be used to predict the behaviour of FRP-plated beams.
- Reversed cyclic loading can be applied to strengthened beams with FRP materials for possible future researches.
- For possible research work, R.C. beams already damaged by previous loadings and then strengthened by FRP materials can be tested under four point loading as well.

APPENDIX A: PICTURES OF THE TESTS AND SPECIMENS

Photos of every stage of this study are shown in the following pictures. Testing procedure may be followed with these pictures:

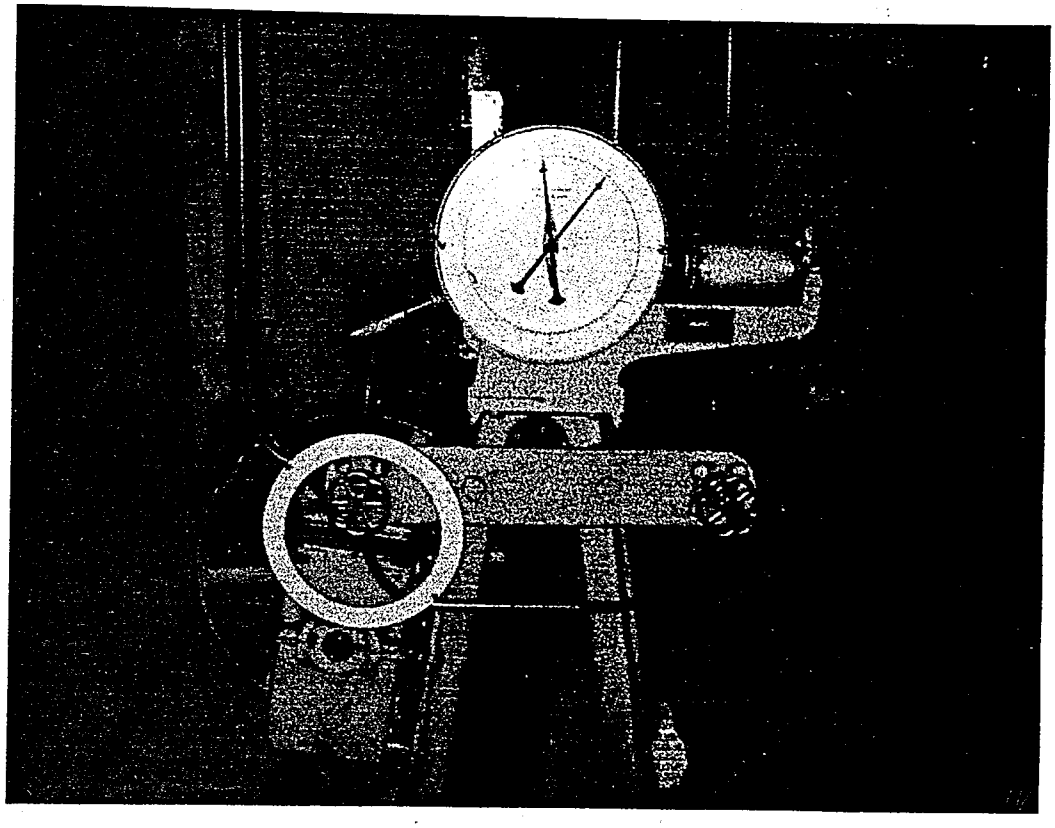

Figure A.1. Test machine used to find yield strength of re-bars

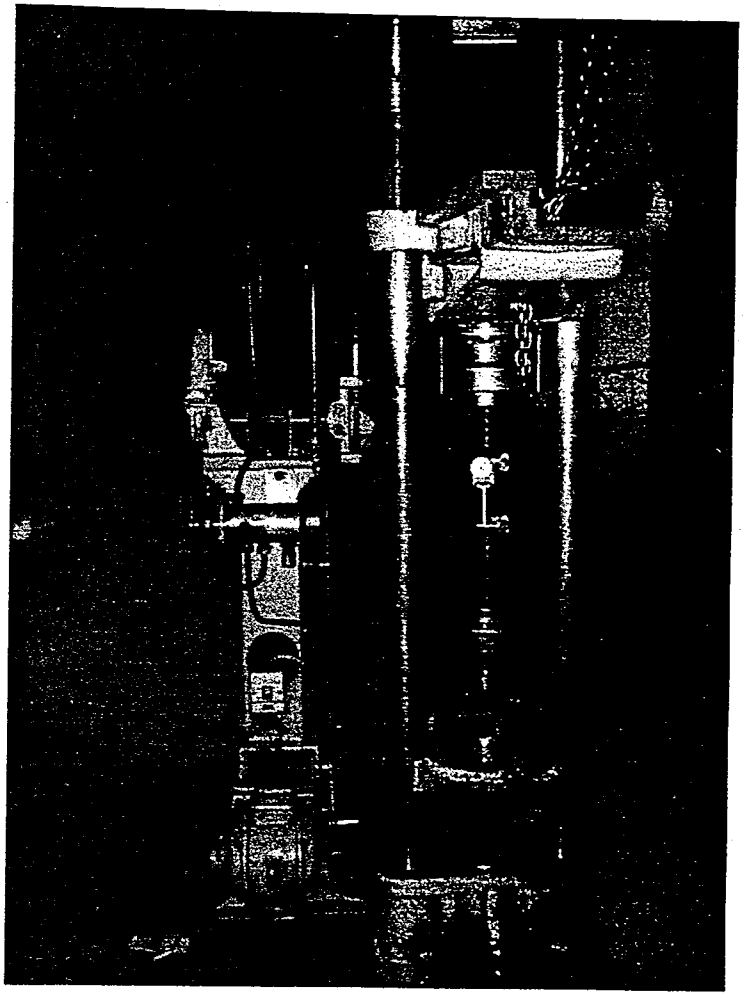

Figure A.2. Test of re-bars

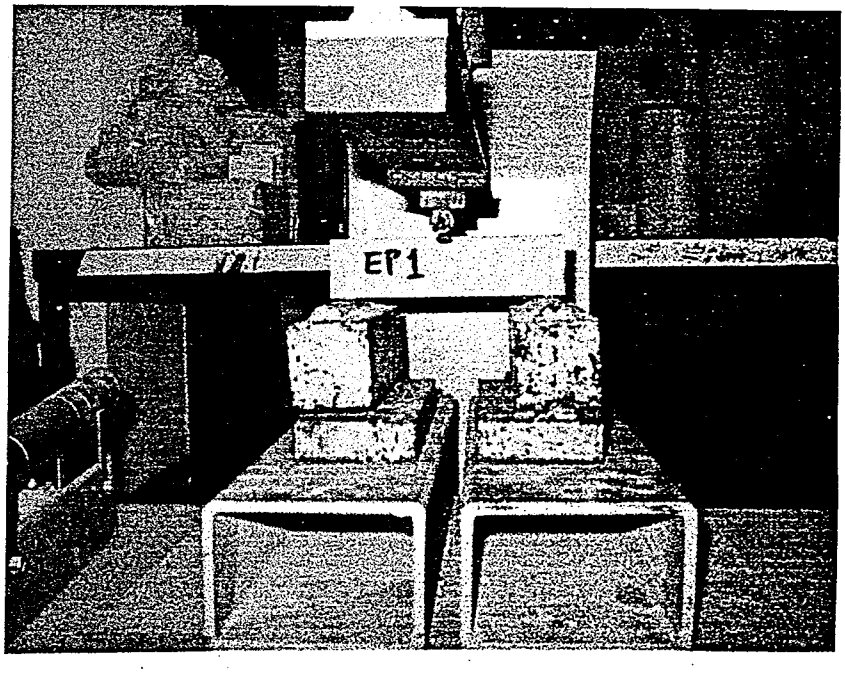

Figure A.3. Flexural test set-up of 40x40x160 mm epoxy specimens

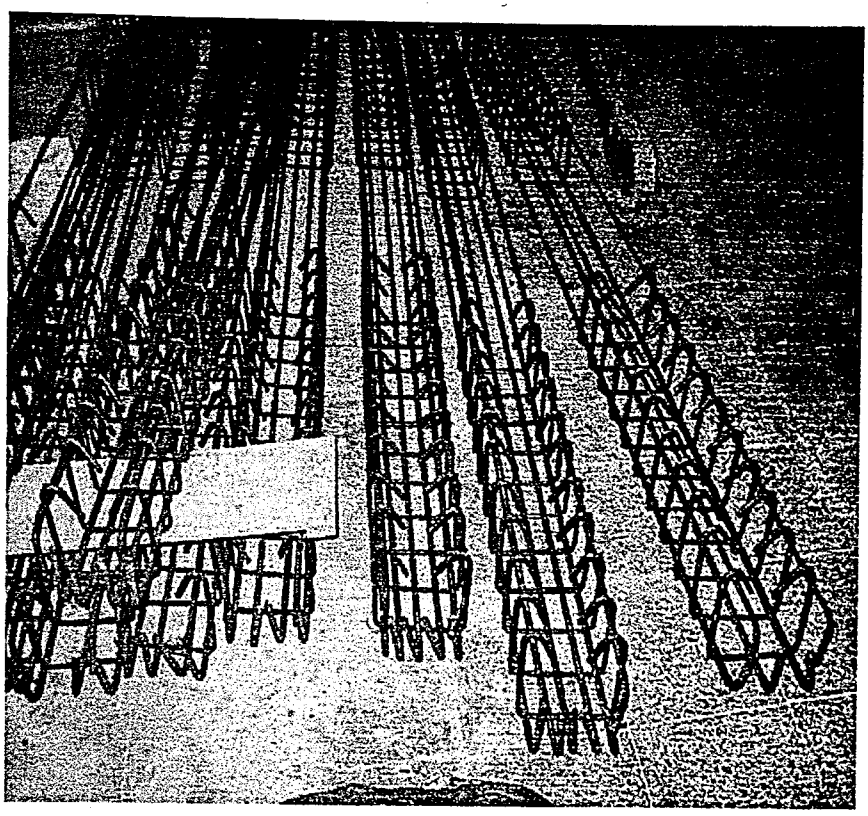

Figure A.4. A view of longitudinal and transverse reinforcements

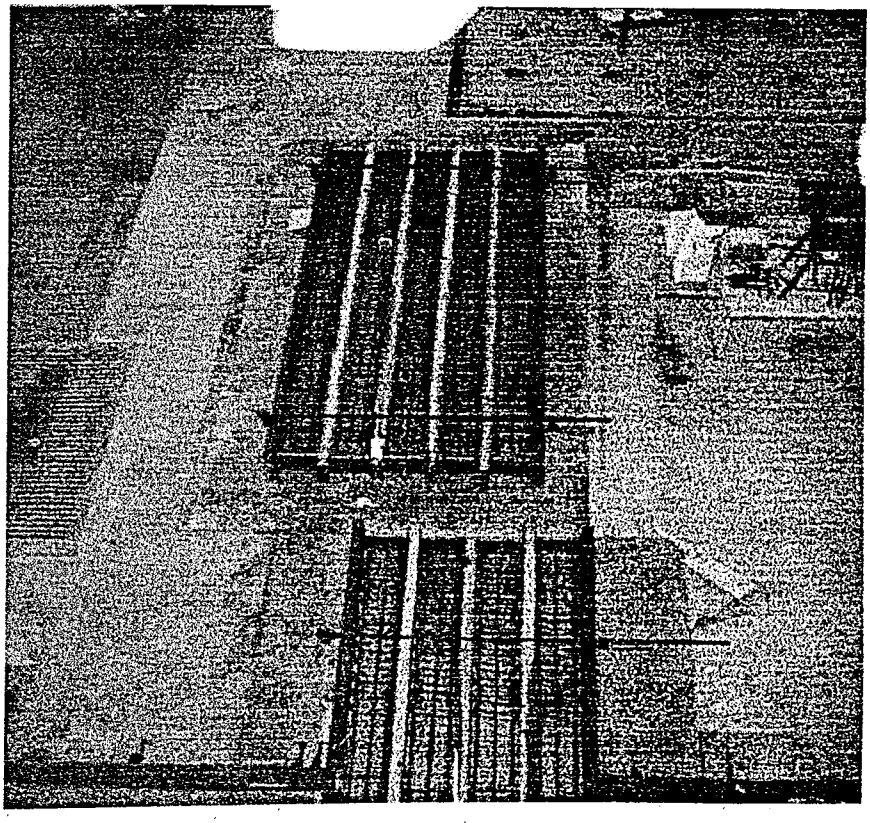

Figure A.5. A view of timber and steel moulds

Figure A.6. A view of reversed test beams

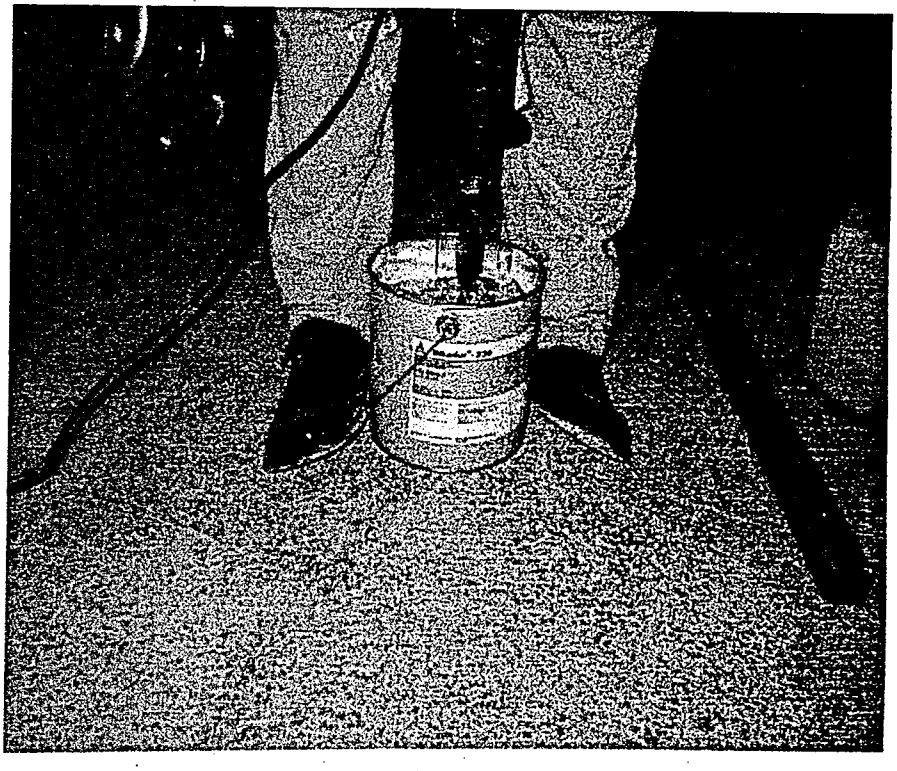

Figure A.7. Mixing of epoxy adhesives

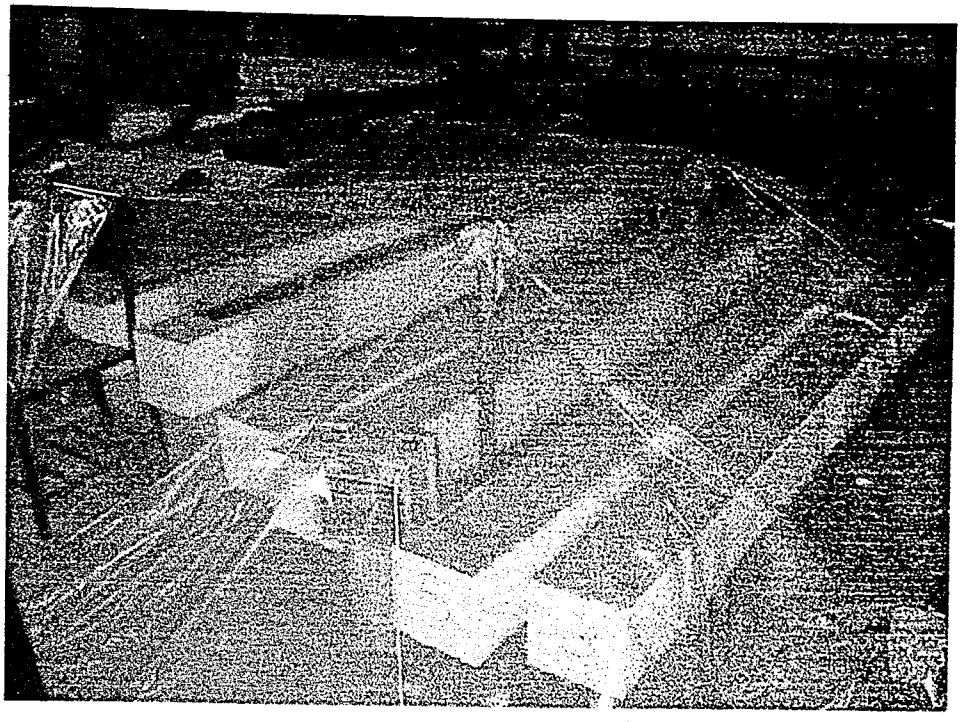

Figure A.8. A view of nylon tent

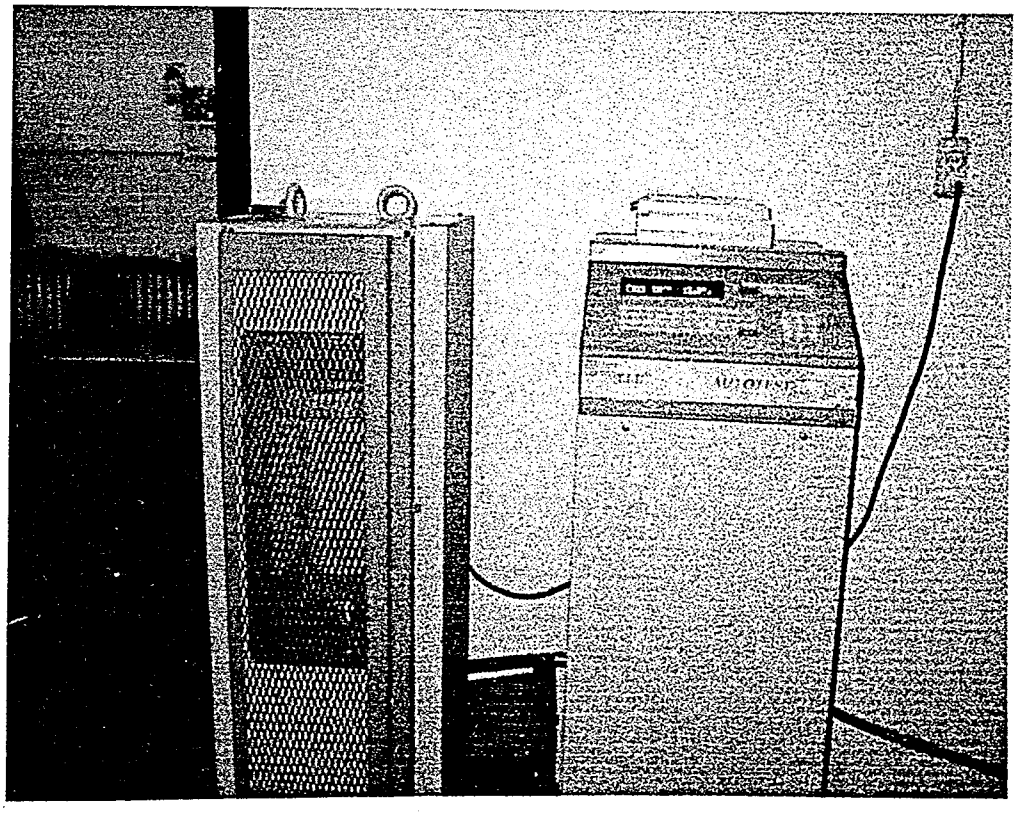

Figure A.9. Compression test of 150x300 mm test cylinders

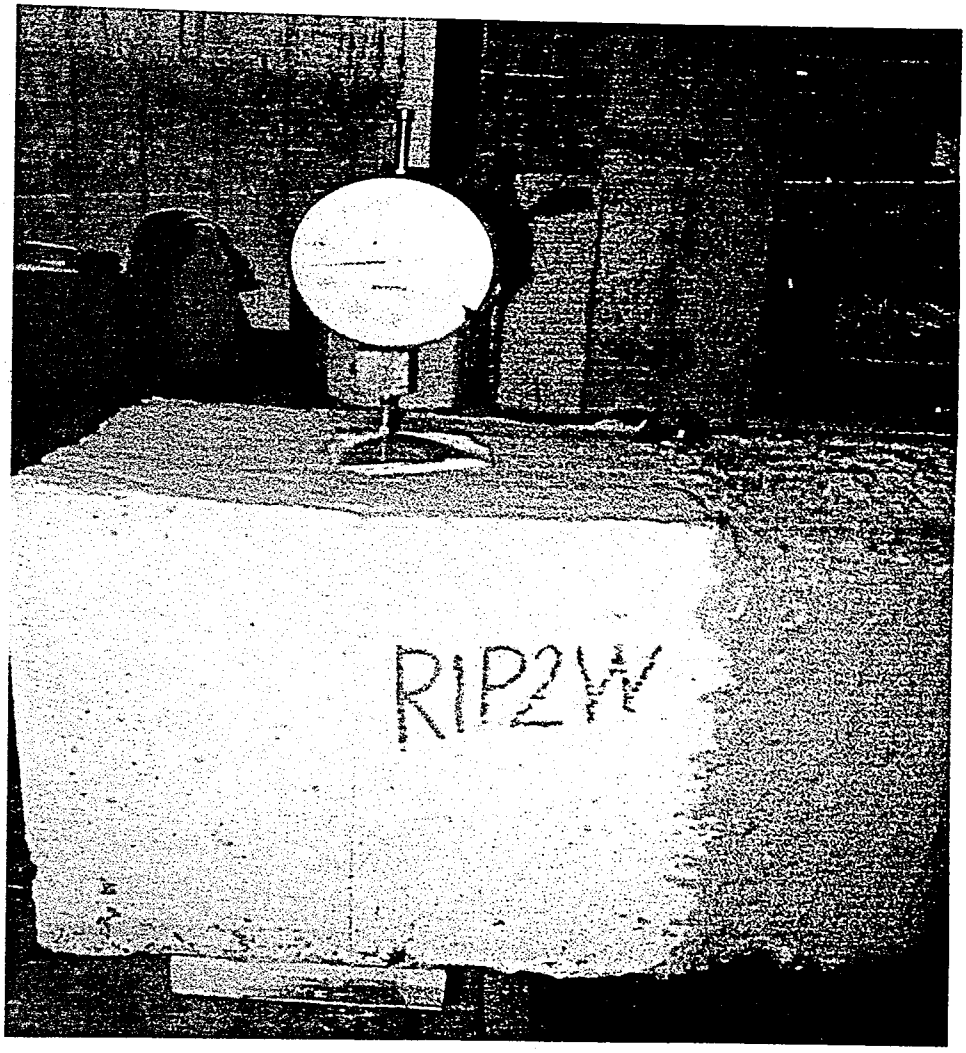

Figure A.10. Location of the dial-gage at the right support

REFERENCES

1. Malek, A.M., H. Saadatmanesh and M.R. Ehsani, "Prediction of Failure Load of R/C Beams Strengthened with FRP Plate Due to Stress Concentration at the Plate End", *ACI Structural Journal,* Vol. 95, No.1, pp. 142-152, March-April 1998.

2. Özkul, M.H. and H. Yıldırım, "Strengthening of Steel Reinforced Concrete Beams with Carbon Fibre Reinforced Plastics", in F. Karadoğan (Ed.), *Repair & Strengthening of Existing Buildings,* Vol. 1, pp. 551-557, Istanbul, February 1998.

3. Triantafillou, T., "Shear Strengthening of Reinforced Concrete Beams Using Epoxy-Bonded FRP Composites", *ACI Structural Journal,* Vol. 95, No. 2, pp. 107-115, March-April 1998.

4. Saadatmanesh, H. and A.M. Malek, "Design Guidelines for Flexural Strengthening of RC Beams with FRP Plates", *Journal of Composites for Construction, ASCE,* Vol. 2, No.4, pp. 158-164, November 1998.

5. Garden, H.N. and L.C. Hollaway, "An Experimental Study of the Failure Modes of Reinforced Concrete Beams Strengthened with Prestressed Carbon Composite Plates", *Composites Part B 29 B, Elsevier Science Limited,* pp. 411-424, 1998.

6. Hamoush, S.A. and S.H. Ahmad, "Debonding of Steel Plate-Strengthened Concrete Beams", *Journal of Structural Engineering, ASCE,* Vol. 116, No.2, pp. 356-371, February 1990.

7. Sharif, A., G.J. Al-Sulaimani, I.A. Basunbul, M.H. Baluch and B.N. Ghaleb, "Strengthening of Initially Loaded Reinforced Concrete Beams Using FRP Plates", *ACI Structural Journal,* Vol. 91, No. 2, pp. 160-168, March-April 1994.

8. Garden, H.N., L.C. Hollaway, and A.M. Thorne, "The Strengthening and Deformation Behaviour of Reinforced Concrete Beams Upgraded Using Prestressed Composites", *RILEM Materials and Structures,* Vol. 31, pp. 247-258, 1998.

9. Plevris, N., T.C. Triantafillou and D. Veneziano, "Reliability of RC Members Strengthened with CFRP Laminates", *Journal of Structural Engineering, ASCE,* Vol. 121, No.7, pp. 1037-1044, July 1995.

10. Meier, U., "Rehabilitation and Retrofitting of Existing Structures Through External Bonding of Thin Carbon Fibre Sheets", *RILEM Materials and Structures,* Vol. 28, No.176, pp. 105-106, March 1995.

11. Koga, M. and M. Ohtsu, "A Retrofitting System for Concrete Structures with CFRP-Sheet and CFRP-Strand-It's Basic Mechanism and Applications-", *Proceedings of the Seventh International Conference on Structural Faults and Repair*, pp. 63-67, Edinbrough, U.K., 1997.

12. Norris, T., H. Saadatmanesh and M.R. Ehsani, "Shear and Flexural Strengthening of R/C Beams with Carbon Fiber Sheets", *Journal of Structural Engineering, ASCE,* Vol. 123, No.7, pp. 903-911, July 1997.

13. Saadatmanesh, H. and M.R. Ehsani, "RC Beams Strengthened with GFRP Plates. I: Experimental Study", *Journal of Structural Engineering, ASCE,* Vol. 117, No.11, pp. 3417-3433, November 1991.

14. Feldman, D., *Polymeric Building Materials,* Elsevier Science Publishers, Essex, 1989.

15. Hull, D., A*n Introduction to Composite Materials,* Cambridge University Press, Cambridge, 1981.

16. Perkins, P.H., *Concrete Structures: Repair, Waterproofing and Protection,* Applied Science Publishers LTD, London, 1976

17. Spadea, G., F. Bencardino and R.N. Swamy, "Structural Behaviour of Composite RC Beams with Externally Bonded CFRP", *Journal of Composites for Construction, ASCE,* Vol. 2, No.3, pp. 132-137, August 1998.

18. David, E., *Mechanical Behaviour of RC Beams Strengthened or Repaired by CFRP Sheets Bonding: Experimental and Numerical Study*"Ph.D. Thesis, Université d'Artois, 1999

19. Spadea, G., F. Bencardino and R.N. Swamy, "Optimizing the Performance Characteristics of Beams Strengthened with Bonded CFRP Laminates", *RILEM Materials and Structures,* Vol. 33, pp. 119-126, March 2000.

20. Triantafillou, T.C. and N. Plevris, "Strengthening of RC Beams with Epoxy-Bonded Fibre-Composite Materials", *RILEM Materials and Structures,* Vol. 25, pp. 201-211, 1992.

21. Ross, C.A., D.M. Jerome, J.W. Tedesco and M.L. Hughes, "Strengthening of Reinforced Concrete Beams with Externally Bonded composite Laminates", *ACI Structural Journal,* Vol. 96, No. 2, pp. 212-220, March-April 1999.

22. An, W., H. Saadatmanesh. and M.R. Ehsani, "RC Beams Strengthened with FRP Plates. II: Analysis and Parametric Study", *Journal of Structural Engineering, ASCE,* Vol. 117, No.11, pp. 3434-3455, November 1991.

23. Grace, N.F., G.A. Sayed, A.K. Soliman and K.R. Saleh, "Strengthening Reinforced Concrete Beams Using Fiber Reinforced Polymer (FRP) Laminates", *ACI Structural Journal,* Vol. 96, No. 5, pp. 865-874, September-October 1999.

24. Buyukozturk, O. and B. Hearing, "Failure behaviour of Precracked Concrete Beams Retrofitted with FRP", *Journal of Composites for Construction, ASCE,* Vol. 2, No.3, pp. 138-144, August 1998.

25. El-Mihilmy, M. and J.W. Tedesco, "Analysis of Reinforced Concrete Beams Strengthened with FRP Laminates", *Journal of Structural Engineering, ASCE,* Vol. 126, No.6, pp. 684-691, June 2000.

26. Triantafillou, T.C., *Guidelines for the Dimensioning of Reinforced Concrete Elements Strengthened with Sika Carbodur/Skawrap*, Sika A.C. Publishment, Zurich, April 1999.

27. Ziraba, Y.N., M.H. Baluch, I.A. Basunbul, A.M. Sharif, A.K. Azad and G.J. Al-Sulaimani, "Guidelines Toward the Design of Reinforced Concrete Beams with External Plates", *ACI Structural Journal,* Vol. 91, No. 6, pp. 639-646, November-December 1994.

28. ACI 318-95, *Building Code Requirements for Reinforced Concrete*, American Concrete Institute, Detroit, Michigan, 1995

29. TS-500, *Betonarme Yapıların Hesap ve Yapım Kuralları,* Turkish Standards, February 2000.

30. Ritchie, P.A., D.A. Thomas, Le-Wu Lu and G.M. Connelly, "External Reinforcement of Concrete Beams Using Fiber Reinforced Plastics", *ACI Structural Journal,* Vol. 88, No. 4, pp. 490-500, July-August 1991.

31. Mukhopadhyaya, P., N. Swamy and C. Lynsdale, "Optimizing Structural Response of Beams Strengthened with GFRP Plates", *Journal of Composites for Construction,* Vol. 2, No. 2, pp. 87-95, May 1998.